
# รายงานวิจัยฉบับสมบูรณ์

# การดัดแปรพื้นผิวอนุภาคนาโนแมกนีไทท์ด้วยปฏิกิริยาพอลิเมอไรเซชันแบบอนุมูลอิสระถ่ายโอนอะตอมและการประยุกต์ใช้

# Surface Modification of Magnetite Nanoparticle *via* Atom Transfer Radical Polymerization and Its Applications

โดย รองศาสตราจารย์ ดร. เมธา รัตนากรพิทักษ์ และคณะ

พฤษภาคม 2556

สัญญาเลขที่ DBG5380001

# รายงานวิจัยฉบับสมบูรณ์

# การดัดแปรพื้นผิวอนุภาคนาโนแมกนีไทท์ด้วยปฏิกิริยาพอลิเมอไรเซชันแบบอนุมูลอิสระถ่ายโอนอะตอมและการประยุกต์ใช้


| คณะผู้วิจัย | สังกัด |
|---|---|
| 1. รองศาสตราจารย์ ดร.เมธา รัตนากรพิทักษ์ | มหาวิทยาลัยนเรศวร |
| 2. ดร.อุทัย วิชัย | มหาวิทยาลัยนเรศวร |
| 3. ผู้ช่วยศาสตราจารย์ ดร.บุญจิรา รัตนากรพิทักษ์ | มหาวิทยาลัยนเรศวร |
| 5. นางสาวยิ่งรัก พรายอินทร์ | มหาวิทยาลัยนเรศวร |
| 6. นางสาวภาวิณี เทียมดี | มหาวิทยาลัยนเรศวร |
| 7. นายบัณฑิต ทองอ่อน | มหาวิทยาลัยนเรศวร |
| 8. นางสาวนิภาพร พวงศิลป์ | มหาวิทยาลัยนเรศวร |



สนับสนุนโดยสำนักงานคณะกรรมการการอุดมศึกษา
และสำนักงานกองทุนสนับสนุนการวิจัย

## กิตติกรรมประกาศ

งานวิจัยนี้ ได้รับการสนับสนุนทุนวิจัยจากสำนักงานคณะกรรมการการอุดมศึกษา (สกว.) ร่วมกับมหาวิทยาลัยนเรศวร ด้วยทุนวิจัยพื้นฐานเชิงยุทธศาสตร์ “นาโนศาสตร์และนาโนเทคโนโลยี” ประจำปี 2553-2556 ข้าพเจ้าขอขอบคุณนักวิจัยร่วมทุกท่านที่มีส่วนร่วมในการวิเคราะห์และวิจารณ์ผลการทดลอง ได้แก่ ดร. อุทัย วิชัยและ ผู้ช่วยศาสตราจารย์ ดร.บุญจิรา รัตนากรพิทักษ์ จากภาควิชาเคมี คณะวิทยาศาสตร์ มหาวิทยาลัยนเรศวร Dr.Véronique Montembault, Dr.Sagrario Pascua และ Prof.Dr.Laurent Fontaine จาก Université du Maine ประเทศฝรั่งเศส และขอขอบคุณนิสิตปริญญาโทและปริญญาเอกทุกท่านที่มีส่วนสำคัญในการทำงานวิจัยนี้ ได้แก่นางสาวยิ่งรัก พรายอินทร์ นางสาวภาวิณี เทียมดี นายบัณฑิต ทองอ่อนและนางสาวนิภาพร พวงศิลป์

ข้าพเจ้าขอขอบคุณทุนการศึกษาและการวิจัยแก่นิสิตปริญญาโทและปริญญาเอก ได้แก่ ทุนจากโครงการปริญญาเอกกาญจนาภิเษก (คปก.) และทุนจากศูนย์ความเป็นเลิศด้านนวัตกรรมทางเคมี (PERCH-CIC) และขอขอบคุณทุนสนับสนุนความร่วมมือด้านงานวิจัยร่วมระหว่างกระทรวงการต่างประเทศของประเทศฝรั่งเศส และ สำนักงานคณะกรรมการการอุดมศึกษา (สกอ.) ของประเทศไทย ประจำปี 2552-2553 (the Franco-Thai Cooperation Program in Higher Education and Research 2009-2010, supported by the Ministry of Foreign Affairs, Ministry of Higher Education and Research of France and the Commission on Higher Education of Thailand)

**Research title: Surface Modification of Magnetite Nanoparticle *via* Atom Transfer Radical Polymerization and Its Applications**

## Abstract

Surface modification and functionalization of magnetite nanoparticle (MNP) have recently attracted a great attention in the biotechnology and biomedical applications. This report presents various strategies for modification and functionalization of MNP surface and its corresponding applications. MNP can be prepared via a thermal decomposition of iron organic precursors and the particle was then surface modified with various kinds of polymers via atom transfer radical polymerization (ATRP) to obtain the MNP with desirable properties such as high magnetic saturation, biocompatibility, water dispersibility and containing interactive functions at the surface. It was found that the stability in the dispersions and the availability for further functionalization of MNP have been improved after the polymeric coatings.

This report presents 4 different approaches for MNP surface modification. The first and second topics present successful surface functionalization of MNP with acrylic acid and azlactone functional groups, respectively, for further attachments of bioentities. The third topic describes the surface functionalization of the particles with UV sensitive polymers (poly(azobenzene acrylate)). The fourth topic describes the surface modification of MNP with block copolymer of poly(ethylene glycol methyl ether) and poly(dimethyl siloxane) to obtain polymeric bilayer surfactant. These surface modified and functionalized MNPs exhibit a great potential for uses in many areas, including biomedical and biotechnology applications.

**Keyword:** nanoparticle, magnetite, surface modification, grafting from, ATRP

**ชื่อเรื่อง: การดัดแปรพื้นผิวอนุภาคนาโนแมกนีไทท์ด้วยปฏิกิริยาพอลิเมอไรเซชันแบบอนุมูลอิสระถ่ายโอนอะตอมและการประยุกต์ใช้**

## บทคัดย่อ

ปัจจุบัน การศึกษาปฏิกิริยาการดัดแปรและการตรึงหมู่ฟังก์ชันบนพื้นผิวอนุภาคนาโนแมกนีไทท์เพื่อการประยุกต์ใช้ทางด้านเทคโนชีวภาพและทางด้านการแพทย์กำลังได้รับความสนใจอย่างมาก โดยงานวิจัยนี้ได้กล่าวถึงการศึกษาและออกแบบการดัดแปรพื้นผิวอนุภาคนาโนแมกนีไทท์ด้วยพอลิเมอร์เพื่อใช้ในการตรึงสารชีวโมเลกุลบนพื้นผิวอนุภาคและการประยุกต์ใช้งานของอนุภาคที่ดัดแปรพื้นผิว อนุภาคนาโนแมกนีไทท์สังเคราะห์จากปฏิกิริยาการแตกสลายที่อุณหภูมิสูงของสารตั้งต้นเหล็ก จากนั้นทำการดัดแปรพื้นผิวอนุภาคด้วยพอลิเมอร์หลากหลายชนิดด้วยปฏิกิริยาพอลิเมอไรเซชันแบบอนุมูลอิสระถ่ายโอนอะตอม เพื่อให้ได้อนุภาคที่มีสมบัติตามต้องการ เช่น มีการตอบสนองต่อแม่เหล็กที่ดี มีความเข้ากันได้เชิงชีวภาพ สามารถกระจายตัวได้ดีในน้ำและมีหมู่ฟังก์ชันบนพื้นผิวที่สามารถเกิดปฏิกิริยาต่อได้ จากผลการทดลองพบว่าอนุภาคนาโนแมกนีไทท์ที่มีการเคลือบด้วยพอลิเมอร์แล้วจะมีความสามารถในการกระจายตัวในตัวทำละลายดีขึ้นและยังมีหมู่ฟังก์ชันบนพื้นผิวสำหรับการเกิดปฏิกิริยาอื่นๆได้

งานวิจัยนี้ได้เสนอการดัดแปรพื้นผิวอนุภาคนาโนแมกนีไทท์ 4 แนวทาง โดยในงานวิจัยเรื่องที่ 1 และ 2 เป็นการออกแบบพื้นผิวอนุภาคให้มีหมู่ฟังก์ชันกรดอะคริลิกและแอซแลคโทนตามลำดับ เพื่อสามารถใช้ในการทำปฏิกิริยาการตรึงสารชีวโมเลกุลที่สนใจบนพื้นผิวอนุภาคได้ เรื่องที่ 3 เป็นการดัดแปรพื้นผิวอนุภาคด้วยพอลิเมอร์ที่ตอบสนองต่อแสงยูวี (พอลิ(เอโซเบนซีนอะคริเลท)) และเรื่องที่ 4 เป็นการออกแบบพื้นผิวอนุภาคนาโนแมกนีไทท์แบบสองชั้นโดยการเคลือบอนุภาคด้วยพอลิเมอร์ร่วมแบบบล๊อกระหว่างพอลิเอทิลีนไกลคอลเมทิลอีเทอร์และพอลิไซลอกเซนเพื่อเกิดเป็นพอลิเมอร์เคลือบบนพื้นผิวอนุภาคแบบสองชั้น โดยจากผลการทดลองเบื้องต้นพบว่าอนุภาคที่มีการดัดแปรและเพิ่มหมู่ฟังก์ชันบนพื้นผิวเหล่านี้ น่าที่จะสามารถนำไปประยุกต์ใช้ทั้งทางด้านเทคโนชีวภาพและทางด้านการแพทย์ได้อย่างมีประสิทธิภาพ

**คำสำคัญ** : อนุภาคนาโน, แมกนีไทท์, การดัดแปรพื้นผิว, การเกิดกิ่งออกจาก, ปฏิกิริยาพอลิเมอไรเซชันแบบอนุมูลอิสระถ่ายโอนอะตอม

# LIST OF CONTENTS

**Page**

**หน้าสรุปโครงการ (Executive Summary)**

**ทุนวิจัยพื้นฐานเชิงยุทธศาสตร์ "นาโนศาสตร์และนาโนเทคโนโลยี" ประจำปี 2553-2556**

**รหัสโครงการ DBG5380001**

---

1. ชื่อโครงการ

การดัดแปรพื้นผิวอนุภาคนาโนแมกนีไทท์ด้วยปฏิกิริยาพอลิเมอไรเซชันแบบอนุมูลอิสระถ่ายโอนอะตอม และการประยุกต์ใช้

Surface Modification of Magnetite Nanoparticle *via* Atom Transfer Radical Polymerization and Its Applications

2. ชื่อหัวหน้าโครงการ หน่วยงานที่สังกัด ที่อยู่ หมายเลขโทรศัพท์ โทรสาร และ e-mail

ผู้หัวหน้าโครงการ นายเมธา รัตนากรพิทักษ์ Mr. Metha Rutnakornpituk

หน่วยงานที่สังกัด ภาควิชาเคมี คณะวิทยาศาสตร์ มหาวิทยาลัยนเรศวร อ.เมือง จ. พิษณุโลก

โทรศัพท์ 055-963464 โทรสาร 055-963401

e-mail: methar@nu.ac.th โทรศัพท์มือถือ 086-589-3736

3. สาขาวิชาที่ทำการวิจัย การสังเคราะห์และดัดแปรพื้นผิวอนุภาคนาโน การสังเคราะห์บล๊อกพอลิเมอร์

Keywords : magnetic, nanoparticle, surface modification, block copolymer

4. ระยะเวลาดำเนินงาน 3 ปี

5. ปัญหาที่ทำการวิจัย และความสำคัญของปัญหา

การออกแบบและสังเคราะห์พอลิเมอร์ให้มีโครงสร้างโมเลกุลและองค์ประกอบที่แน่นอน (well-defined structure and composition) และมีหมู่ฟังก์ชันเฉพาะ (functionality) นั้นเป็นสิ่งสำคัญ โดยเฉพาะเพื่อการประยุกต์ใช้ทางด้านเทคโนโลยีชีวภาพและในทางการแพทย์ ทั้งนี้เนื่องจากจะทำให้ได้พอลิเมอร์ที่มีสมบัติตรงตามวัตถุประสงค์การใช้งาน ในปัจจุบัน การพัฒนาความรู้ด้านปฏิกิริยาพอลิเมอไรเซชันแบบอนุมูลอิสระแบบลิฟวิ่ง/ควบคุมได้ (controlled/living radical polymerization, CRP) เช่น nitroxide mediated

radical polymerization (NMRP), reversible addition-fragmentation chain transfer (RAFT) และปฏิกิริยาพอลิเมอไรเซชันแบบอนุมูลอิสระถ่ายโอนอะตอม (atom transfer radical polymerization, ATRP) ทำให้สามารถออกแบบโครงสร้างโมเลกุลของพอลิเมอร์ได้อย่างแม่นยำ โดยเฉพาะปฏิกิริยา ATRP มีข้อเด่นกว่าปฏิกิริยา CRP อื่นหลายประการ เช่น สภาวะในการเกิดปฏิกิริยา ATRP ไม่ซับซ้อนมากเมื่อเทียบกับปฏิกิริยา CRP อื่นและสามารถใช้เตรียมพอลิเมอร์ที่มีหมู่ฟังก์ชันได้หลากหลายชนิด

การดัดแปรพื้นผิวด้วยเทคนิค ATRP ทำได้สองแนวทางได้แก่ แบบ “grafting from” ซึ่งเป็นการพอลิเมอไรเซชันของโมโนเมอร์ออกจากพื้นผิว และแบบ “grafting to” ซึ่งเป็นการตรึงพอลิเมอร์ที่มีหมู่ที่สามารถเกิดอัตรกิริยากับพื้นผิวได้ แนวทางแรกมีข้อเด่นกว่าหลายประการ เช่น หลีกเลี่ยงผลของหมู่เกะกะ (steric effect) จากการเข้าทำปฏิกิริยาของสายโซ่พอลิเมอร์บนพื้นผิว ซึ่งส่งผลให้การดัดแปรพื้นผิวแบบแนวทางที่หนึ่งสามารถควบคุมหมู่ฟังก์ชัน (functionality) ความหนา (thickness) และความหนาแน่น (density) ของพอลิเมอร์บนพื้นผิวได้ดีกว่าแนวทางที่สอง ในปัจจุบันการศึกษาการดัดแปรพื้นผิวแบบ “grafting from” ด้วยเทคนิค ATRP ของอนุภาคนาโนแมกนีไทท์ (magnetite nanoparticle) นั้นกำลังได้รับความสนใจอย่างมาก เนื่องจากอนุภาคนาโนแมกนีไทท์มีสมบัติเป็นแม่เหล็ก จึงมีการนำมาประยุกต์ใช้งานอย่างแพร่หลายทั้งทางด้านการแพทย์และเทคโนโลยีชีวภาพ เช่น การใช้เป็นวัสดุนำพาและปลดปล่อยตัวยาไปยังอวัยวะเป้าหมายเพื่อเพิ่มประสิทธิภาพในการรักษาโรคใช้ในการรักษาโรคมะเร็งด้วยความร้อน (hypothermia) การติดฉลากอนุภาคด้วยสารชีวโมเลกุล (bio-separation) หรือการประยุกต์ใช้เป็นสารขยายสัญญาณของเทคนิค magnetic resonance imaging (MRI) เพื่อใช้ตรวจดูอวัยวะต่างๆ ภายในร่างกาย อนุภาคนาโนแมกนีไทท์สามารถเกิดการรวมกลุ่มกัน (agglomeration) ทำให้เกิดการตกตะกอนเป็นอนุภาคขนาดใหญ่และสูญเสียสมบัติความเป็นอนุภาคนาโนการเสถียรอนุภาคด้วยพอลิเมอร์จะทำให้อนุภาคนาโนสามารถกระจายตัวได้ดีและมีความเสถียรในตัวทำละลายเป็นระยะเวลานานได้

ดังนั้น งานวิจัยนี้จะใช้เทคนิคการพอลิเมอไรเซชันแบบ ATRP เพื่อดัดแปรพื้นผิวของอนุภาคนาโนแมกนีไทท์แบบ “grafting from” เพื่อให้ได้พอลิเมอร์ที่เป็นสารเสถียรอนุภาค (polymeric surfactant) ที่สามารถควบคุมความหนา ความหนาแน่นและหมู่ฟังก์ชันบนพื้นผิวได้ และยังเป็นการออกแบบโครงสร้างและองค์ประกอบของพอลิเมอร์ให้มีสมบัติเฉพาะเพื่อการประยุกต์ใช้ที่แตกต่างกัน โดยออกแบบพื้นผิวอนุภาคนาโนแมกนีไทท์ให้มีหมู่ฟังก์ชันที่ต่างกัน 4 แบบได้แก่ 1) พื้นผิวอนุภาคที่มีหมู่คาร์บอกซิลิกเพื่อใช้ในการตรึงโมเลกุลกรดโฟลิกบนพื้นผิวอนุภาค 2) พื้นผิวอนุภาคที่มีหมู่อิเล็คโตรไฟล์ชนิดแอซแลคโตน ซึ่งสามารถทำปฏิกิริยากับสารชีวโมเลกุลที่มีหมู่นิวคลีโอไฟล์ได้ 3) พื้นผิวอนุภาคที่มีหมู่เอโซเบนซีนที่สามารถ

ตอบสนองต่อการกระตุ้นด้วยแสงยูวีได้ และ 4) พื้นผิวอนุภาคที่มีพอลิเมอร์แบบสองชั้นเพื่อการประยุกต์ใช้ด้านการดักเก็บและควบคุมการปลดปล่อยยา

7. วัตถุประสงค์

7.1 สามารถดัดแปรพื้นผิวของอนุภาคนาโนแมกนีไทท์ด้วยปฏิกิริยาพอลิเมอไรเซชันแบบอนุมูลอิสระถ่ายโอนอะตอม (ATRP) เพื่อให้พื้นผิวอนุภาคมีสมบัติเฉพาะ

7.2 ศึกษาจลนศาสตร์ (kinetics) ของปฏิกิริยาพอลิเมอไรเซชันและองค์ประกอบของพอลิเมอร์ร่วมบนพื้นผิวอนุภาคนาโนแมกนีไทท์

7.3 สามารถตรึงสารชีวโมเลกุล เช่น โปรตีน โมเลกุลยาหรือสารฟลูออโรฟอร์ บนพื้นผิวอนุภาคนาโนแมกนีไทท์ด้วยอัตรกิริยาแบบต่างๆ เช่น การดูดซับเชิงกายภาพ (physical adsorption) อัตรกิริยาแบบไอออนิก (ionic interaction) และการเกิดพันธะโควาเลนต์ (covalent bonding)

8. วิธีการทดลอง

งานวิจัยนี้จะใช้ปฏิกิริยาพอลิเมอไรเซชันแบบอนุมูลอิสระถ่ายโอนอะตอม (ATRP) เพื่อการดัดแปรพื้นผิวอนุภาคนาโนแมกนีไทท์เพื่อให้มีสมบัติเฉพาะในการประยุกต์ใช้งานที่แตกต่างกัน โดยออกแบบลักษณะพื้นผิวอนุภาคที่แตกต่างกัน 4 แบบดังนี้

1) พื้นผิวอนุภาคที่มีหมู่คาร์บอกซิลิกเพื่อใช้ในการตรึงโมเลกุลกรดโฟลิกบนพื้นผิวอนุภาค

2) พื้นผิวอนุภาคที่มีหมู่อิเล็คโตรไฟล์ชนิดแอซแลคโตน ซึ่งสามารถทำปฏิกิริยากับสารชีวโมเลกุลที่มีหมู่นิวคลีโอไฟล์ได้

3) พื้นผิวอนุภาคที่มีหมู่เอโซเบนซีนที่สามารถตอบสนองต่อการกระตุ้นด้วยแสงยูวีได้ และ

4) พื้นผิวอนุภาคที่มีพอลิเมอร์แบบสองชั้นเพื่อการประยุกต์ใช้ด้านการดักเก็บและควบคุมการปลดปล่อยยา

โดยแบ่งการทดลองออกเป็นขั้นตอนต่างๆ ดังนี้

*ขั้นตอนที่ 1 การสังเคราะห์อนุภาคนาโนแมกนีไทท์ (Synthesis of magnetite nanoparticle)*

สังเคราะห์อนุภาคนาโนแมกนีไทท์ด้วยปฏิกิริยาการแตกสลายสารตั้งต้นเหล็ก (Iron precursor) ชนิด Iron acetylacetonate ($Fe(acac)_3$) โดยใช้อุณหภูมิสูง (Thermal decomposition) อนุภาคนาโนที่เตรียมโดยวิธีนี้มีขนาดประมาณ 10 นาโนเมตรและมีการกระจายของขนาดที่แคบหรือมีขนาดที่ใกล้เคียงกัน ศึกษาขนาดและการกระจายของขนาดด้วยเทคนิค Transmission Electron Microscopy (TEM) และเทคนิค Photocorrelation Spectrophotometry (PCS) เพื่อหาขนาดไฮโดรไดนามิกและประจุบนพื้นผิว

*ขั้นตอนที่ 2 การสังเคราะห์สารเริ่มต้นสำหรับปฏิกิริยา ATRP บนพื้นผิวอนุภาค (Synthesis of ATRP initiator on the particle surface)*

สังเคราะห์สารเริ่มต้นสำหรับปฏิกิริยา ATRP บนพื้นผิวอนุภาค โดยการทำปฏิกิริยาระหว่างหมู่ Fe-OH บนพื้นผิวอนุภาคกับ 3-aminopropyl triethoxysilane (APS) ตามด้วยปฏิกิริยากับ 2-bromoisobutyryl bromide (BIBB) เกิดเป็นหมู่ฟังก์ชันที่สามารถเริ่มต้นปฏิกิริยา ATRP ได้บนพื้นผิวอนุภาค ศึกษาหมู่ฟังก์ชันบนพื้นผิวด้วยเทคนิค FTIR หาสัดส่วนระหว่างอนุภาคแมกนีไทท์และสารอินทรีย์ที่เคลือบบนพื้นผิวด้วยเทคนิค Thermogravimetric analysis (TGA)

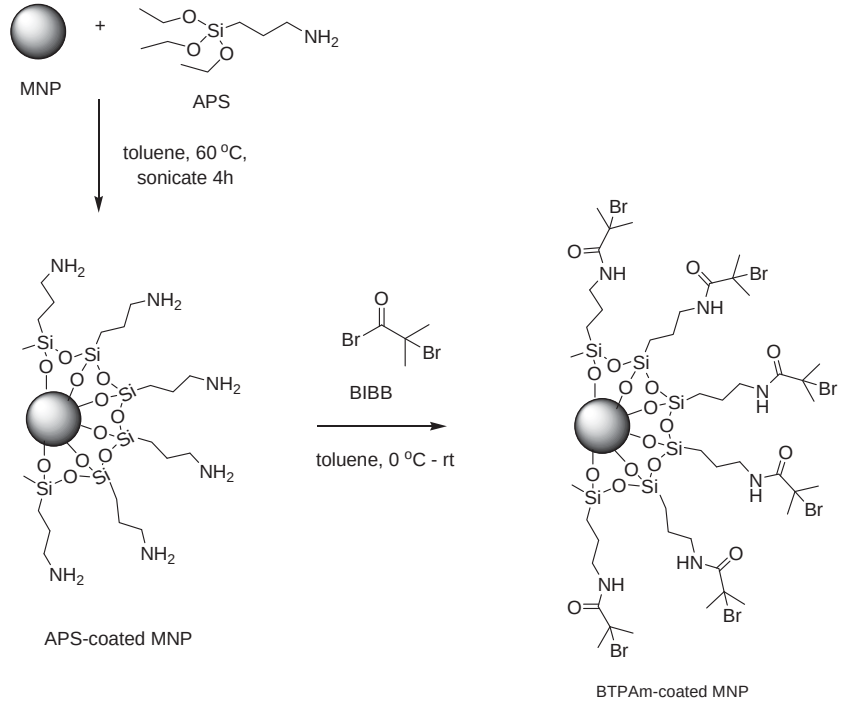


**รูปที่ 1** ปฏิกิริยาการสังเคราะห์สารเริ่มต้นปฏิกิริยา ATRP บนพื้นผิวอนุภาคนาโนแมกนีไทท์

*ขั้นตอนที่ 3 การดัดแปรพื้นผิวอนุภาคด้วยปฏิกิริยา ATRP (Surface modification via ATRP) และการประยุกต์ใช้*

*แนวทางที่ 1 การดัดแปรพื้นผิวอนุภาคนาโนแมกนีไทท์ด้วยหมู่คาร์บอกซิลิกเพื่อใช้ในการตรึงโมเลกุลกรดโฟลิกบนพื้นผิวอนุภาค* ดัดแปรพื้นผิวอนุภาคด้วย poly(acrylic acid)(PAA) เทคนิค ATRP เพื่อให้เกิดพอลิเมอร์ที่มีหมู่คาร์บอกซิลิกเคลือบบนพื้นผิวอนุภาคซึ่งสามารถเกิดปฏิกิริยาต่อกับโมเลกุลกรดโฟลิกได้แนวทางนี้จะได้อนุภาคนาโนแมกนีไทท์ที่มีกรดโฟลิกบนพื้นผิวและมีความเสถียรในสารละลายน้ำได้

*แนวทางที่ 2 การดัดแปรพื้นผิวอนุภาคนาโนแมกนีไทท์ให้มีหมู่อิเล็คโตรไฟล์ชนิดแอซแลคโตน ซึ่งสามารถทำปฏิกิริยากับสารชีวโมเลกุลที่มีหมู่นิวคลีโอไฟล์ได้* ดัดแปรพื้นผิวอนุภาคด้วยเทคนิค ATRP เพื่อให้เกิดพอลิเมอร์เคลือบบนพื้นผิวอนุภาคมีสารอิเล็คโทรไฟล์ชนิดแอซแลคโตน ซึ่งเป็นสารที่มีความว่องไวต่อการเกิดปฏิกิริยากับสารนิวคลีโอไฟล์ใดๆ เช่น โปรตีน โมเลกุลยาหรือสารฟลูออโรฟอร์ ซึ่งทำให้สามารถตรึงสารชีวโมเลกุลบนพื้นผิวด้วยพันธะโควาเลนต์ แนวทางนี้จะได้โมเลกุลสารชีวโมเลกุลบนพื้นผิวที่มีความเสถียรในสารละลาย

*แนวทางที่ 3 การดัดแปรพื้นผิวอนุภาคนาโนแมกนีไทท์ให้มีหมู่เอโซเบนซีนที่สามารถตอบสนองต่อการกระตุ้นด้วยแสงยูวีได้เพื่อการประยุกต์ใช้เป็นกลไกในการกระตุ้นการปลดปล่อยยา* ดัดแปรพื้นผิวอนุภาคด้วย poly(azobenzene) ด้วยเทคนิค ATRP เพื่อให้เกิดพอลิเมอร์ที่มีหมู่ azobenzene ที่ตอบสนองต่อการกระตุ้นด้วยแสงยูวีเคลือบบนพื้นผิวอนุภาค โดยหมู่ azobenzene จะมีความเป็นขั้วต่ำที่สภาวะปกติเนื่องจากมีโครงสร้างแบบ trans และเมื่อกระตุ้นด้วยแสงยูวีจะเปลี่ยนโครงสร้างเป็น cis ในสภาวะกระตุ้นซึ่งจะมีความเป็นขั้วสูงขึ้นซึ่งการเปลี่ยนโครงสร้างเมื่อกระตุ้นด้วยแสงยูวีนี้จะใช้เป็นกลไกในการปลดปล่อยยาได้

*แนวทางที่ 4 การดัดแปรพื้นผิวอนุภาคนาโนแมกนีไทท์ให้มีพอลิเมอร์แบบสองชั้นเพื่อการประยุกต์ใช้ด้านการดักเก็บและปลดปล่อยยา* ทำการดัดแปรพื้นผิวอนุภาคให้เกิดเป็นสารเสถียรพอลิเมอร์แบบชั้นในและนอก โดยการเกิดปฏิกิริยา ATRP ของพอลิเมอร์บล็อกแรกที่มีสมบัติเป็นไฮโดรโฟบิก เช่น พอลิไซลอกเซน (PDMS) เพื่อเกิดเป็นสารเสถียรอนุภาคชั้นใน จากนั้นทำปฏิกิริยา ATRP ต่อจากชั้นแรกด้วยพอลิเมอร์ที่มีสมบัติไฮโดรฟิลิก เช่น พอลิเอทิลีนไกลคอล (PEG) เพื่อเกิดเป็นสารเสถียรชั้นนอก สารเสถียรชั้นในที่มีสมบัติเป็นสารไฮโดรโฟบิกทำหน้าที่ในการดูดซับยาที่มีสมบัติไฮโดรโฟบิกไว้บนพื้นผิว

ชั้นใน ขณะที่ชั้นนอกที่มีสมบัติเป็นสารไฮโดรฟิลิกทำหน้าที่ในการเสถียรอนุภาคและการกระจายอนุภาคในชั้นน้ำ (Stability and dispersibility) ทั้งนี้เพื่อให้อนุภาคสามารถกระจายในน้ำได้ดีและมีความเสถียรเป็นระยะเวลานาน

9. ผลการทดลอง

จากผลงานงานวิจัยนี้เราสามารถใช้เทคนิคการพอลิเมอไรเซชันแบบ ATRP เพื่อดัดแปรพื้นผิวของอนุภาคนาโนแมกนีไทท์แบบ “grafting from” เพื่อให้ได้พอลิเมอร์ที่เป็นสารเสถียรอนุภาค (polymeric surfactant) ที่สามารถควบคุมความหนา ความหนาแน่นและหมู่ฟังก์ชันบนพื้นผิวได้ และเป็นการออกแบบโครงสร้างและองค์ประกอบของพอลิเมอร์ให้มีสมบัติเฉพาะเพื่อการประยุกต์ใช้ที่แตกต่างกัน โดยในรายงานการวิจัยนี้ได้เสนอการออกแบบพื้นผิวอนุภาคนาโนแมกนีไทท์ที่ต่างกัน 4 แบบได้แก่ 1) พื้นผิวอนุภาคที่มีหมู่คาร์บอกซิลิกเพื่อใช้ในการตรึงโมเลกุลกรดโฟลิกบนพื้นผิวอนุภาค 2) พื้นผิวอนุภาคที่มีหมู่อิเล็คโตรไฟล์ชนิดแอซแลคโตน ซึ่งสามารถทำปฏิกิริยากับสารชีวโมเลกุลที่มีหมู่นิวคลีโอไฟล์ได้ 3) พื้นผิวอนุภาคที่มีหมู่เอโซเบนซีนที่สามารถตอบสนองต่อการกระตุ้นด้วยแสงยูวีได้ และ 4) พื้นผิวอนุภาคที่มีพอลิเมอร์แบบสองชั้นเพื่อการประยุกต์ใช้ด้านการดักเก็บและควบคุมการปลดปล่อยยา โดยองค์ความรู้ใหม่ที่ได้จากงานวิจัยนี้ ได้แก่

1) การออกแบบ การสังเคราะห์และการติดตามการเกิดปฏิกิริยา ATRP บนพื้นผิวอนุภาคนาโนแมกนีไทท์ ของพอลิเมอร์ร่วม (copolymer) ชนิดใหม่ 4 แบบ ซึ่งมีชื่อแต่ละหัวข้องานวิจัย ดังนี้
   - Poly(acrylic acid)-grafted magnetic nanoparticle for conjugation with folic acid
   - Azlactone functionalization of magnetic nanoparticles using ATRP and their bioconjugation
   - Surface modification of magnetite nanoparticle with azobenzene-containing water dispersible polymer
   - Magnetite nanoparticle coated with amphiphilic bilayer surfactant of polysiloxane and poly(poly(ethylene glycol) methacrylate)
2) การศึกษาจลนศาสตร์ของปฏิกิริยา ATRP ของพอลิเมอร์ร่วมชนิดใหม่บนพื้นผิว
3) การประยุกต์ใช้งานอนุภาคนาโนที่มีการออกแบบพื้นผิวเฉพาะเพื่อการประยุกต์ใช้งานเฉพาะด้าน

และผลกระทบขององค์ความรู้นี้ต่อความก้าวหน้าในเชิงวิชาการของสาขาที่ทำการวิจัย ได้แก่ เป็นการใช้เทคนิค ATRP เพื่อการออกแบบโครงสร้างพอลิเมอร์เพื่อให้ได้สมบัติเฉพาะที่ต้องการ เพื่อการประยุกต์ใช้งานเฉพาะด้าน ซึ่งจากความรู้และความเข้าใจพื้นฐานที่ได้รับจากงานวิจัยนี้ จะนำไปสู่การ

พัฒนาการออกแบบโมเลกุลพอลิเมอร์บนพื้นผิวอนุภาคนาโนชนิดอื่นหรือโครงสร้างแบบอื่นๆที่ซับซ้อน และมีประโยชน์มากยิ่งขึ้น

# เนื้อหางานวิจัย

ประกอบด้วย 4 เรื่อง ดังนี้

1) Poly(acrylic acid)-grafted magnetic nanoparticle for conjugation with folic acid

2) Azlactone functionalization of magnetic nanoparticles using ATRP and their bioconjugation

3) Surface modification of magnetite nanoparticle with azobenzene-containing water dispersible polymer

4) Magnetite nanoparticle coated with amphiphilic bilayer surfactant of polysiloxane and poly(poly(ethylene glycol) methacrylate)

# Poly(acrylic acid)-grafted magnetic nanoparticle for conjugation with folic acid

*Metha Rutnakornpituk*[*], *Nipaporn Puangsin, Pawinee Theamdee, Boonjira Rutnakornpituk and Uthai Wichai*

**Abstract**: Poly(acrylic acid) (poly(AA))-grafted magnetic nanoparticles (MNPs) prepared *via* surface-initiated atom transfer radical polymerization (ATRP) of *t*-butyl acrylate, followed by acid-catalyzed deprotection of *t*–butyl groups, is herein presented. In addition to serve as both steric and electrostatic stabilizers, poly(AA) grafted on MNP surface also served as a platform for conjugating folic acid, a cancer cell targeting agent. Fourier transform infrared spectroscopy (FTIR) was used to monitor the reaction progress in each step of the syntheses. The particle size was 8 nm in diameter without significant aggregation during the preparation process. Photocorrelation spectroscopy (PCS) indicated that, as increasing pH of the dispersions, their hydrodynamic diameter was decreased and negatively charge surface was obtained. According to thermogravimetric analysis (TGA), up to 14 wt% of folic acid (about 400 molecules of folic acid per particle) was bound to the surface-modified MNPs. This novel nanocomplex is hypothetically viable to efficiently graft other affinity molecules on their surfaces and thus might be suitable for use as an efficient drug delivery vehicle particularly for cancer treatment.

## 1. Introduction

Synthesis of magnetite nanoparticles (MNPs) coated with a thin film of organic polymer has recently attracted much attention due to their potential biomedical applications such as magnetic resonance imaging [1-6], magnetic separation, controlled drug release [7] and hyperthermia treatment of tumor cells [8]. A thin shell of polymeric coating on the particle surface is necessary to prevent nanometer-sized particle aggregation due to their inherent anisotropic dipolar interaction, resulting in losing the specific properties associated with their nanometer dimensions [9-10]. In addition, the polymers on their surface can provide a platform for incorporating biological functional molecules, such as amino acid [11], protein [12-13] and DNA [14-16], for particle labeling with fluorescent molecules [17-18] and for attaching folic acid [19-20], a receptor for tumor cells.

Recently, atom transfer radical polymerization (ATRP) has been reported as a potential “grafting-from” method for surface modification [21-23]. ATRP is a living/controlled radical polymerization method, which does not require stringent

experimental conditions [24-25]. ATRP enables for the polymerization and block copolymerization of a wide range of functional monomers such as styrene [26-28], methacrylate [29], acrylate [30-31] and methacrylamide [32], yielding polymers with narrowly dispersed molecular weights. Surface modification of nanoparticles *via* ATRP has attracted a great attention in recent years. As compared to a conventional radical polymerization, surface-initiated ATRP from nanoparticles produced polymers with narrow polydispersity index (PDI) and proceeded in a controlled fashion [33]. In addition, the advantage of ATRP technique as compared to other controlled radical polymerization (CRP) techniques is that the polymerization can be initiated at low reaction temperature, while other CRP techniques such as reversible addition-fragmentation chain transfer (RAFT) and nitroxide-mediated polymerizations require relatively high reaction temperature to generate radicals from azo or peroxide initiators. Moreover, functionalization of the particle surface with alkyl halide, the ATRP initiating species, can be easily carried out either by physical absorption of acid-containing halides [34] or covalent bonding of ATRP initiating halides *via* silanization [35]. The “grafting from” strategy *via* ATRP has thus been mostly adopted for MNP surface modification with a variety of polymeric surfactants such as polystyrene [23], poly(methyl methacrylate) [36], poly(ethylene glycol) methacylate [37-38] and poly(acrylamide) [39].

The aim of the current work is to adopt a “grafting from” method to modify MNP surfaces with poly(*t*-butyl acrylate) (poly(*t*-BA)) *via* ATRP, followed by acid-catalyzed deprotection of *t*-butyl groups to obtain poly(AA)-grafted MNP. It is thought that ATRP can offer well-defined water dispersible poly(AA) stabilizers with low molecular weight distribution on the particle surface. The carboxylic acid groups over expressed on its surface are readily reactive toward molecules containing functional groups such as amine and alcohol. It has thus gained our attention because, not only serving as steric and electrostatic surfactants [40], poly(AA) can also be used as a key intermediate for grafting a large range of functional molecules [41-42]. Folic acid (FA) is of particular interest in this work because it can specifically conjugate with folate receptors overexpressed on cancer cell membranes [43]. Precedents have reported the immobilization of FA on the outermost surface of MNPs coated with other polymeric surfactants [44-47]. Therefore, it is expected that the multifunctional FA-grafted MNPs prepared in this work should bind to cancer cell membranes specifically and consequently improve uptake efficiency of the MNP to the cells.

The detail studies on the efficiency on treating cancer cells of this complex are warranted for a future investigation.

In the present work, poly(AA)-coated MNPs were thus prepared *via* surface-initiated ATRP of *t*-BA, followed by acid-catalyzed hydrolysis of *t*-butyl groups. FTIR was used to monitor the reaction progress in each step. Thermogravimetric analysis (TGA) was used to investigate percent of each composition in the polymer-MNP complex. Transmission electron microscopy (TEM) technique was also used to monitor the particle size and the presence of the polymer in the complex. Vibrating sample magnetometry (VSM) was performed to reveal their magnetic properties. In combination with UV-visible spectrophotometry and FTIR, TGA technique was conducted to evidence the existence of FA in the complexes.

## 2. Experimental Section

### *2.1 Materials*

Unless otherwise stated, all reagents were used without further purification: iron (III) acetylacetonate ($Fe(acac)_3$), 99% (Acros), benzyl alcohol (Unilab), 3-aminopropyl triethoxysilane (APS), 99% (Acros), triethylamine (TEA) (Carto Erba), 2-bromoisobutyryl bromide (BIBB), 98% (Acros), copper (I) bromide (CuBr), 98% (Acros), *N,N,N´,N´´,N´´*-pentamethyldiethylenetriamine (PMDETA), ethyl-α-bromoisobutyrate (Aldrich), 99% (Acros), folic acid, 97% (Fluka), N-hydroxyl succinamide (NHS), 98% (Acros), dicyclohexyl carbodiimide (DCC), 99% (Acros), di-*t*-butyl dicarbonate ($Boc_2O$), 99% (Aldrich), ethylene diamine (EDA), 99.5% (Fluka), trifluoroacetic acid (TFA), 99.5% (Fluka). *t*-Butyl acrylate (*t*-BA), 99% (Fluka), was distilled under vacuum prior to use.

### *2.2 Synthesis*

#### *2.2.1 Synthesis of oleic acid-coated magnetite nanoparticles (MNPs)*

MNPs were prepared *via* thermal decomposition following the method previously described [48]. In a typical procedure, $Fe(acac)_3$ (1.0 g, 2.81 mmol) and benzyl alcohol (20 ml) were mixed by magnetic stirring in a three-neck flask with nitrogen flow. The mixture was heated to 200 °C for 48 h. The precipitant was then removed from the dispersion using an external magnet and washed with ethanol and $CH_2Cl_2$ repeatedly to remove benzyl alcohol. The particles were then dried at room temperature under reduced pressure. To prepare oleic acid-coated MNPs, the dried MNPs (0.6 g) were introduced into an oleic acid solution in dried toluene (4 ml oleic acid in 30 ml THF) and ultrasonicated for 3 h.

#### *2.2.2 Synthesis of 2-bromo-2-methyl-N-(3-(triethoxysilyl) propanamide (BTPAm)*

To a stirred solution of 3-aminopropyl triethoxysilane (APS) (0.18 ml, 0.8 mmol) and triethylamine (TEA) (0.12 ml, 0.8 mmol) in dried toluene (10 ml), 2-bromoisobutyryl bromide (BIBB) (0.1 ml, 0.8 mmol) in dried toluene (10 ml) was added dropwise at 0 °C for 2 h under nitrogen. The reaction mixture was warmed to room temperature and stirred for 24 h. The mixture was passed through a filter paper to remove salts and the filtrate was evaporated to remove the unreacted TEA under reduced pressure. The resulting product, BTPAm, was yellowish thick liquid (78% yield). $^{1}$H NMR (400 MHz, $CDCl_3$) $\delta_H$ : 0.60 [m, 2H, Si-C$\underline{H}_2$, 1.20 [t, 9H, O-$CH_2$-C$\underline{H}_3$], 1.65 [m, 2H, Si-$CH_2$-C$\underline{H}_2$], 1.95, [s, 6H, C$\underline{H}_3$-C-Br], 3.25 [m, 2H, C$\underline{H}_2$-NH], 3.80 [m, 6H, $CH_3$-C$\underline{H}_2$-O]. FT-IR (KBr disc) $\lambda_{max}$ : 3345 $cm^{-1}$ (NH stretching), 2975 - 2889 $cm^{-1}$ (C-H stretching), 1738 $cm^{-1}$ (C=O of acid bromide stretching), 1658 $cm^{-1}$ (C=O of amide stretching), 1532 $cm^{-1}$ (NH bending), 1442 $cm^{-1}$ (C-N stretching), 1286 $cm^{-1}$ (C-Br stretching), 1112-1026 (Si-O stretching).

*2.2.3 Immobilization of 2-bromo-2-methyl-N-(3-(triethoxysilyl) propanamide (BTPAm) onto MNP surface (BTPAm-coated MNPs) (Figure 1)*

To immobilize BTPAm on the oleic acid-coated MNP surface, the MNP-toluene dispersion (0.1 g of oleic acid-coated MNPs in 5 ml toluene) (30 ml), BTPAm (0.90 ml) and 2 M TEA in toluene (6 ml) were added into a round bottom flask. The mixture was stirred for 24 h at room temperature under nitrogen. The particles were subsequently precipitated in methanol, following by magnet separation to obtain the BTPAm-modified MNPs. Then, the MNPs were re-dispersed in toluene and re-precipitated in methanol. This procedure was repeated several times to completely remove unreacted BTPAm. The particles were finally dried *in vacuo.*

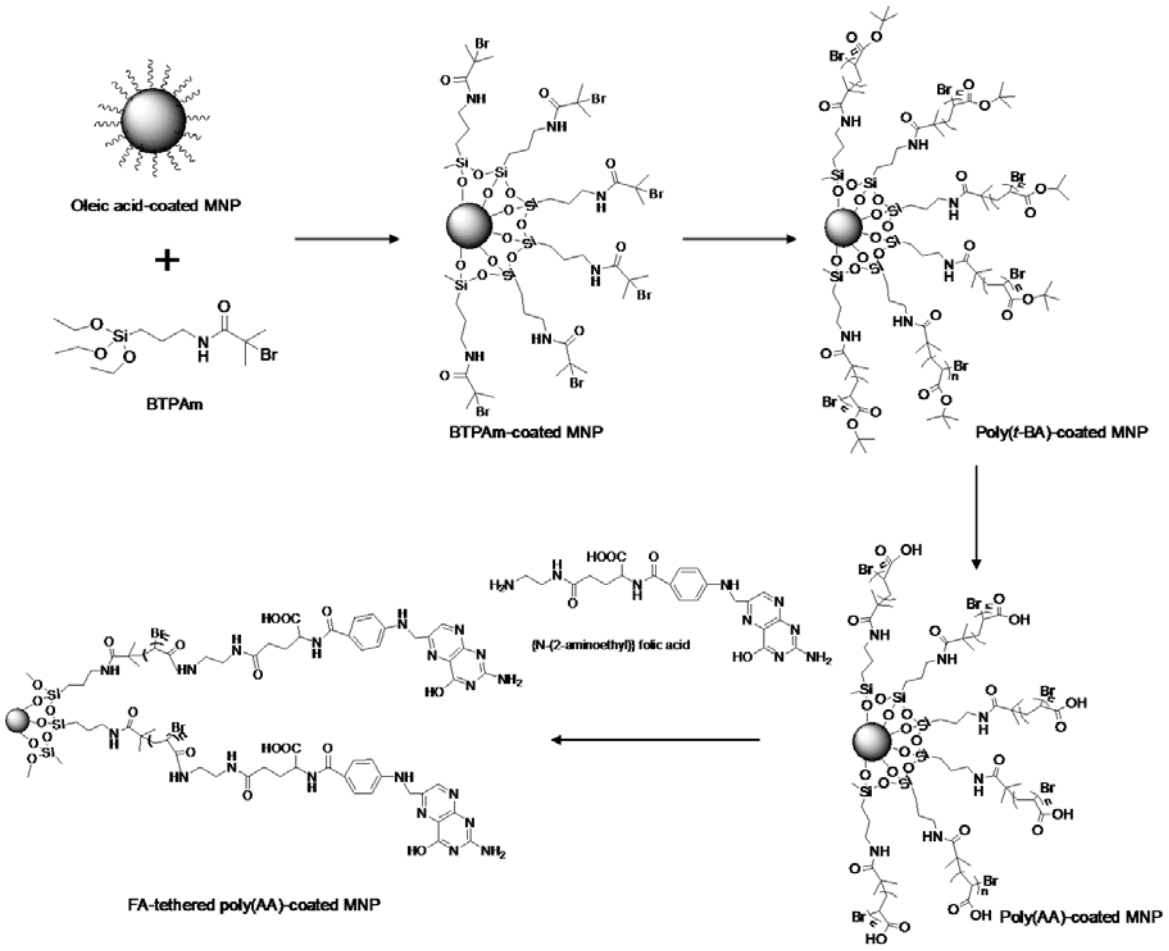


**Figure 1** Synthesis of poly(AA)-coated MNPs *via* ATRP reaction and immobilization of folic acid (FA)

*2.2.4 Synthesis of poly(t-butyl acrylate)-coated MNPs (poly(t-BA)-coated MNPs) via ATRP reaction*

To a schlenk tube containing dioxane (1 ml), CuBr (0.3 g, 0.0021 mol), and PMDETA (0.42 ml, 0.0021 mol) were added under nitrogen blanket. The mixture was stirred until homogenous blue color was observed. Then, *t*-butyl acrylate (*t*-BA) (3 ml, 0.021 mol) monomer and BTPAm-immobilized MNPs (0.3 g) were added *via* a syringe. The mixture was degassed and nitrogen-purged by three freeze-thaw cycles. The solution was then heated to 90 °C for 24 h to commence ATRP reaction. At a given time, the reactions were ceased and poly(*t*-BA)-grafted MNPs were magnetically separated and washed thoroughly with methanol and dried *in vacuo*.

*2.2.5 Synthesis of poly(acrylic acid)-coated MNPs (poly(AA)-coated MNPs) via hydrolysis of poly(t-butyl acrylate)-coated MNPs )*

Poly(*t*-BA)-coated MNPs were hydrolyzed to obtain acrylic acid functional groups on MNP surfaces. Briefly, poly(*t*-BA)-coated MNPs (0.05 g) were hydrolyzed in a 20-ml TFA solution (0.1 M of TFA in THF) at room temperature for 24 h. The solution was concentrated under reduced pressure, diluted with $CH_2Cl_2$, and repeatedly precipitated in cold hexane. The precipitate was separated by a permanent magnet and dried *in vacuo*. The possible reactions between TFA and polymers coated on MNP surface are illustrated in supplementary data.

*2.2.6 Synthesis of N-(2-aminoethyl) folic acid (EDA-FA) (Figure 2)*

*2.2.6.1 Protection of an amino group of ethylene diamine (EDA) with t-butyl carbamate (Boc)*

A solution of di-*t*-butyl dicarbonate ($Boc_2O$) (0.23 ml, 1 mmol) in anhydrous $CH_2Cl_2$ (10 ml) was added dropwise to a cold solution of ethylene diamine (EDA) (0.67 ml, 10 mmol) in anhydrous $CH_2Cl_2$ (10 ml) at 0 °C under nitrogen atmosphere. The mixture was magnetically stirred at 0 °C for 2 h and at room temperature for 24 h. Then, distilled water (5 ml) was added into the mixture to dissolve the precipitate. The organic layer was washed with brine (15 ml) 5 times, dried over anhydrous $Na_2SO_4$, and then concentrated under reduced pressure to give *t*-butyl *N*-(2-aminoethyl) carbamate (EDA-Boc), appearing as thick oil (82% yield). $^1$H NMR (400 MHz, $CDCl_3$) $\delta_H$ : 1.40 [s, 9H, C<u>H</u>$_3$ Boc], 2.80 [m, 2H, C<u>H</u>$_2$-$NH_2$], 3.20[m, 2H, $CH_2$-C<u>H</u>$_2$-NH-Boc]. FT-IR (KBr disc) $\lambda_{max}$ : 3360 cm$^{-1}$ (NH stretching), 2955 - 2923 cm$^{-1}$ (C-H stretching), 1693 cm$^{-1}$ (C=O of amide stretching), 1525 cm$^{-1}$ (NH bending), 1366-1277 cm$^{-1}$ (C-N bending), 1172 cm$^{-1}$ (C-O stretching).

*2.2.6.2 Coupling folic acid with the amino-protected EDA*

To a stirred solution of FA (0.275 g, 6.25x10$^{-4}$ mol) in anhydrous DMSO (5 ml) and pyridine (4 ml), the solution of EDA-Boc (0.10 g, 6.25x10$^{-4}$ mol) and DCC (0.21 g, 7.5x10$^{-4}$ mol) in anhydrous DMSO (5 ml) were added. The mixture was stirred at room temperature for 18 h under nitrogen blanket. After the reaction completed, the mixture was gradually poured into a vigorously stirred diethyl ether (20 ml) at 0 °C. The yellow precipitate was collected and washed with cold diethyl ether several times and dried under high vacuum to obtain {*t*-butyl N-(2-aminoethyl) carbamate} folic acid (Boc-EDA-FA), appearing as a yellow solid (85% yield). $^1$H NMR (400 MHz, DMSO-$d_6$) $\delta_H$ : 1.40 [s, 9H, C<u>H</u>$_3$ Boc], 2.0 [m, 2H, C<u>H</u>$_2$-$CH_2$-CO-NH], 2.40 [m, 2H, C<u>H</u>$_2$-CO-NH], 2.90 [m, 2H, C<u>H</u>$_2$-NH-CO], 3.10 [m, 2H, C<u>H</u>$_2$-NH-Boc], 4.30 [m, 1H, HOOC-C<u>H</u>-NH], 4.50 [d, 2H, phenyl-NH-C<u>H</u>$_2$ folic acid],

6.60 [d, *J= 8Hz*, 2H, 2CH=CH phenyl folic acid ], 6.90 [t, 1H, phenyl-NH-$CH_2$], 7.60 [d, *J= 8Hz*, 2H, 2CH=CH phenyl folic acid], 8.60 [s, 1H, N=CH Ar folic acid]. FT-IR (KBr disc) $\lambda_{max}$ : 3360-2600 $cm^{-1}$ (OH and NH stretching), 1700 $cm^{-1}$ (C=O of amide stretching), 1605 $cm^{-1}$ (C-O of acid stretching), 1168 $cm^{-1}$ (C-O stretching).

TFA (2 ml) was then added to Boc-EDA-FA and stirred at room temperature. After 2 h stirring, TFA was removed under reduced pressure and the resulting residue was dissolved in anhydrous DMF. Pyridine was added until a formation of yellow precipitate and it was subsequently washed with diethyl ether and dried to give *N*-(2-aminoethyl) folic acid (EDA-FA) (80% yield, $T_m$ 290°C). $^1$H NMR (400 MHz, DMSO-$d_6$) $\delta_H$ : 2.0 [m, 2H, $CH_2$-$CH_2$-CO-NH], 2.40 [m, 2H, $CH_2$-CO-NH], 2.60 [m, 2H, $CH_2$-NH-CO], 3.30 [m, 2H, $CH_2$-$NH_2$], 4.20 [m, 1H, HOOC-CH-NH], 4.40 [d, 2H, phenyl-NH-$CH_2$ folic acid], 6.60 [d, *J= 8Hz*, 2H, 2CH=CH phenyl folic acid], 6.90 [t, 1H, Phenyl-NH-$CH_2$], 7.70 [d, *J= 8Hz*, 2H, 2CH=CH phenyl folic acid] , 8.60 [s, 1H, N=CH Ar folic acid]. FT-IR (KBr disc) $\lambda_{max}$ : 3600-2800 $cm^{-1}$ (OH and NH stretching), 1684 $cm^{-1}$ (C=O of amide stretching), 1605 $cm^{-1}$ (C-O of acid stretching), 1532-1335 $cm^{-1}$ (C-N bending), 1202-1132 $cm^{-1}$ (C-O stretching).

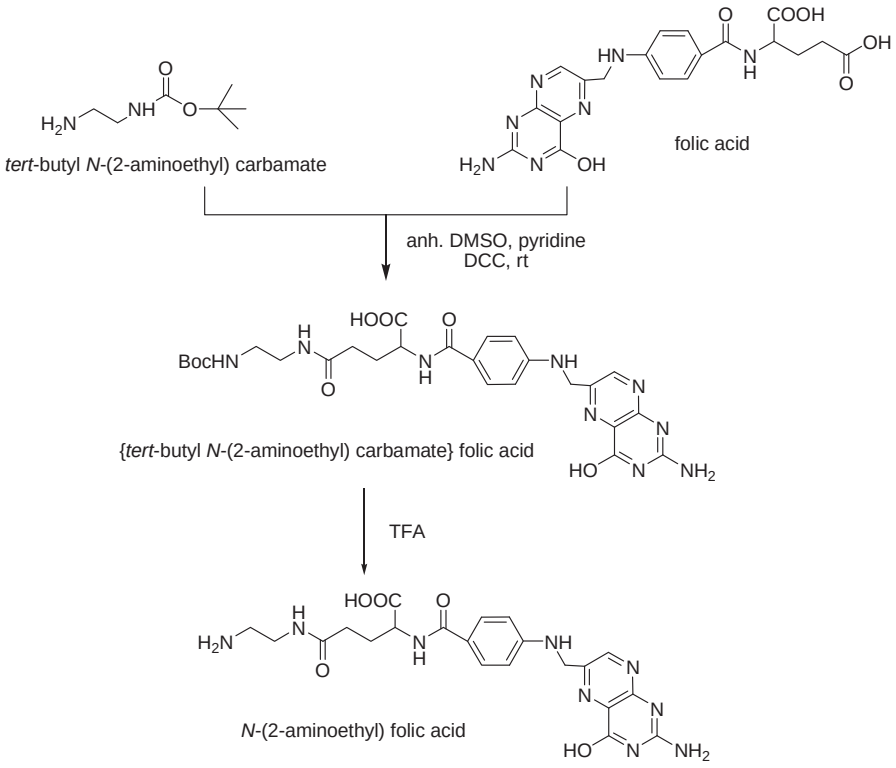


**Figure 2** Synthesis of *N*-(2-aminoethyl) folic acid (EDA-FA)

*2.2.7 Immobilization of folic acid on the surfaces of poly(AA)-coated MNPs*

Poly(AA)-coated MNPs were dispersed in a 10 ml aqueous solution containing NHS (40 mg) and EDC·HCl (20 mg) and the mixture was kept in a dark place for 2 h. The particles were recovered, washed with water and dried *in vacuo*. Then, the particles were added in a solution of 200 mg of EDA-FA and 50 mg of EDC in 10 ml anhydrous DMSO. The suspension was agitated overnight at 37 °C in dark. The particles were then recovered, washed with DMSO and methanol several times and dried *in vacuo*.

*2.3 Characterization*

FTIR was performed on a Perkin-Elmer Model 1600 Series FTIR Spectrophotometer. The solid samples were mixed with KBr to form pellets. Nuclear magnetic resonance spectroscopy (NMR) was performed on a 400 MHz Bruker NMR spectrometer using $CDCl_3$ as a solvent. Gel permeation chromatography (GPC) data was conducted on PLgel 10 μm mixed B2 columns and a refractive index detector. Tetrahydrofuran (THF) was used as a solvent with a flow rate of 1 ml/min at 30$^{o}$C. TEM were performed using a Philips Tecnai 12 operated at 120 kV equipped with Gatan model 782 CCD camera. TGA was performed on SDTA 851 Mettler-Toledo at the temperature ranging between 25-600 $^{o}$C at a heating rate of 20$^{o}$C/min under oxygen atmosphere. VSM was performed at room temperature using a Standard 7403 Series, Lakeshore vibrating sample magnetometer. The magnetic moment was investigated over a range of applied magnetic fields from -10,000 to +10,000 G using 30 min sweep time. Hydrodynamic diameter of the particles was measured *via* PCS using NanoZS4700 nanoseries Malvern instrument. The sample dispersions were sonicated for 10 min before the measurement at 25$^{o}$C. The presence of FA was investigated using SPECORD S100 UV-Visible spectrophotometer (Analytikjena AG) coupled with a photo diode array detector at $\lambda_{max}$ = 371 nm.

**3. Results and discussion**

The aim of this work is to modify MNP surfaces with poly(AA) and immobilize folic acid on their surfaces. Poly(AA) grafted on the particle surfaces is thought to provide steric and electrostatic stabilizations and dispersibility of the particles in aqueous media. Another major advantage of this system was that the carboxylic acid-enriched surfaces of poly(AA)-grafted MNPs provided a platform for efficient surface immobilization of any functional molecules such as DNA, drugs, protein and fluorescent molecules. Hence, the novelty of this current work is that this is the first report on synthesizing multifunctional poly(AA)-coated MNPs for attaching folic acid (FA), a model molecule in this work. Precedents have reported

the immobilization of biomolecules on the distal ends of MNPs coated with other polymeric surfactant [44-47]. This novel system is hypothesized to increase the loading efficiency of FA on the MNP surfaces.

To perform surface-initiated ATRP from MNPs, BTPAm, a molecule containing an ATRP initiating site was first synthesized through amidization between APS and BIBB, followed by silanization of triethoxy silane of BTPAm on MNP surface. The results of the synthesis of BTPAm including FTIR and $^{1}$H NMR are illustrated in supplementary data. To immobilize BTPAm on MNP surfaces, bare MNPs were first coated with oleic acid to form well dispersed MNPs in toluene. The advantage of this procedure was that the MNPs were well dispersible in the media before reacting with BTPAm, allowing BTPAm to effectively silanize to their surfaces due to its greater surface approaching ability in the dispersed MNPs.

Figure 3 displays FTIR spectra of poly(*t*-BA)-coated MNPs withdrawn from the dispersions at 1, 6, 12 and 24 h of ATRP reaction. Because ATRP is known as a controlled radical polymerization, the time period for the ATRP reaction is thus crucial for tuning the molecular weight of the polymers. A progressive growth of ester linkage signals (-O(C=O)- stretching, ~ 1724 $cm^{-1}$ and C-O stretching, ~ 1147 $cm^{-1}$) of *t*-BA repeating units in relative to those of a Si-O signal of the linker (~ 1100-1020 $cm^{-1}$ and ~ 800 $cm^{-1}$) indicated that the molecular weights of poly(*t*-BA) on MNP surfaces increased as increasing ATRP reaction time. It should be noted that the signal corresponding to Fe-O bonds from MNP core (~589 $cm^{-1}$) were observed throughout the reactions without significant change in its intensity.

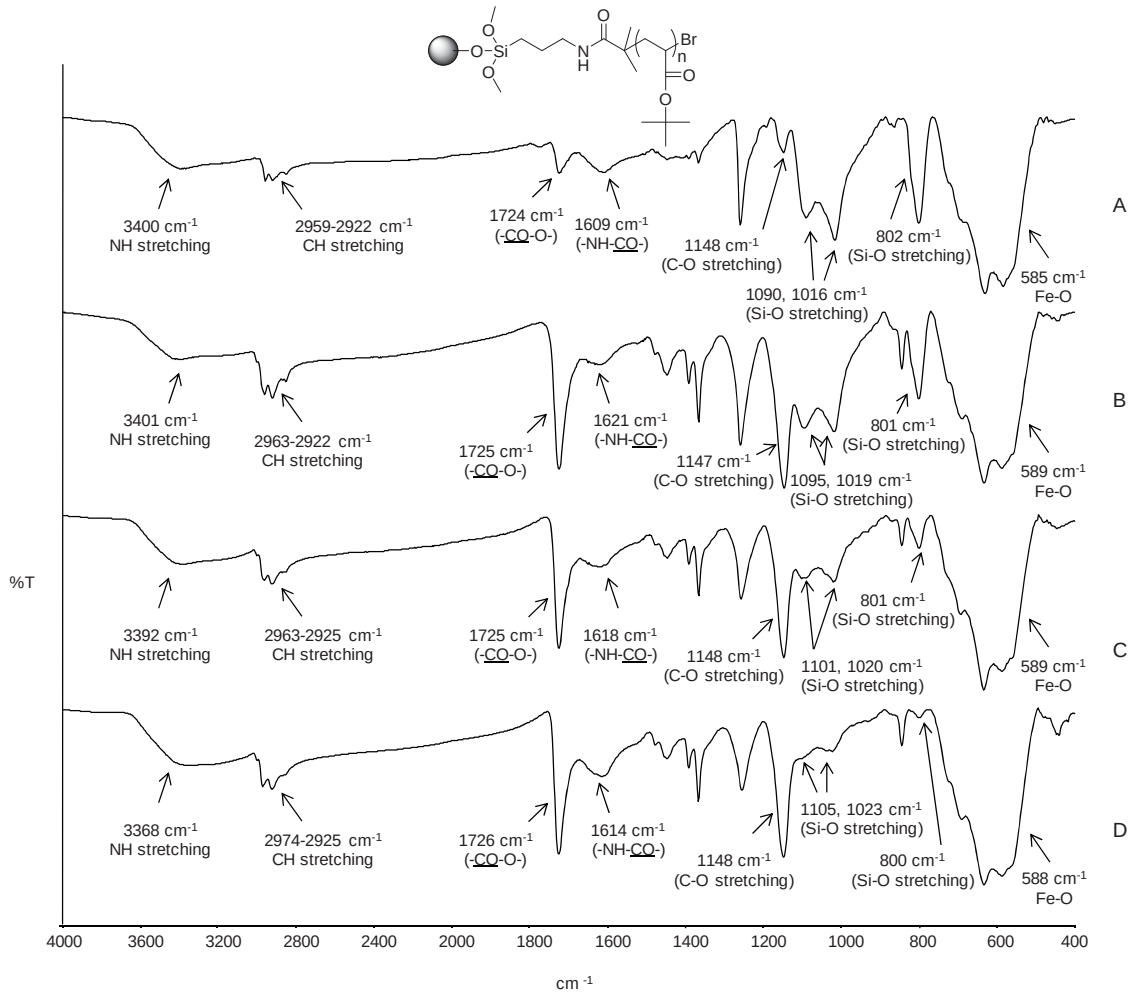


**Figure 3** FTIR spectra of poly(*t*-BA)-coated MNP at various ATRP reaction times, A) 1 h, B) 6 h, C) 12 h and D) 24 h

Weight loss from TGA technique of poly(*t*-BA)-coated MNPs at various ATRP reaction times was investigated to determine the relative amount of poly(*t*-BA) that can be grafted on the particle surface. It should be noted that the particles were separated from the uncoordinated species using an external magnet. Using an assumption that % char yield was the weight of magnetite remaining at 600 $^{o}$C, the weight loss of the surface-modified MNPs was thus attributed to the decomposition of organic components including BTPAm and poly(*t*-BA) that complexed to the particle surface. Hence, percent char yield of bare MNP and MNP coated with BTPAm were determined to obtain percent of BTPAm in the complexes in each sample. According to TGA results, percent of BTPAm in the complexes was about 2 wt%, while percents of poly(*t*-BA) were 3 wt%, 15 wt%, 26 wt% and 43 wt% of the complexes at 1, 6, 12 and 24 h ATRP reaction times, respectively (Figure 4). This was a

supportive result to FTIR that poly(*t*-BA) chain length was prolonged when ATRP reaction time was extended.

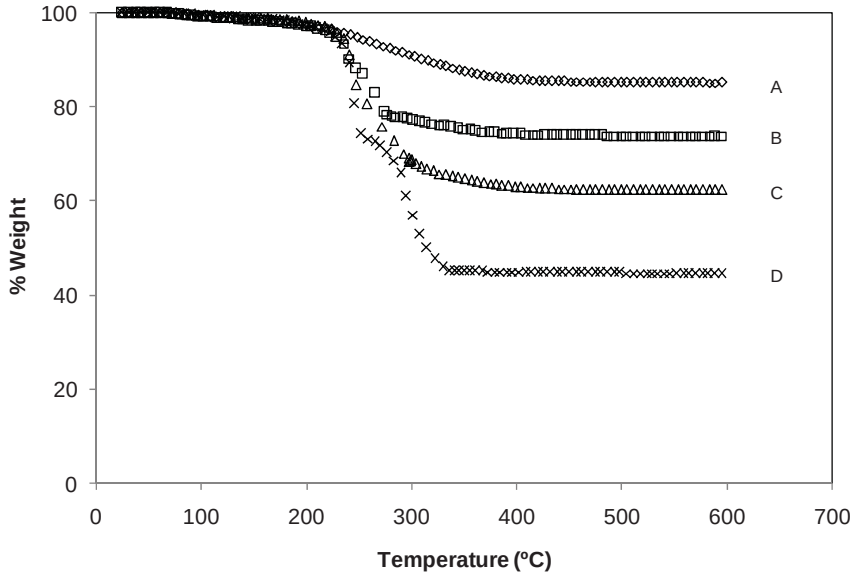


**Figure 4** TGA thermograms of poly(*t*-BA)-coated MNPs at various ATRP reaction times, A) 1 h, B) 6 h, C) 12 h and D) 24 h

To investigate the molecular weight and the molecular weight distribution of poly(*t*-BA), small amount of ethyl bromoisobutylate (EBiB) was added in the dispersion as a "sacrificial initiator" to form free poly(*t*-BA) along with poly(*t*-BA) grafted on MNP. After 24 h of the reaction, the free poly(*t*-BA) was removed from the MNP complex using an external magnet. According to GPC results, molecular weight of poly(*t*-BA) was about 18,600 g/mol and its molecular weight distribution was about 1.22. This narrow molecular weight distribution indicated the living mechanism of controlled radical polymerization. $^{1}$H NMR spectrum of free poly(*t*-BA) is shown in supplementary data.

TEM images of MNP complexes at each step of the reaction are illustrated in Figure 5. Bare MNPs observed in Figure 5A were well organized because they were somewhat uniformed in size, which was in the range of 6-10 nm in diameter with the average of about 8 nm. Surface modification of the MNPs resulted in a slightly broader size distribution due to the presence of organic compounds coated on their surface (Figure 5B-5D). However, the average particle size was not significant difference from those of bare MNPs. It should be noted that poly(*t*-BA)-coated MNPs were well dispersed in toluene due to the existence of hydrophobic poly(*t*-BA) on their surface (Figure 5C), while poly(AA)-coated MNPs were

well dispersed in water because of the presence of hydrophilic and charge surfactants of poly(AA) (Figure 5D).

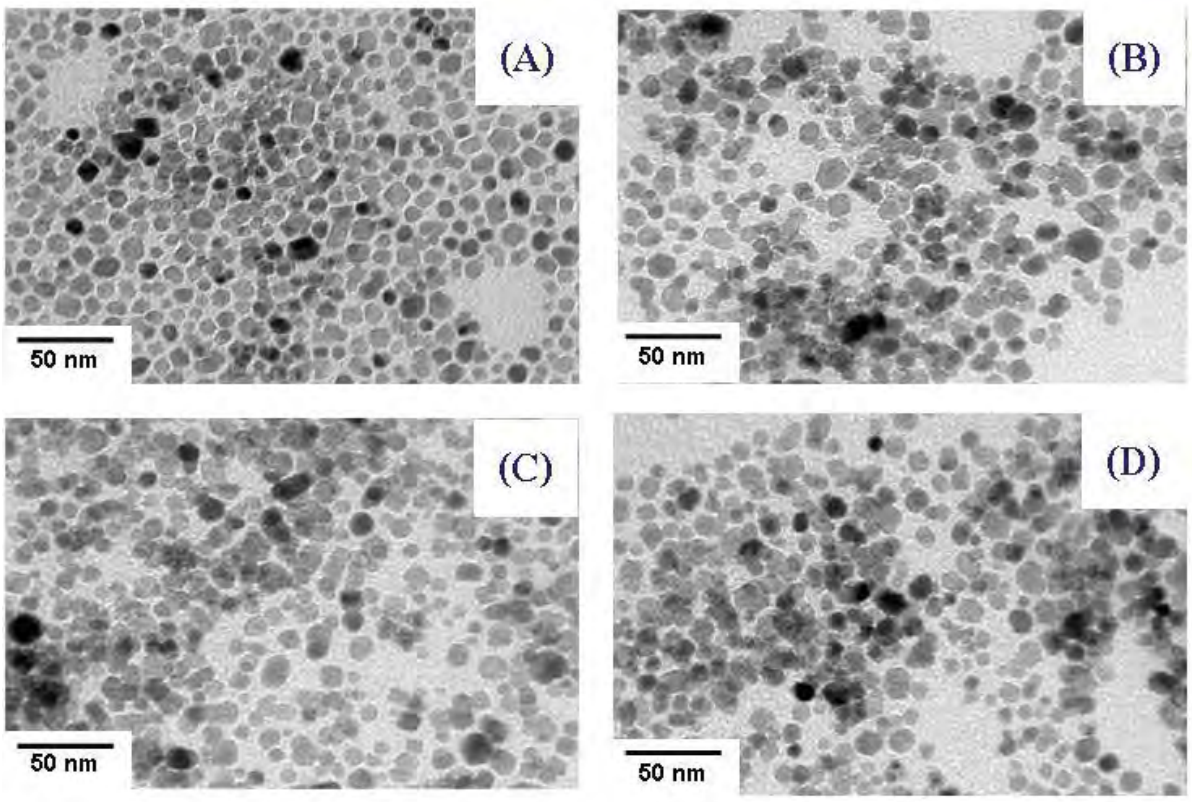


**Figure 5** TEM images of A) bare MNPs, B) BTPAm-coated MNPs, C) poly(*t*-BA)-coated MNPs, D) poly(AA)-coated MNPs**.** In the TEM sample preparation, MNPs in Figure A-C were dispersed in toluene and those in Figure D were dispersed in water.

The *M*-*H* curves of bare MNP, BTPAm-coated MNP, poly(*t*-BA)-coated MNPs and poly(AA)-coated MNP were illustrated in Figure 6. They showed superparamagnetic behavior at room temperature as indicated by the absence of reminance and coercivity upon removing an external applied magnetic field. According to the results in Table 1, the decrease of saturation magnetization ($M_s$) from 59 emu/g of bare MNPs to 27 emu/g of poly(*t*-BA)-coated MNPs was attributed to the presence of the organic surfactant on their surface, resulting in the decrease of percent of magnetite in the complexes. After the hydrolysis of poly(*t*-BA) to form poly(AA)-coated MNP, its $M_s$ value increased from 27 to 39 emu/g sample due to the removal of *t*-BA groups in poly(*t*-BA), which subsequently increased percent of magnetite in the complexes. Interestingly, when taking percent of magnetite in the complex into account, the $M_s$ values in emu/g magnetite basis of these complexes were not significantly different from each other, indicating that magnetic properties of the particles

were not considerably affected upon ATRP of poly(*t*-BA) and hydrolysis to form poly(AA)-coated MNPs.

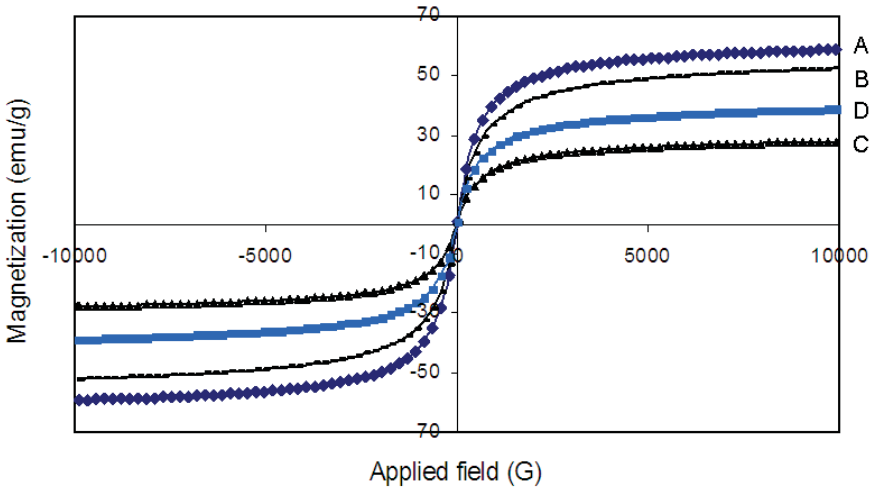


**Figure 6** *M-H* curves of A) bare MNP, B) BTPAm-coated MNP, C) poly(*t*-BA)-coated MNP and D) poly(AA)-coated MNP

**Table 1** Percentage of magnetite in the complex and their magnetic properties

| Sample | emu/g sample [a] | % $Fe_3O_4$ [b] | emu/g $Fe_3O_4$ |
|---|---|---|---|
| Bare MNP | 59 | 90 | 65 |
| BTPAm-coated MNP | 53 | 88 | 60 |
| Poly(*t*-BA)-coated MNP | 27 | 45 | 61 |
| Poly(AA)-coated MNP | 39 | 63 | 62 |

[a] Estimated from the saturation magnetization ($M_s$) at 10,000 G from VSM technique, [b] Estimated from % char yield at 600 ºC from TGA technique

After the hydrolysis reaction, it was conceived that MNPs having carboxylic acid-enriched surfaces were obtained. These carboxylic acid functional groups are readily reactive toward coupling reactions with other molecules having affinity functional groups such as amine and alcohol. In the current work, folic acid (FA) was chemically immobilized on the surface-modified MNPs. FA has two carboxylic acid groups at the $\alpha$ and $\gamma$ positions, which can covalently react with amino functional groups of EDA. However, it has already been

verified that $\gamma$-COOH is more accessible to covalently react with amino groups due to its high reactivity [49-50]. FA needs to be first activated with ethylene diamine (EDA) to obtain primary amine-terminated FA (*N*-(2-aminoethyl) folic acid or EDA-FA). This logical strategy enhanced the reactivity of FA to efficiently react with carboxylic acid over-expressed on the surface of poly(AA)-coated MNPs through amidization reaction. Results of the synthesis of EDA-FA including FTIR and $^{1}$H NMR spectra were detailed in supplementary data.

In the grafting reaction between poly(AA)-coated MNPs and EDA-FA, *N*-hydroxyl succinimide (NHS) was used to activate the dangling carboxylic acid groups. FTIR spectra of the products in each step were thus illustrated in comparison with the starting compounds (Figure 7). Figure 7A showed the FTIR spectrum of poly(AA)-coated MNPs and those of NHS was depicted in Figure 7B. In Figure 7C, the sharp and strong characteristic signal of ester linkages appeared at 1723 $cm^{-1}$, indicating the coupling reaction between carboxylic acid of poly(AA)-coated MNPs and NHS. In addition, Fe-O linkages of magnetite core were also observed at 586 $cm^{-1}$. After the coupling reaction with EDA-FA (Figure 7D), the characteristic signals of FA, such as 1700-1500 $cm^{-1}$ and 1153-1069 $cm^{-1}$, appeared in the FA-bound MNPs (Figure 7E), indicating the successful conjugation of FA on the MNP surfaces.

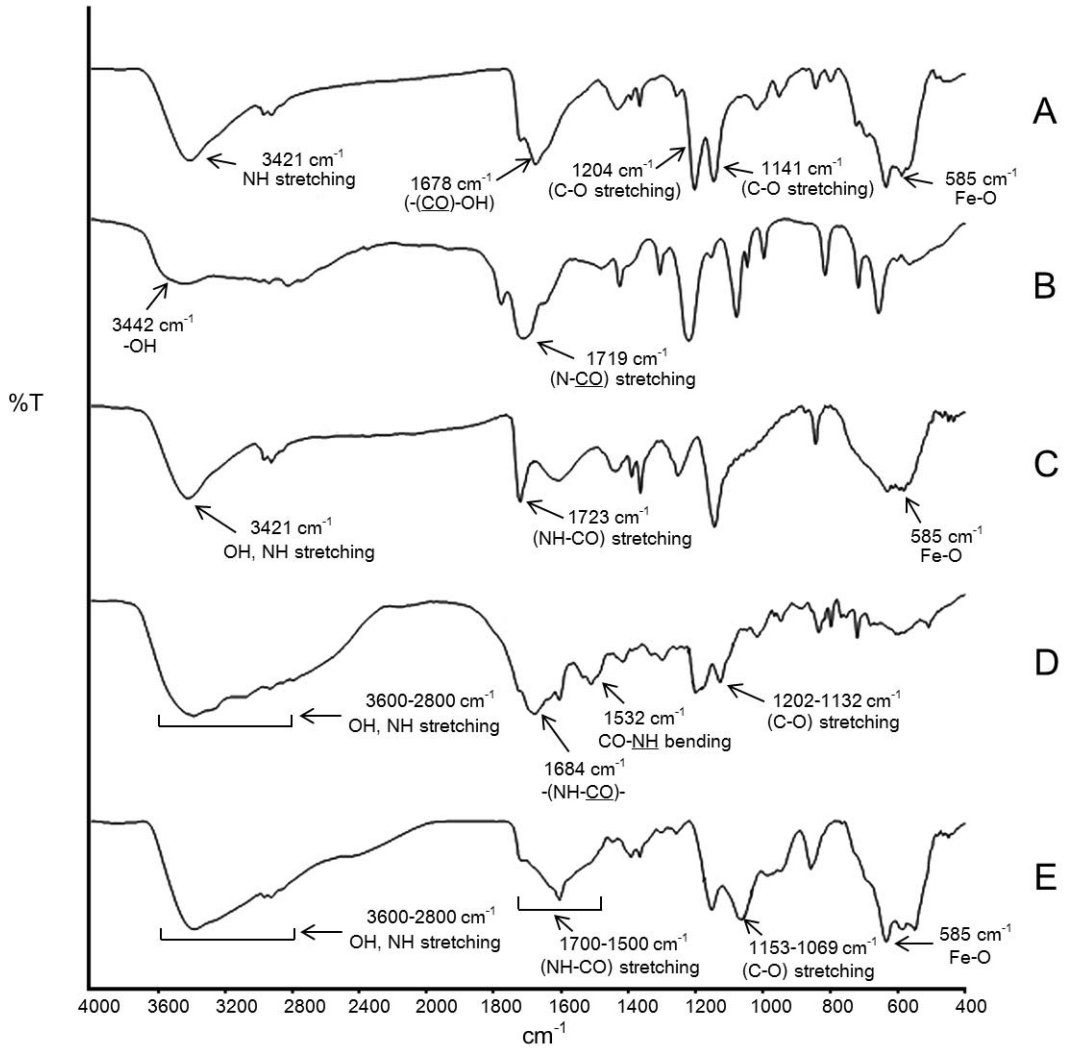


**Figure 7** FTIR spectra of (A) poly(AA)-coated MNP, (B) NHS, (C) NHS-poly(AA)-coated MNPs, (D) EDA-FA and (E) FA-poly(AA)-coated MNPs

UV-visible spectrophotometry was also applied to confirm the presence of FA in the conjugated MNP complex. FA showed a $\lambda_{max}$ value at 371 nm (Figure 8A), whilst those of FA-conjugated MNPs also exhibited a weak absorbance signal at the same wavelength (Figure 8B). It is worth to mention that poly(AA)-coated MNPs before FA loading did not show any absorbance signal at the same wavelength (Figure 8C). This result implied that FA was, to some extent, covalently conjugated to the MNP surfaces.

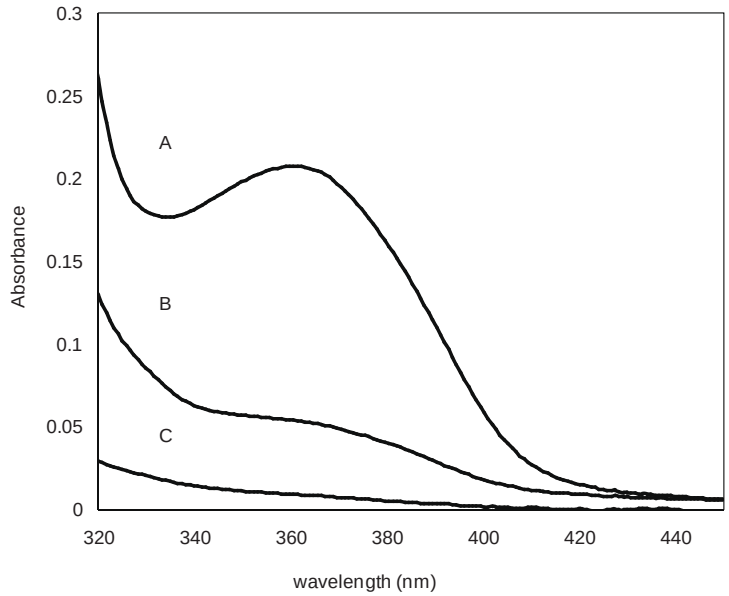


**Figure 8** UV-visible spectra of (A) folic acid (FA), (B) FA-conjugated MNPs and (C) poly(AA)-coated MNPs without FA

To determine percentage of magnetite core and organic shell in the complexes in each step of the reactions, the complexes were characterized *via* TGA to investigate their mass loss. Bare MNPs manifested a drastic weight loss between 200-350 $^{o}$C with 90 % char yield (Figure 9A). This was attributable to the decomposition or desorption of the absorbed ammonium salt at elevated temperature and eventually loss some weight [51-52]. The weight loss of MNPs coated with BTPAm, poly(*t*-BA) and poly(AA) were attributed to the decomposition of organic components complexing to the particle surface and % char yields were the weight of magnetite core. From TGA thermograms in Figure 9B and 9C, there was about 2 wt% of BTPAm and 49 wt% of poly(*t*-BA) in poly(*t*-BA)-coated MNPs. The grafting density of BTPAm, the initiating site for ATRP on the particle, can be calculated and it was found that there was about 0.8 molecule/nm$^2$ (150 molecules/particle). Examples of the calculation are illustrated in supplementary data. The grafting density of poly(*t*-BA) were comparable to that of BTPAm on the surface.

After the hydrolysis of poly(*t*-BA), percent of organic components in the case of poly(AA)-coated MNPs significantly dropped (from 49 to 27 wt%) due to the removal of *t*-BA groups from the polymeric layer of the particles (Figure 9D). The 27 wt% of poly(AA) corresponded to 23 carboxylic acid/nm$^2$ (4,600 acid/particle). From Figure 9E, there was about 14 wt% of FA in the complex, corresponding to about 2 FA molecules/nm$^2$ (400 FA molecules/particle). Therefore, percent conversion of carboxylic acid to FA was about 8%. The lowering temperature of TGA curve in Figure 9E (FA-poly (AA)-coated MNP) as

compared to that in Figure 9D (poly (AA)-coated MNP) was attributed to the weight loss of FA component in the complex. The decomposed TGA thermogram of free FA has been investigated and shown in supplementary data. In addition, it was also found that there was about 2.7 FA molecules/site of the ATRP initiator (400 FA molecule/150 sites of BTPAm in a single particle). The limited number of the %conversion and grafting density of FA on the particle surface was attributed to limited accessibility of bulky FA to react with steric poly(AA). However, the grafting density of FA might be improved by copolymerization of poly(AA) with other polymers to lessen steric hindrance of the compact poly(AA), so that FA con be more effectively conjugated. Also, utilization of spacer from the particle surface is another approach that can diminish steric hindrance on the dense surface.

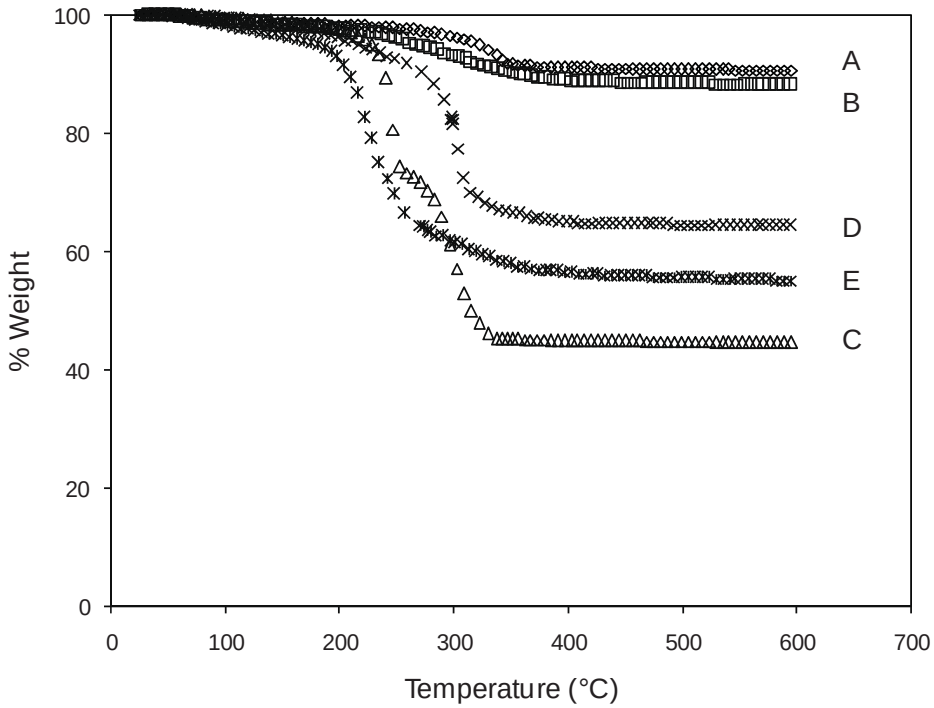


**Figure 9** TGA thermograms of (A) bare MNP, (B) BTPAm-coated MNP, (C) poly(*t*-BA) coated MNP, (D) poly(AA)-coated MNP and (E) FA-poly(AA)-coated MNP

Because carboxylic acid functional groups can be easily ionized in an aqueous solution, it is thus interesting to understand how pH of the dispersions affect hydrodynamic diameter and surface charge of poly(AA)-coated MNPs and FA-poly(AA)-coated MNP. pH of the aqueous dispersions containing the complexes (0.2 mg/ml) were varied from

approximately 1 to 11 and their hydrodynamic diameters were determined *via* PCS technique. In both samples, as pH of the dispersions increased, their hydrodynamic diameters rapidly decreased at acidic pH (ranging between pH 1.2-5.4) and gradually decreased at pH ranging between 5.4-11.3 (Figure 10). It was hypothesized that as increasing pH of the dispersions, ionization of carboxylic acid on the surface of poly(AA)-coated MNPs took place, resulting in the formation of carboxylate ions on their surfaces. The negative charges of carboxylate ions led to additional electrostatic repulsion toward neighboring particles and thus prevented massive flocculation.

The results from zeta potential measurements also supported this assumption. The surface charges of poly(AA)-coated MNPs were positive at the pH ranging between 1.2-6.5 and negative at the pH range of 6.5-11.3, implying that point of zero charge (PZC) of this complex was pH 6.5 (Figure 10). It was also found that FA-containing complex showed a slightly higher zeta potential than the other at pH ranging between 1.2-6.5. This was attributed to the presence of amines in FA structure, resulting in protonated amino groups. Similarly, the enriched amines in the complex might also influence the lower zeta potential in FA-containing complex at basic pH.

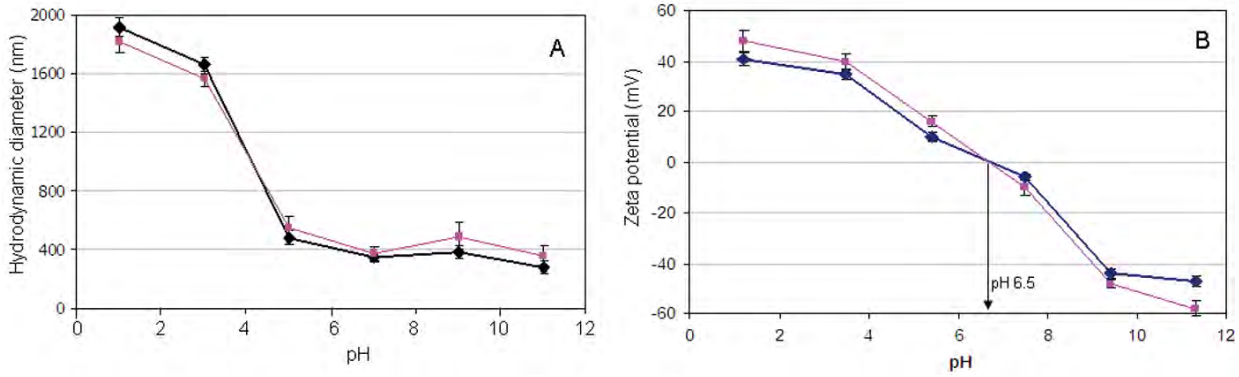


**Figure 10** The effect of pH of the aqueous dispersions containing poly(AA)-coated MNP (●) and FA-poly(AA)-coated MNP (■) on their hydrodynamic diameter and zeta potential. The experiments were performed at 25$^{o}$C.

The large size of the particles in DLS as compared to those from TEM measurements (8 nm in diameter) might come from the fact that there were some nano-clusters of particles in the dispersions. These nano-clusters of the particles can be observed in TEM

measurements from the first step of the particle synthesis (shown in supplementary data). When poly(AA) was chemically grafted on their surface, these clusters still presented. Although these nano-clusters existed in the dispersions, the particles were well dispersible in aqueous dispersions without macroscopic aggregation visibly observed because there were poly(AA) coated on their surface.

Cytotoxicity testings of poly(AA)-coated MNP and FA-poly(AA)-coated MNP were also performed. According to our preliminary results, it was found that the dispersions were not toxic against Vero cell line up to 50 μg/ml concentration of the sample (sulforhodamine B (SRB) assay method). Detail studies regarding the toxicity of the magnetite complexes are warranted for future studies.

## 4. Conclusions

This work presented a "grafting from" strategy to modify MNP surfaces with poly(*t*-BA) *via* ATRP, followed by a hydrolysis of *t*-BA groups to obtain poly(AA) and finally immobilization of folic acid on their surfaces. The originality of this work is that this is the first report on modifying MNP surface with poly(AA) which serves as a platform for folic acid immobilization. Because the folate receptor is overexpressed on the surface of cancer cells, it is for this reason that folic acid is of particular interest in the current work in an attempt to facilitate the intracellular uptake by specific cancer cells for cancer therapy. Folic acid was successfully activated with ethylene diamine (EDA) to obtain primary amine-terminated folic acid derivative. This logical strategy enhanced the reactivity of folic acid to be efficiently immobilized on MNP surfaces through amidization reaction.

In addition to the use of binding affinity of carboxylic acid functional groups, poly(AA) on their surface can also provide stabilization mechanisms through both steric repulsion due to the long chain polymers and electrostatic repulsion owing to the formation of negative charges in basic pH dispersions. Furthermore, poly(AA) on their surfaces also promoted particle dispersibility in water, which is a minimum requirement for biomedical uses. This novel magnetically guidable nanocomplex might be suitable for use as an efficient drug delivery vehicle particularly for cancer treatment.

**Acknowledgement** The authors thank the Thailand Research Fund (TRF) and Naresuan University (DBG5380001) for financial funding. The Center of Excellence for Innovation in

Chemistry (PERCH-CIC), Commission on Higher Education, Ministry of Education is also gratefully acknowledged for financial support.

**Supplementary data**: Proposed reaction mechanisms of trifluoroacetic acid (TFA) with the polymers on MNP surface. FTIR and $^{1}$H NMR spectra of 2-bromo-2-methyl-*N*-(3-(triethoxysilyl) propanamide (BTPAm) and *N*-(2-aminoethyl) folic acid (EDA-FA). $^{1}$H NMR spectrum of poly(t-BA), TEM images showing some nano-aggregation. Examples of calculation of grafting density. TGA thermogram of folic acid.

**References**

[1] Pei W, Kumadaa H, Natusmea T, Saitoa H, Ishio S. J Magn. Magn Mater 2007; 310: 2375-7.

[2] Sun S, Murray CB, Weller D, Folks L, Moser A. Science 2000;287:1989-92.

[3] Teng X, Yang H. J Am Chem Soc 2003:125,14559-63.

[4] Casula MF, Floris P, Innocenti C, Lascialfari A, Marinone M, Corti M, Sperling RA, Parak WJ, Sangregorio C. Chem Mater 2010:22,1739-48.

[5] Anders S, Sun S, Murray CB, Rettner CT, Best ME, Thomson T, Albrecht M, Thiele JU, Fullerton EE, Terris BD. Microelectron Eng 2002;61-62:569-75.

[6] Woo K, Hong J, Choi S, Lee HW, Ahn JP, Kim CS, Lee SW. Chem Mater 2004;16:2814-8.

[7] Zhang J, Misra RDK. Acta Biomater 2007;3:838-50.

[8] Laurent S, Forge D, Port M, Roch A, Robic C, Elst LV, Muller RN. Chem Rev 2008;108:2064-110.

[9] Veiseh O, Gunn JW, Zhang M. Adv. Drug Delivery Rev 2010;62:284-304.

[10] Sahoo Y, Goodarzi A, Swihart MT, Ohulchanskyy TY, Kaur N, Furlani EP. J Phys Chem 2005;109:3879-85.

[11] Hayashi K, Ono K, Suzuki H, Sawada M, Moriya M, Sakamoto W, Yogo T. Chem Mater 2010; 22:3768-72.

[12] Feng PB, Gao F, Gu HC. J Colloid Interface Sci 2005;284:1-6.

[13] Liu X, Xing J, Guan Y, Shan G, Liu H. Colloids Surf A: Physicochem Eng 2004;238:127-31.

[14] Mornet S, Vekris A, Bonnet J, Duguet E, Grasset F, Choy JH, Portier J. Mater Lett 2000; 42:183-8.

[15] Cheng G, Zhao J, Tu Y, He P, Fang Y. Anal Chem Acta 2005;533:11-6.

[16] Lellouche J, Senthil G, Joseph A, Buzhansky L, Bruce I, Bauminger ER, Schlesinger J. J Am Chem Soc 2005;127:11998-2006.

[17] Corr SA, Rakovich YP, Gun'ko YK. Nanoscale Res Lett 2008;3:87-104.

[18] Sahoo Y, Goodarzi A, Swihart MT, Ohulchanskyy TY, Kaur N, Furlani EP, Prasad PN. J Phys Chem B 2005;109:3879-85.

[19] Zhang Y, Kohler N, Zhang M. Biomaterials 2002;23:1553-61.

[20] Sonvico F, Mornet S, Vasseur S, Dubernet C, Jaillard D, Degrouard J, Hoebeke J, Duguet E, Colombo P, Couvreur P. Bioconjugate Chem 2005;16:1181-8.

[21] Zhou Y, Wang S, Ding B, Yang Z. Chem Eng J 2008;138:578-85.

[22] Fischer H. Chem Rev 2001;101:3581-610.

[23] Sun Y, Ding X, Zheng Z, Cheng X, Hu X, Peng Y. Eur Polym J 2007;43:762-72.

[24] Pyun J, Jia S, Kowalewski T, Patterson GD, Matyjaszewski K. Macromolecules 2003;36:5094-104.

[25] Hu B, Fuchs A, Huseyin S, Gordaninejad F, Evrensel C. Polymer 2006;47:7653-63.

[26] Zhao H, Shipp DA. Chem Mater 2003;15:2693-5.

[27] Liu G, Yan X, Lu Z, Curda SA, Lal J. Chem Mater 2005;17:4985-91.

[28] Sun Y, Ding X, Zheng Z, Cheng X, Hu X, Peng Y. Euro Polym J 2007;43:762-72.

[29] Hermann High LR, Holder SJ, Penfold HV. Macromolecules 2007;40:7157-65.

[30] Shipp DA, Wang JL, Matyjaszewski K. Macromolecules 1998;31:8005-8.

[31] Xia J, Gaynor SG, Matyjaszewski K. Macromolecules 1998;31:5958-9.

[32] Teodorescu M, Matyjaszewski K. Macromolecules 1999;32:4826-31.

[33] Raghuraman G K, Rühe J, Dhamodharan R. Nanopart Res 2008;10:415–27.

[34] Fan QL, Neoh KG, Kang ET,Shuter B,Wang SC. Biomaterials 2007;28:5426–36.

[35] Czaun M, Hevesi L, Takafuji M, Ihara H. Chem Commun 2008;2124–6.

[36] Marutanil E, Yamamoto S, Ninjbadgar T, Tsujii Y, Fukuda T, Takano M. Polymer 2004;45: 2231-5.

[37] Zhou Y, Wang S, Ding B, Yang Z. Chem Eng J 2007;40:6217-23.

[38] Fan QL, Neoh KG, Kang ET, Shuter B, Wang SC. Biomaterials 2007;28:5426-36.

[39] Frimpong RA, Hilt JZ. Nanotechnology 2008;19:1-7.

[40] Si S, Kotal A, Mandal TK, Giri S, Nakamura H, Kohara T. Chem Mater. 2004;16:3489-96.

[41] Zhang M, Breiner T, Mori H, Muller AHE. Polymer 2003;44:1449-58.

[42] Wan S, Zheng Y, Liu Y, Yan H, Liu KJ. Mater Chem 2005;15:3424-30.

[43] Sauzedde F, Elaïssari A, Pichot C. Colloid Polym Sci 1999;277:846-55.

[44] Ng V, Lee YV, Chen BT, Adeyeye AO. Nanotechnology 2002;13:554-8.

[45] Hayashi K, Moriya M, Sakamoto W, Yogo T. Chem Mater 2009;21:1318-25.

[46] Kohler N, Fryxell GE, Zhang M. J Am Chem Soc 2004;126:7206-11.

[47] Landmark KJ, DiMaggio S, Ward J, Kelly C, Vogt S, Hong S, Kotlyar A, Myc A, Thomas TP, Penner-Hahn JE, Baker JJR, Banaszak Holl MM, Orr BG. ACS Nano 2008;2:773-83.

[48] Pinna N, Grancharov S, Beato P, Bonville P, Antonietti M, Niederberger M. Chem Mater 2005; 17:3044-9.

[49] Mohapatra S, Mallick SK, Maiti TK, Ghosh SK, Pramanik P. Nanotechnology 2007;18:385102.

[50] Park EK, Lee SB, Lee YM. Biomaterials 2005;26:1053–61.

[51] Rutnakornpituk M, Meerod S, Boontha B, Wichai U. Polymer 2009;50:3508-15.

[52] Tao K, Dou H, Sun K. Chem Mater 2006;18:5273-8.

**Supporting information 1 : Synthesis of 2-bromo-2-methyl-*N*-(3-(triethoxysilyl) propanamide (BTPAm)**

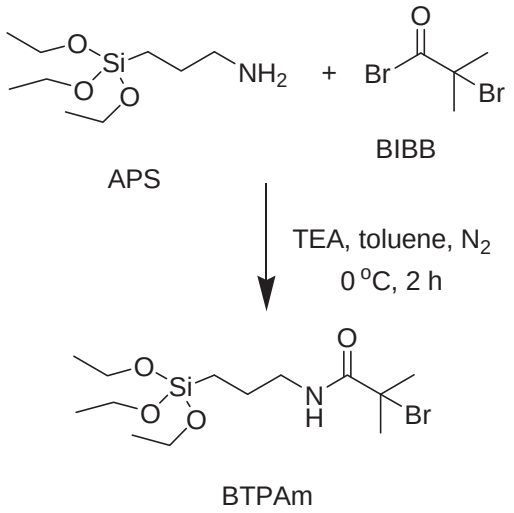


**Figure s1-1** Amidization reaction between APS and BIBB to obtain BTPAm

BTPAm was prepared through an amidization reaction between APS and BIBB. Comparing with the FTIR spectrum of APS (Figure s1-2A) and BIBB (Figure s1-2B), Figure s1-2C exhibited FTIR characteristic absorption peaks of BTPAm (1658 $cm^{-1}$ of -NH-CO- carbonyl stretching, 1112-1026 $cm^{-1}$ of Si-O stretching, 1532 $cm^{-1}$ of N-H bending and 3345 $cm^{-1}$ of N-H- stretching). The signal at 1738 $cm^{-1}$ belonging to -(CO)-Br carbonyl stretching indicated the slight remaining of unreacted BIBB after the reaction. It is important to mention that the molar ratio of APS to BIBB used in this step was 1:1; it is possible to have some unreacted BIBB or APS remaining after the reaction. However, the mixture was used in the next step without further purification.

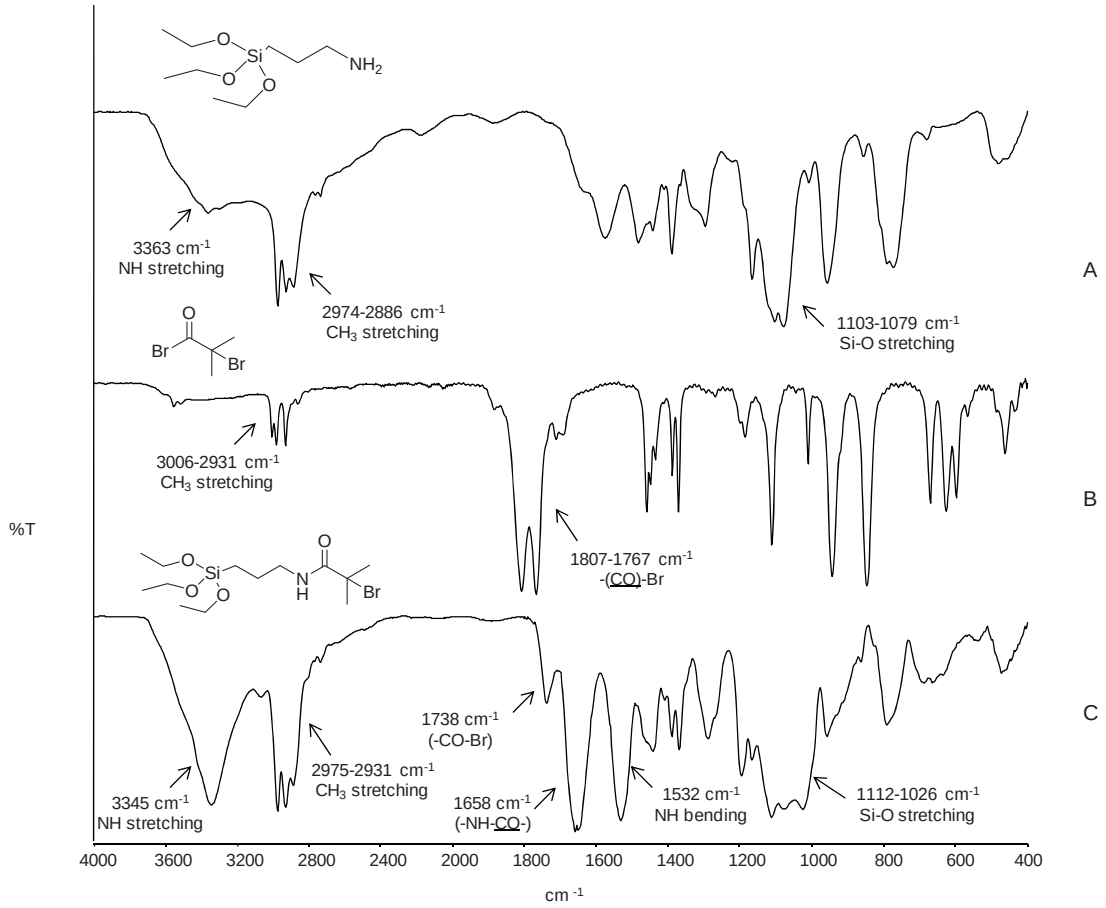


**Figure s1-2** FTIR spectra of A) 3-aminopropyl triethoxysilane (APS), B) 2-bromoisobutyryl bromide (BIBB) and C) (2-bromo-2-methyl-*N*-(3- (triethoxysilyl) propanamide (BTPAm)

**Table s1-1** Functional group annotation of BTPAm (Figure s1-2C)

| Wavenumber ($cm^{-1}$) | Functional group |
|---|---|
| 3345 | N-H stretching |
| 2975-2889 | C-H stretching |
| 1738 | Acid bromide (-(CO)-Br) stretching |

| | |
|---|---|
| 1658 | Amide (-(NH)-(CO) stretching |
| 1532 | N-H bending |
| 1442 | C-N stretching |
| 1286 | C-Br stretching |
| 1112-1026 | Si-O stretching |
| 794 | N-H out-of-plane bending |

Figure s1-3C showed a $^{1}$H NMR spectrum of BTPAm in comparison with APS (Figure s1-3A) and BIBB (Figure s1-3B) starting reagents. In good agreement with FTIR results, a distinctive shift of the $^{1}$H NMR signal corresponding to methylene protons adjacent to NH group (from 2.50 ppm, signal *a*, to 3.22 ppm, signal *a'*) indicated the formation of BTPAm. In addition, slight shifts of other signals such as methylene protons of signal *b* (1.45 ppm) to signal *b'* (1.62 ppm), and methyl protons of signal *f* (2.50 ppm) to signal *f'* (2.40 ppm) also confirmed the formation of BTPAm.

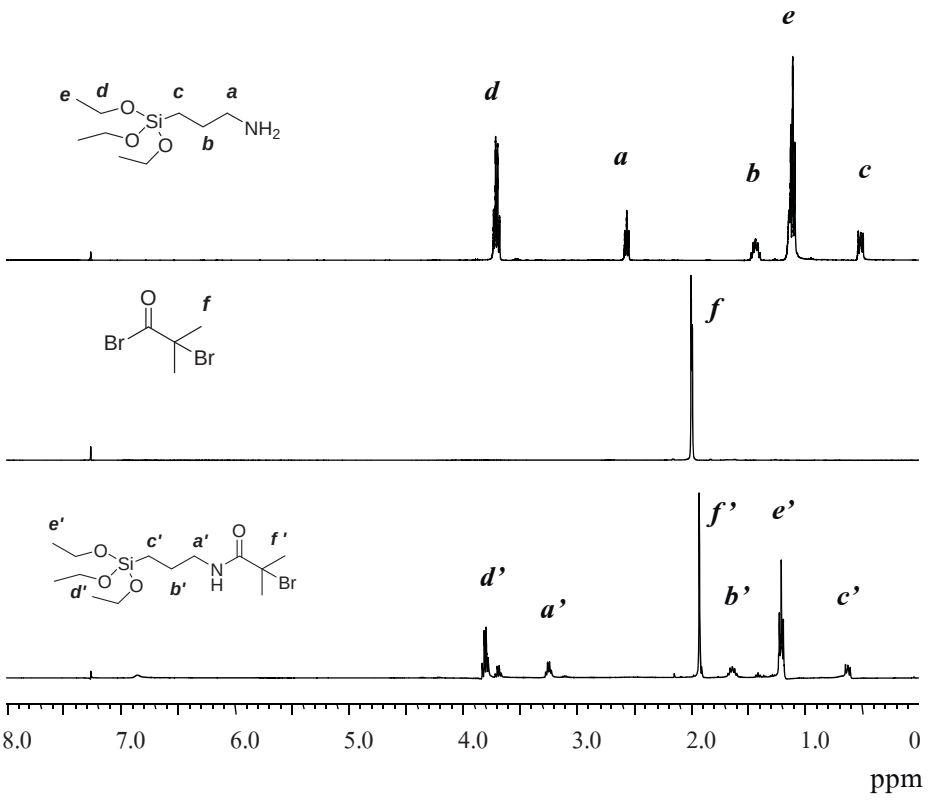


**Figure s1-3** $^{1}$H NMR spectra of A) 3-aminopropyl triethoxysilane (APS) (solvent: $CDCl_3$), B) 2-bromoisobutyryl bromide (BIBB) (solvent: $CDCl_3$) and C) (2-bromo-2-methyl-*N*-(3-(triethoxysilyl) propanamide (BTPAm) (solvent: $CDCl_3$)

**Supporting information 2: Synthesis of *N*-(2-aminoethyl) folic acid (EDA-FA)**

*N*-(2-aminoethyl) folic acid (EDA-FA) is a derivative of folic acid containing an active primary amino functional group. The purpose of this step was to activate folic acid such that it can readily react with carboxylic acid overexpressed on the surface-modified MNPs prepared from the previous step. EDA-FA was synthesized from ethylene diamine (EDA) starting reagent *via* a two-step synthesis; 1) protection of single amino group of EDA and 2) coupling folic acid with the amino-protected EDA.

*1. Protection of single amino group of ethylene diamine (EDA) with tert-butyl carbamate (Boc)*

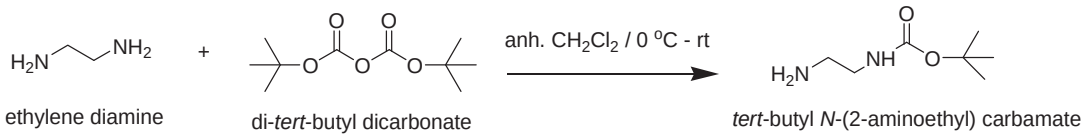


**Figure s2-1** Synthesis of *tert*-butyl *N*-(2-aminoethyl) carbamate (EDA-Boc)

Comparing with the FTIR spectrum of di-*tert*-butyl dicarbonate ($Boc_2O$) (Figure s2-2A), Figure s2-2B exhibited FTIR characteristic absorption signals of *N*-*tert*-butoxycarbonyl-1,2-diaminoethane (EDA-Boc) (1693 $cm^{-1}$ of -NH-CO- carbonyl stretching, 1172 $cm^{-1}$ of C-O stretching, 1525 $cm^{-1}$ of N-H bending and 3360 $cm^{-1}$ of N-H- stretching). In good agreement with FTIR, $^1$NMR results also indicated the formation of EDA-Boc due to the presence of the methylene protons (signal *b*) at 3.15 ppm; (Figure s2-3); $^1$H NMR ($CDCl_3$): $\delta$ = 1.43 (s, 9H, $CH_3$); 2.79 (m, 2H, $CH_2$); 3.15 (m, 2H, $CH_2$); 4.88 (bs, 1H, amide proton). EDA-Boc appeared as colorless oil.

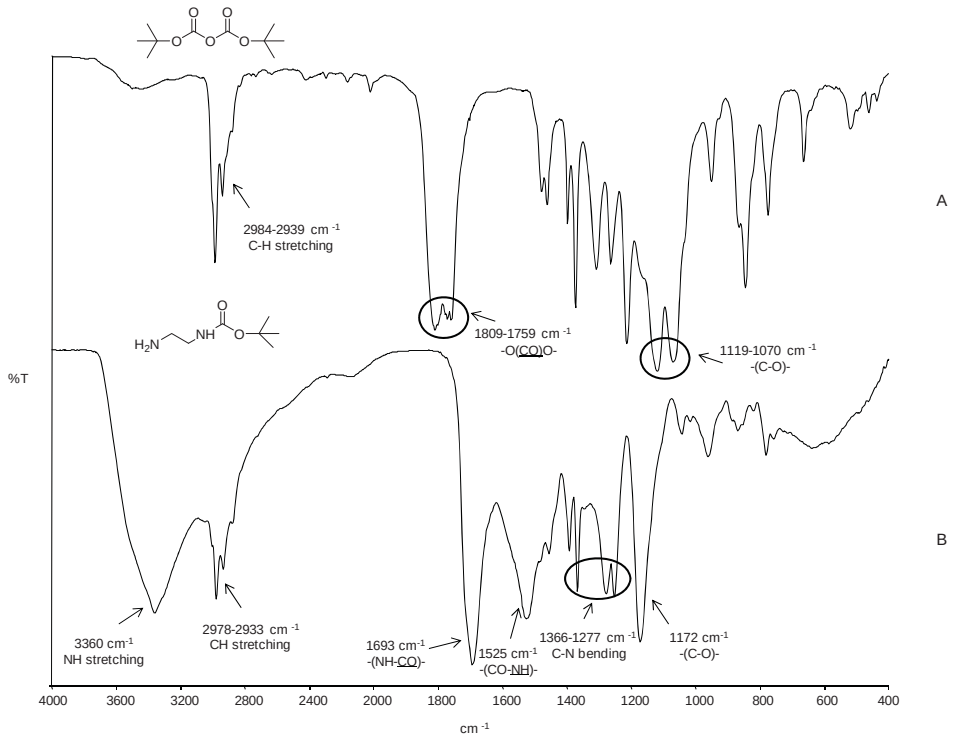


**Figure s2-2** FTIR spectra of A) di-*tert*-butyl dicarbonate ($Boc_2O$) and B) N-*tert*-butoxycarbonyl-1,2-diaminoethane (EDA-Boc)

**Table s2-2A** Functional group annotation of di-*tert* dicarbonate ($Boc_2O$) (Figure s2-2A)

| Wavenumber ($cm^{-1}$) | Functional group |
|---|---|
| 2984-2939 | C-H stretching |
| 1809-1759 | Carbonate -O(CO)O- stretching |
| 1119-1070 | C-O stretching |

**Table s2-2B** Functional group annotation of *N-tert*-butoxycarbonyl-1,2-diaminoethane (EDA-Boc) (Figure s2-2B)

| Wavenumber ($cm^{-1}$) | Functional group |
|---|---|
| 3360 | N-H stretching |
| 2978-2933 | C-H stretching |
| 1693 | Amide -(NH-CO)- stretching |
| 1525 | Amide -(CO-NH)- bending |
| 1366-1277 | C-N bending |
| 1172 | C-O stretching |

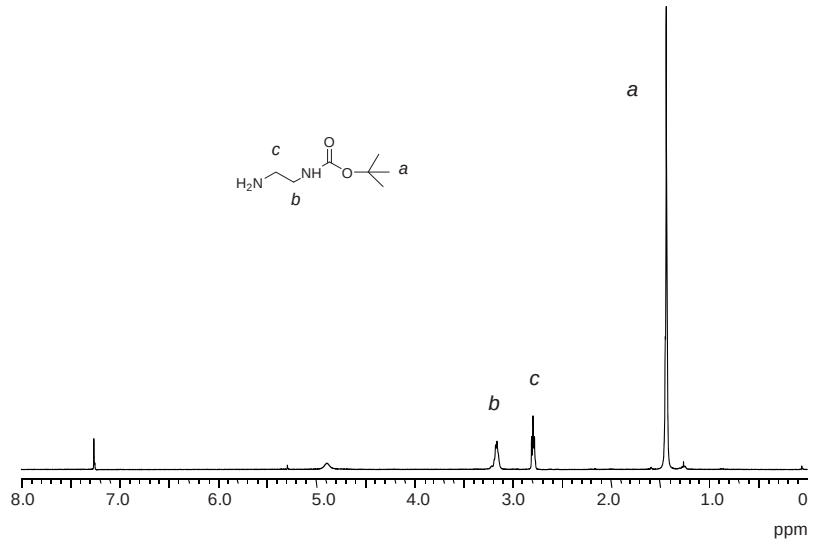


**Figure s2-3** The $^{1}$H MNR spectrum of *N*-*tert*-butoxycarbonyl-1,2-diaminoethane (EDA-Boc) (solvent: $CDCl_3$)

*2. Coupling folic acid with the amino-protected EDA*

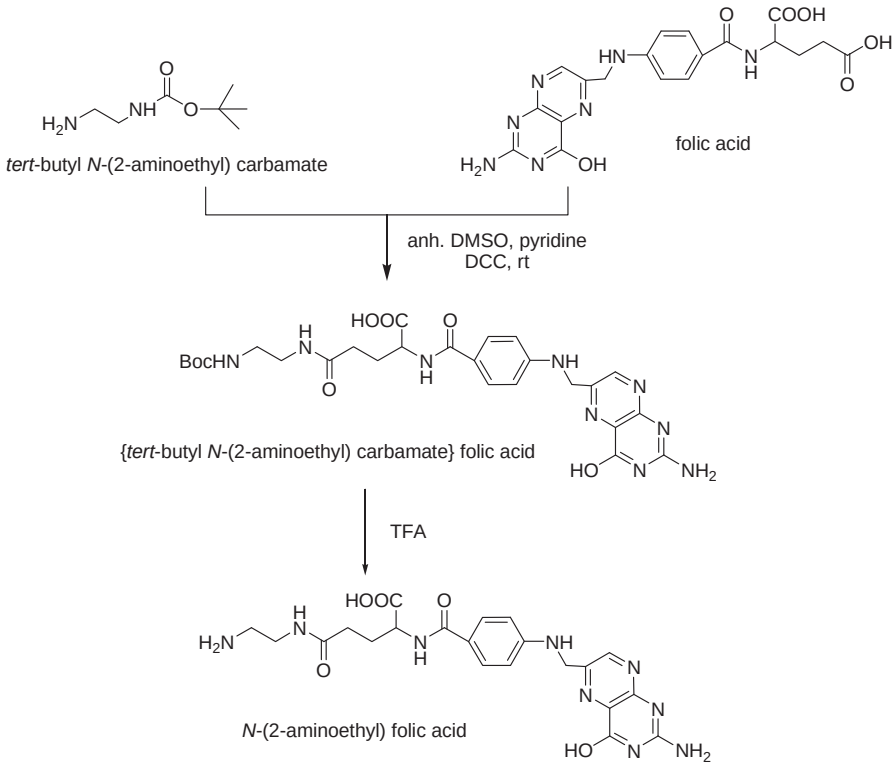

**Figure s2-4** Synthesis of *N*-(2-aminoethyl) folic acid (EDA-FA)

A coupling reaction between the remaining amino group of EDA-Boc and carboxylic acid of FA was performed. In comparison with those of EDA-Boc and FA (Figure s2-5A and s2-5B, respectively), an FTIR spectrum of the resultant product (Boc-EDA-FA) from the amidization reaction was depicted in Figure s2-5C. The spectrum showed the characteristic peaks of both EDA-Boc and FA such as N-H stretching (3392 $cm^{-1}$), NH-CO-stretching (1700 $cm^{-1}$), 1606 $cm^{-1}$ ((OC-OH) and 1513 $cm^{-1}$ (CO-NH bending). Upon removal of Boc protecting groups, most of the characteristic signals still remained (Figure s2-5D).

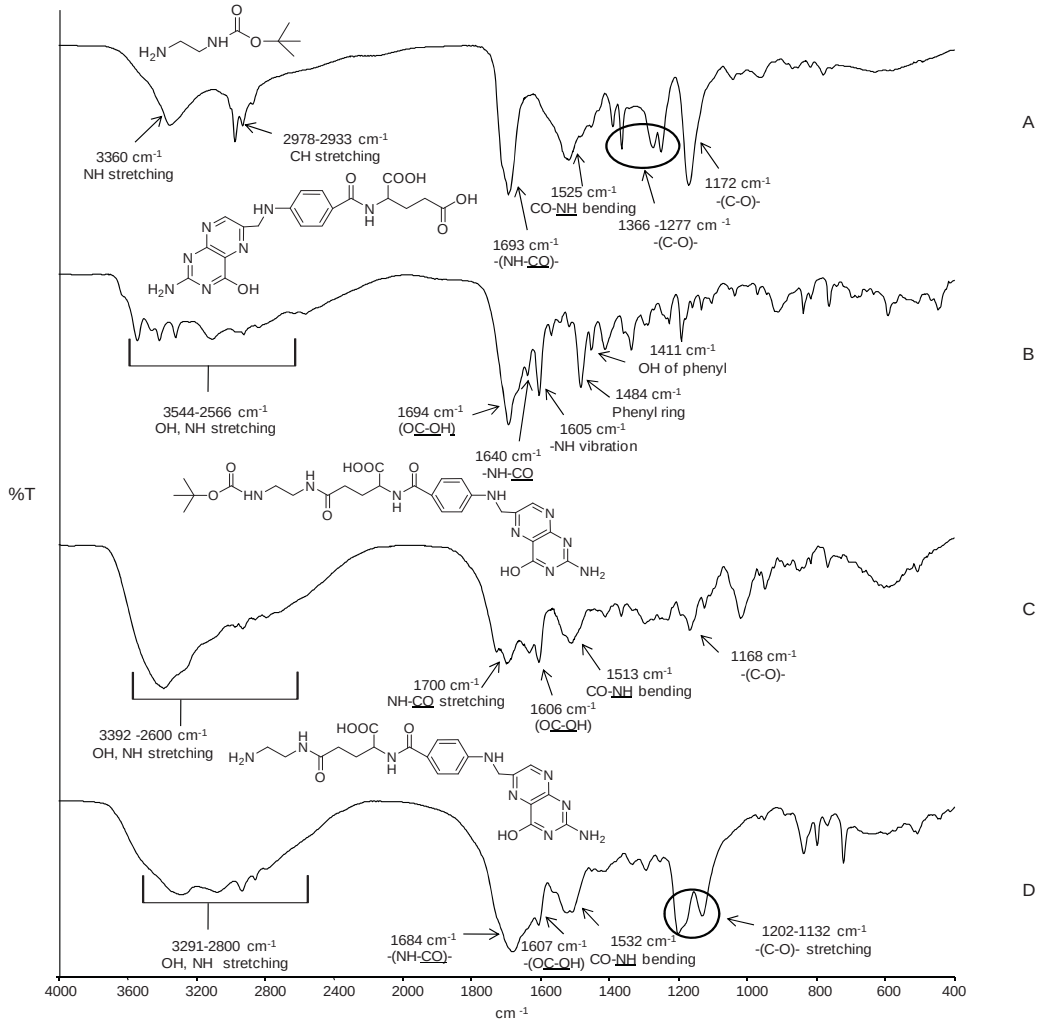

**Figure s2-5** FTIR spectra of A) N-*tert*-butoxycarbonyl-1,2-diaminoethane (EDA- Boc), B) folic acid (FA), C) (*tert*-butyl *N*-(2-aminoethyl) carbamate) Folic acid (Boc-EDA-FA) and D) *N*-(2-aminoethyl) folic acid (EDA-FA)

**Table s2-5B** Functional group annotation of folic acid (FA) (Figure s2-5B)

| Wavenumber ($cm^{-1}$) | Functional group |
|---|---|
| 3544-2566 | (OH) stretching, N-H stretching vibration |
| 1694 | (COOH) stretching vibration |
| 1605 | NH- vibration |
| 1484 | phenyl ring |
| 1411 | OH of phenyl |

**Table s2-5C** Functional group annotation of {*tert*-butyl *N*-(2- aminoethyl) carbamate}folic acid (Boc-EDA-FA) (Figure s2-5C)

| Wavenumber ($cm^{-1}$) | Functional group |
|---|---|
| 3392-2600 | OH, N-H stretching |
| 1700 | Amide -(NH-CO)- stretching |
| 1605 | -(OC-OH)- stretching |
| 1513-1299 | C-N bending |
| 1168 | C-O stretching |

**Table s2-5D** Functional group annotation of *N*-(2-aminoethyl) folic acid (EDA-FA) (Figure s2-5D)

| Wavenumber ($cm^{-1}$) | Functional group |
|---|---|
| 3600-2800 | N-H, O-H stretching |
| 1684 | Amide -(NH-CO)- stretching |
| 1605 | -(OC-OH) stretching |
| 1532-1335 | C-N bending |
| 1202-1132 | C-O stretching |

Similarly to those of FTIR, $^{1}H$ NMR spectra of all related compounds were investigated and shown in Figure s2-6. Figure s2-6A depicted $^{1}H$ NMR of EDA-Boc and Figure s2-6B illustrated those of FA. It was observed that there were signals of trace water in DMSO appearing at (1.2, 2.5 and 3.3 ppm) in Figure s2-6B-6D. In Figure s2-6C, *tert*-butyl *N*-(2-aminoethyl) carbamate) folic acid (Boc-EDA-FA), the coupling product of EDA-Boc and FA, exhibited all characteristic signals of the expected product, indicating the formation of Boc-EDA-FA. A slight shift of signal *c* in Figure s2-6A to signal *c'* in Figure s2-6C also

indicated the occurrence of amidation reaction between EDA-Boc and FA. After removal of the Boc protecting group, the methyl protons corresponding to *t*-butyl groups of Boc (peak *a*', 1.33 ppm) disappeared (Figure s2-6D), indicating the formation of EDA-FA.

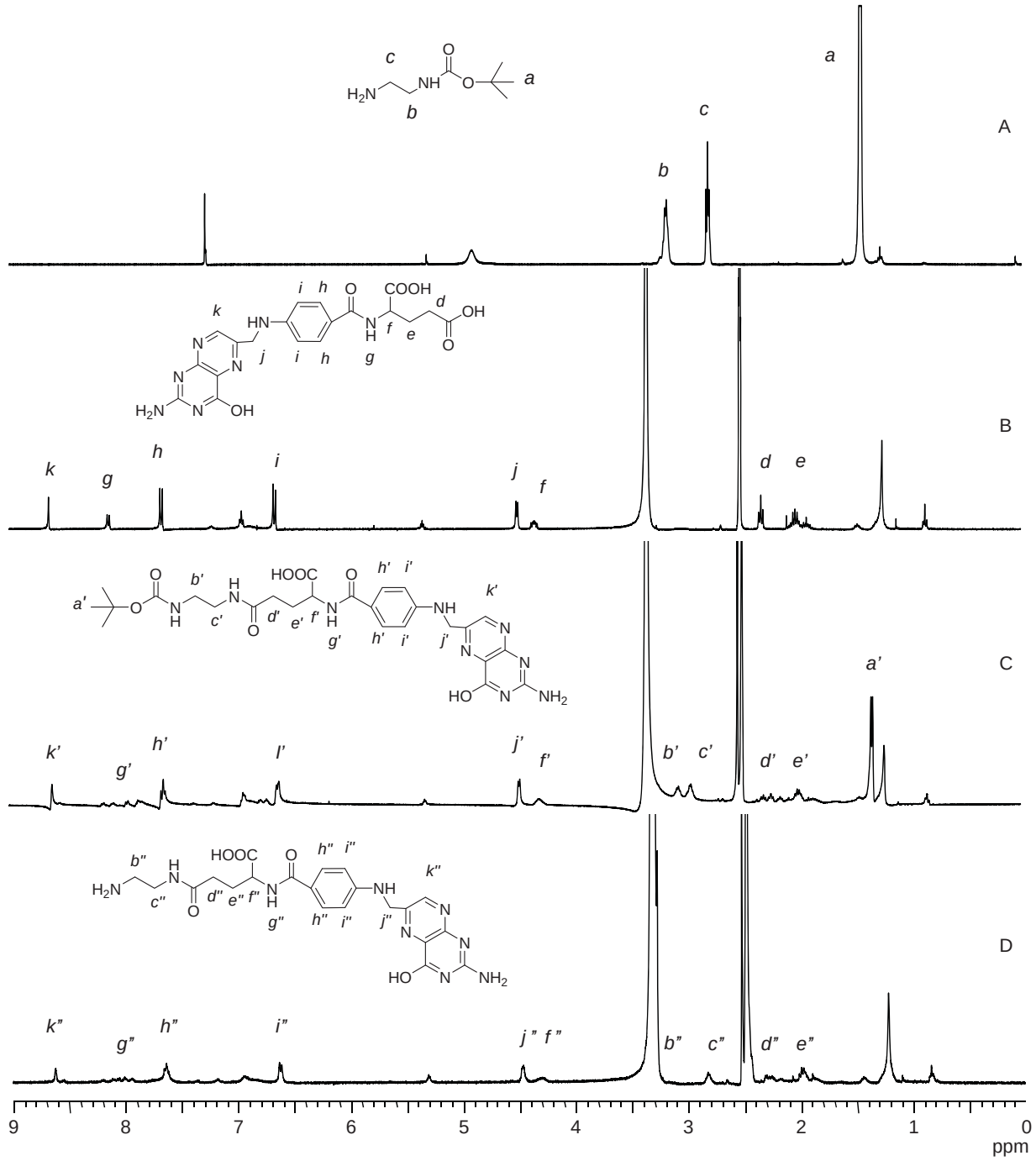


**Figure s2-6** $^{1}$H NMR spectra of (A) *N*-*tert*-butoxycarbonyl-1,2-diaminoethane (EDA-Boc) (solvent: $CDCl_3$), B) folic acid (FA) (solvent: DMSO-$D_6$), C) (*tert*-butyl *N*-(2-aminoethyl) carbamate) folic acid (Boc-EDA-FA) (solvent: DMSO-$D_6$) and D) *N*-(2-aminoethyl) folic acid (EDA-FA) (solvent: DMSO-$D_6$)

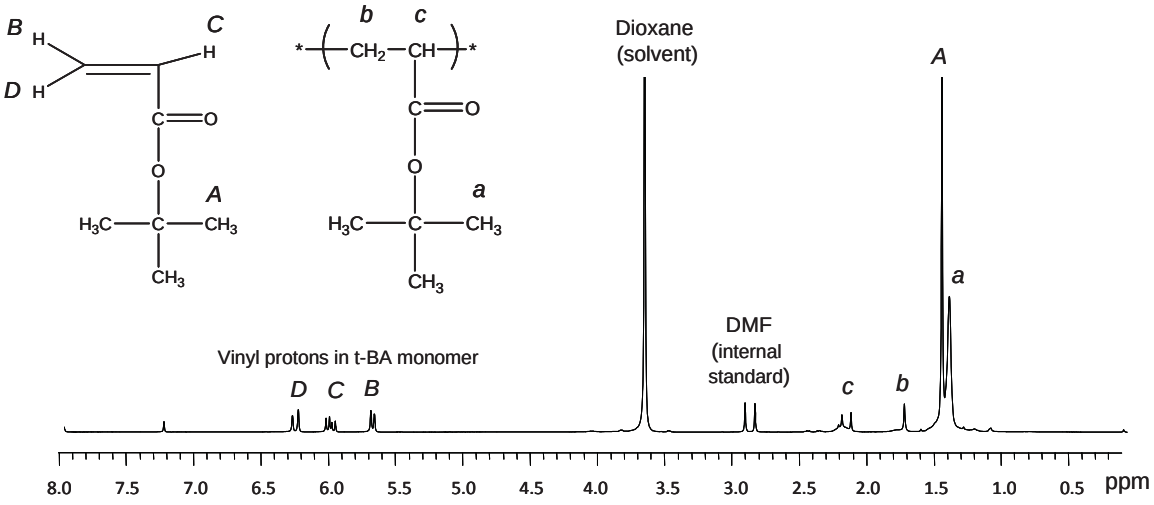


$^1$H NMR spectrum of poly(t-BA) prepared *via* ATRP in dioxane and using DMF as an internal standard. From the spectrum, the signals of poly(t-BA) were observed (peak *a*, *b* and *c*). The sample was removed from the reaction without removal of t-BA monomer; the signals of the monomer were thus observed in the spectrum.

**Examples of the calculation of grafting density of BTPAm, poly(t-BA), carboxylic acid and FA**

From TEM analysis, particle diameter is 8 nm.

Surface area = $4.r^2$, where r = 4 nm

Thus, surface area of a single particle = 4 x 22/7 x $4^2$ =201 $nm^2$

Volume = $4/3.r^3$, where r = 4 nm

Thus, volume of a single particle = 4/3 x 22/7 x $4^3$ = 268 $nm^3$

Because density of magnetite = 5.26 $g/cm^3$ [reference 1-2] = mass/volume

Mass of a single particle = 5.26 $g/cm^3$ x 268 $nm^3$

= 1.41 x $10^{-18}$ g

References

[1] Tebble RS, Craik DJ. Magnetic Materials, Wiley-Interscience, London, 1969.

[2] Cornell RM, Schertmann U. The Iron Oxides: Structure, Properties, Reactions, Occurrence and Uses, VCH Publishers, Weinheim, 1996.

From TGA result, FA-poly(AA)-coated MNPs possessed 60.8% $Fe_3O_4$, 1.7% BTPAm, 23.5% PAA and 14% FA.

Weight of BTPAm coated on a single particle = $(1.41 \times 10^{-18}$ g).(1.7/60.8)

$= 3.94 \times 10^{-20}$ g

Moles of BTPAm = $(3.94 \times 10^{-20}$ g)/(156 g/mol) ; MW of BTPAm =156 g/mol

Number of BTPAm = $(3.94 \times 10^{-20}$ g).$(6.02 \times 10^{23}$ molecule/mol)/(156 g/mol)

$\approx$ 150 molecules/particle

$\approx$ 150 molecules/201 $nm^2$

$\approx$ 0.8 molecule/$nm^2$

Similarly, weight of poly(AA) coated on a single particle = $(1.41 \times 10^{-18}$ g).(23.5/60.8)

$= 5.48 \times 10^{-19}$ g

Moles of carboxylic acid = $(5.48 \times 10^{-19}$ g)/(72 g/mol) ; MW of acrylic acid unit = 72 g/mol

Number of carboxylic acid = $(5.48 \times 10^{-19}$ g).$(6.02 \times 10^{23}$ acid/mol)/(72 g/mol)

$\approx$ 4,600 acid/particle

$\approx$ 4,600 acid/201 $nm^2$

$\approx$ 23 acid/$nm^2$

Similarly, weight of FA in a single particle = $(1.41 \times 10^{-18}$ g).(14/60.8)

$= 3.26 \times 10^{-19}$ g

Moles of FA = (3.26 x $10^{-19}$ g)/(483 g/mol) ; MW of EDA-FA = 483 g/mol

Number of FA = (3.26 x $10^{-19}$ g).(6.02 x $10^{23}$ molecules/mol)/(483 g/mol)

≈ 400 FA molecules/particle

≈ 400 FA molecules/201 $nm^2$

≈ 2 FA molecule /$nm^2$

Therefore, percent conversion of carboxylic acid to FA ≈ 400/(400+4,600)

≈ 8%

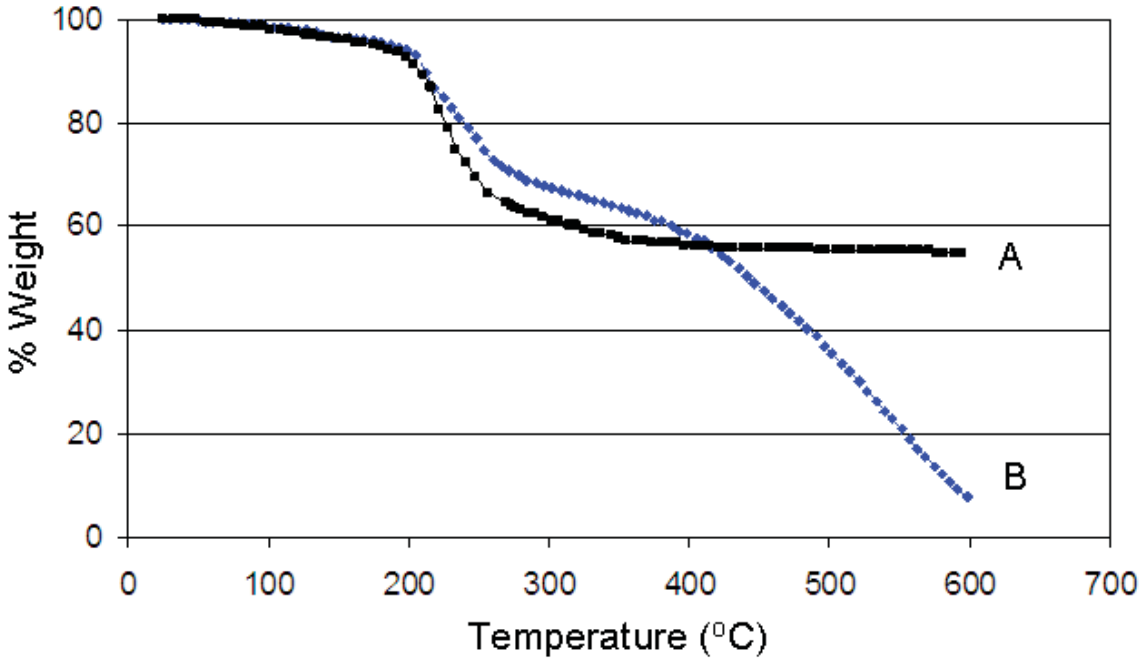

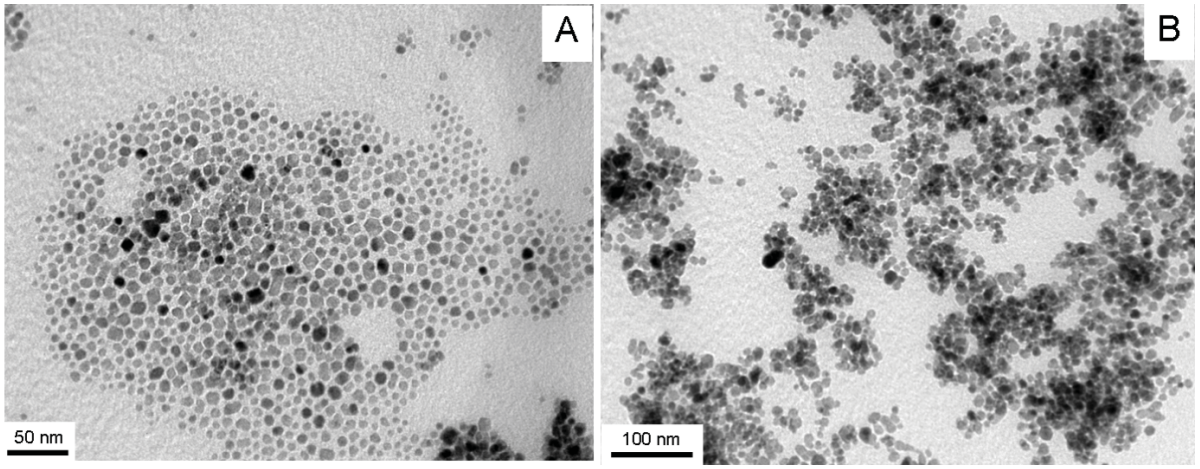
A
50 nm
B
100 nm

# Azlactone functionalization of magnetic nanoparticles using ATRP and their bioconjugation

*Yingrak Prai-in, Kritsada Tankanya, Boonjira Rutnakornpituk, Uthai Wichai, Véronique Montembault, Sagrario Pascual, Laurent Fontaine* and Metha Rutnakornpituk**

**Abstract:** Surface modification of magnetite nanoparticle (MNP) with poly(poly(ethylene glycol) methyl ether methacrylate-*stat*-2-vinyl-4,4-dimethylazlactone) copolymers (Poly(PEGMA-*stat*-VDM)) *via* atom transfer radical polymerization (ATRP) and its application to anchor thymine peptide nucleic acid (PNA) monomer are reported. ATRP of PEGMA and VDM was first performed in a solution system to optimize the reaction condition and the optimal condition was then applied in the surface-initiated ATRP of MNP. Fourier transform infrared spectroscopy (FTIR) indicated the presence of the copolymer in the MNP complexes. After immobilization of thymine PNA monomer, thermogravimetric analysis (TGA) results indicated that there were 4 wt% of the PNA monomer in the complex (1.2 μmol/g complex). The existence of the PNA monomer in the complex was also confirmed *via* FTIR and vibrating sample magnetometry (VSM). The MNP complex with active surface might be efficiently used as magnetically guidable nanosolid support for PNA oligomers and other molecules containing affinity functional groups.

*Keywords*: magnetite; azlactone; ATRP

## Introduction

Magnetite iron oxide nanoparticles (MNP, $Fe_3O_4$) are widely studied in the present days. MNP have been used for many biomedical applications such as magnetic resonance imaging [1-3], drug delivery system [4-5], enzyme and protein immobilization [6-8], RNA and DNA purification [9-11], and gene therapy [12-14]. The minimum requirements of MNP for these applications are that it should be chemically stable, biocompatible, non-toxic, well dispersible in liquid media and able to be bound with biological molecules such as peptides, hormones, nucleotides or drugs [1-14]. Therefore, surface modification of MNP with various polymers becomes a good choice to obtain biocompatible MNP and to enhance the interaction between MNP and biological species.

Several methods, including physical adsorption of polymers to MNP surface, emulsion polymerization in the presence of MNP and so-called “grafting-to” and “grafting-

from" methods have been developed to prepare polymer-coated MNP [15-18]. Among these methods, the "grafting-from" technique has been preferable because polymer chains are grown from initiator-functionalized MNP surface by *in situ* polymerization to obtain a permanent linkage of the polymers on its surface. Recently, several groups have applied atom transfer radical polymerization (ATRP) based on a "grafting-from" method to prepare polymeric layers on surface of MNP [19-21]. The advantages of this method are that the as-synthesized polymer possesses low polydispersity index, controllable molecular weight, functionality, composition distribution and desired polymer architecture [19-21].

In this work, we have applied a copper-mediated ATRP technique to synthesize grafted statistical copolymer of poly(ethylene glycol) methacrylate (PEGMA) and 2-vinyl-4,4-dimethylazlactone (VDM) onto MNP containing an ATRP initiator immobilized on its surface. The azlactone ring of 4,4-dimethyl-5-oxazolone displays a high reactivity towards nucleophilic molecules such as primary amines, alcohol and thiols by means of a ring-opening addition reaction without the use of catalysts. In addition, there is no by-product eliminated from the ring-opening reaction between VDM and nucleophiles [22-28]. Moreover, the azlactone functionality shows a good resistance to hydrolysis at neutral pH: this is a considerable advantage compared to other activated acid forms [29].

We have previously studied the dependence of the molecular architecture of VDM-styrene copolymer on accessibility of benzylamine as a model nucleophilic compound to react with the azlactone rings grafted on a solid support. It was found that the statistical architecture of VDM-styrene copolymer exhibited a good result in terms of reactivity and efficiency in the azlactone-ring opening reaction due to the existence of styrene spacers resulting in the open access to VDM units [24]. In the present work, water dispersibility of MNP could be greatly improved by introducing a thin layer of PEGMA to its surface and the presence of the azlactone rings of VDM serves as a site for immobilization of biological nucleophilic molecules, such as enzymes [30] or proteins [31] on its surface. In this work, thymine PNA monomer was used as a model compound for immobilization onto the VDM-grafted particles. FTIR, VSM and TGA techniques were used to verify the existence of thymine PNA monomer on its surface.

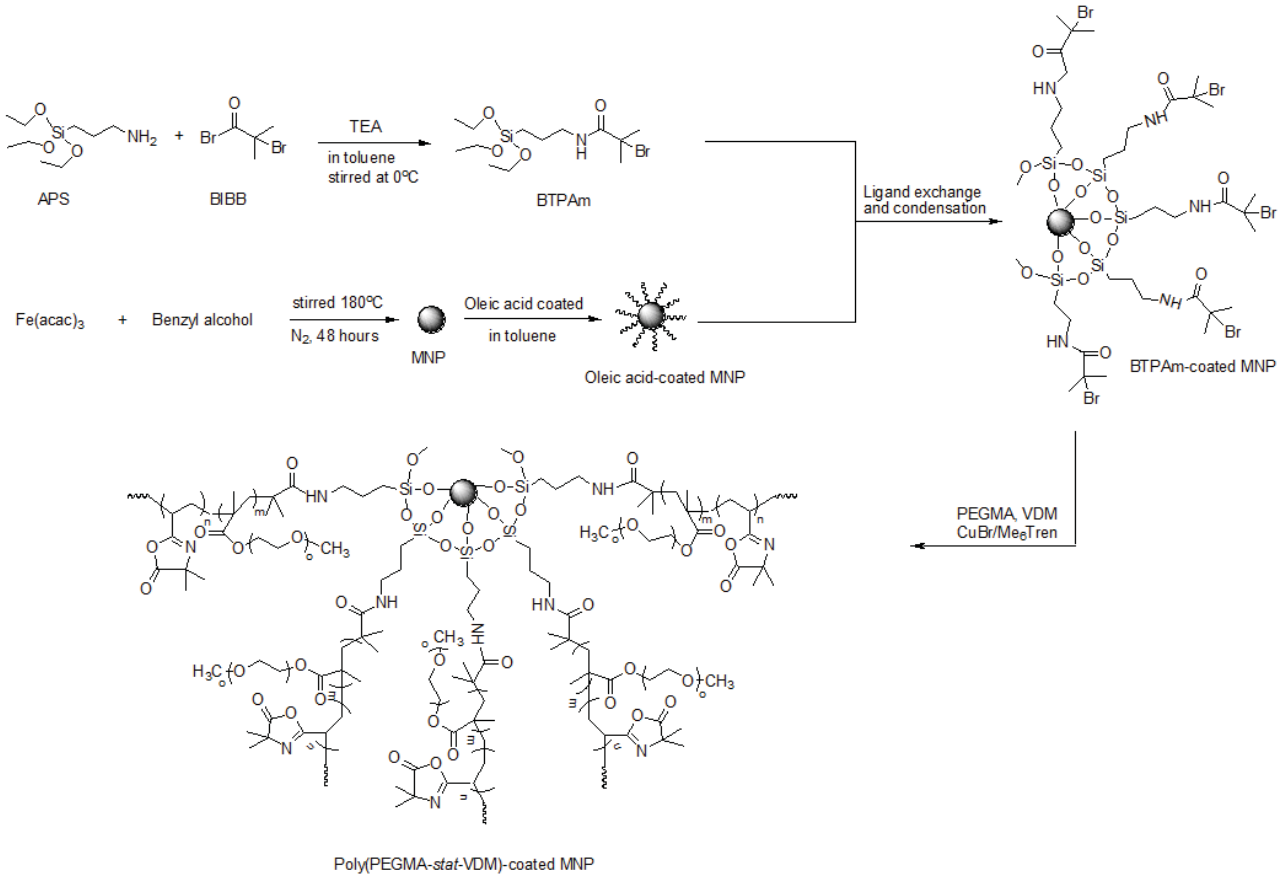


**Scheme 1** Surface modification of MNP with poly(PEGMA-*stat*-VDM) copolymer *via* ATRP reaction

## Experimental

### Materials

Unless otherwise stated, all reagents were used without further purification: iron (III) acetylacetonate ($Fe(acac)_3$, 99.9%, Acros), benzyl alcohol (98%, Unilab), oleic acid (Fluka), copper(I)bromide (99.999%, Aldrich), triethylamine (TEA, 97%, Carto Erba), ethyl-2-bromoisobutyrate (EBiB, 98%, Aldrich), and thymine PNA (Acros). Poly(ethylene glycol) methyl ether methacrylate (PEGMA, Aldrich) with average molecular weight $\overline{M_n}$ = 300 $g.mol^{-1}$ was purified by passing through basic alumina and stored at -4°C after purification. 2-Vinyl-4,4-dimethylazlactone (VDM, 99.4%, ISOCHEM), was distilled *in vacuo* and stored at -15°C after purification. Tris-[2-(dimethylamino) ethyl]amine ($Me_6Tren$) [32] and 2-bromo-2-methyl-*N*-(3-(triethoxysilyl)propyl)propanamide (BTPAm) [21] were prepared according to previously reported procedures. $CH_2Cl_2$ and diethyl ether were dried with $P_2O_5$ and distilled

prior to use. *N*,*N*-dimethylformamide (DMF, Acros), toluene (Acros) and $CDCl_3$ (99%, Euriso-Top) were used as received.

**Characterization**

$^1H$ NMR spectra were obtained from a Bruker AC 200-MHz spectrometer using $CDCl_3$ as a solvent. Molar masses and molar mass distributions were determined *via* size exclusion chromatography (SEC) at 35°C on a system equipped with a Spectra System AS1000 autosampler with a guard column (Polymer Laboratories, PL gel 5 μm guard, 50 × 7.5 mm) followed by two columns (Polymer Laboratories, two PL gel 5 μm Mixed – D columns, 2 × 300 × 7.5 mm). Polystyrene standards (580-483 × $10^3$ $g.mol^{-1}$) were used to calibrate the SEC. Fourier transform infrared (FTIR) analyses were recorded using a Nicolet Avatar 370 DTGS spectrometer in the attenuated total reflection (ATR) mode. Elemental analysis was performed by the Service Central d'Analyses du Centre National de Recherche Scientifique, Gif-sur-Yvette (France). TEM images were taken using a Philips Tecnai 12 operated at 120 kV equipped with Gatan model 782 CCD camera. The particles were re-suspended in toluene or DMF with sonication before deposition on a TEM grid. Magnetic properties of the particles were measured at room temperature using a Standard 7403 Series, Lakeshore vibrating sample magnetometer (VSM). Magnetic moment of each sample was investigated over a range of ± 10000 G of applied magnetic fields using 30 min sweep time. Thermogravimetric analysis (TGA) was performed on SDTA 851 Mettler-Toledo at the temperature ranging between 25-600°C at a heating rate of 20°C/min under oxygen atmosphere. XRD patterns of the particles were collected on a Philips X'pert X-ray diffractometer under $CuK_\alpha$ radiation (λ = 1.540598 Å) operated at 30 kV and 2θ ranging from 0-90°.

**General procedure for the synthesis of poly(PEGMA-*stat*-VDM) copolymers *via* ATRP in solution**

An example of the synthesis of poly(PEGMA-*stat*-VDM) using EBiB/CuBr/$Me_6$Tren/PEGMA/VDM of 1/1/1/50/50 is illustrated. CuBr (0.0287 g, 0.2 mmol) was added to a Schlenk tube equipped with a stir bar. After sealing with a rubber septum, the Schlenk tube was deoxygenated with three vacuum/argon fill cycles. A degassed solution of PEGMA (6 g, 20 mmol), VDM (2.78 g, 20 mmol), toluene (70 % v/v, 6 mL), EBiB (0.039 g, 0.2 mmol) and DMF (5 % v/v, 0.4 mL) (used as an internal standard) was added to the Schlenk tube containing CuBr *via* a cannula. The resulting solution was further degassed

using freeze/pump/thaw cycles *in vacuo*. Degassed $Me_6Tren$ (0.046 g, 0.2 mmol) was added (*t= 0*) to the Schlenk tube and it was then placed in an oil bath preheated to a desired temperature. The samples were withdrawn periodically *via* a degassed syringe for conversion measurements and SEC analyses.

**Synthesis of MNP coated with ATRP initiators (BTPAm-coated MNP)**

BTPAm-coated MNP was prepared *via* a three-step reaction; (1) synthesis of MNP core, (2) coating the MNP with oleic acid and (3) grafting BTPAm onto the oleic acid-coated MNP. MNP was synthesized *via* a thermal decomposition reaction according to the procedure previously reported [33]. Namely, $Fe(acac)_3$ (5 g, 14.05 mmol) and benzyl alcohol (90 mL) were mixed in a three-necked round bottomed flask equipped with a mechanical stirrer and septum. The mixture was set at 180$^{o}$C for 48 h with nitrogen flow. After the reaction, the precipitant was removed from the dispersion using an external magnet and washed with ethanol and $CH_2Cl_2$ repeatedly to remove benzyl alcohol. The particles were then dried at room temperature under reduced pressure. To prepare oleic acid-coated MNP, and MNP-toluene dispersion (0.8 g of dried MNP in 30 mL of toluene) was sonicated for 1 h. Oleic acid (4 mL) was then slowly dropped into the dispersion and sonicated for 3 h under nitrogen atmosphere. To immobilize BTPAm onto the MNP surface, the oleic acid-coated MNP dispersed in toluene was mixed with BTPAm using TEA as a catalyst. The reaction was carried out at room temperature for 24 h under nitrogen atmosphere. The dispersion was precipitated in methanol and washed with toluene to remove oleic acid and ungrafted BTPAm from the dispersion. The Br loading calculated from elemental analysis (%Br = 0.71%) was estimated to $8.89 \times 10^{-2}$ mmol.g$^{-1}$.

**Synthesis of poly(PEGMA-*stat*-VDM)-coated MNP *via* ATRP**

BTPAm-coated MNP dispersed in toluene was sonicated for 20 min and degassed using argon. This suspension was then added to a degassed Schlenk tube containing CuBr, PEGMA, VDM, EBiB (used as a free initiator), and DMF (used as an internal standard) *via* a cannula. Degassed $Me_6Tren$ ligand was added to the above dispersion (*t=0*) and the mixture was set in an oil bath preheated at 30$^{o}$C. The samples were withdrawn periodically *via* a degassed syringe to monitor the monomer conversions *via* $^{1}$H NMR spectroscopy and to determine molecular characteristics of the copolymer *via* SEC analyses. At the end of the copolymerization, the surface-modified MNP were separated from the mixture by external

magnet, precipitated into diethyl ether and dried *in vacuo*. The as-synthesized poly(PEGMA-*stat*-VDM)-coated MNP resulted as a fine black powder.

**Immobilization of thymine PNA monomer on the poly(PEGMA-*stat*-VDM)-coated MNP**

The synthesis procedure of thymine PNA monomer is explained in details in the supporting information. Thymine PNA monomer (10 mg) was added into a dispersion of poly(PEGMA-*stat*-VDM)-coated MNP (10 mg) in DMF (10 mL). The mixture was sonicated at room temperature for 6 h under argon atmosphere. The particle was then collected using an external magnet and washed with DMF repeatedly to remove ungrafted thymine PNA monomer from the particle surface.

**Results and discussion**

**Synthesis of poly(PEGMA-*stat*-VDM) *via* ATRP in solution**

In the present work, a statistical copolymer of PEGMA and VDM was first synthesized in toluene using CuBr/$Me_6$Tren catalytic complex in the presence of EBiB as an initiator. CuBr and $Me_6$Tren were selected as a catalytic complex in the present work. Fontaine *et al*. have reported that using $Me_6$Tren ligand led to a good control in polymerization of VDM: the experimental molecular weights were comparable to the theoretical values and narrow polydispersities were obtained [34]. Molar ratio of CuBr/$Me_6$Tren/EBiB was studied in order to determine the best experimental conditions to obtain a good control in molecular weight and molecular weight distribution. The selected reaction conditions would then be used for surface-initiated ATRP of PEGMA and VDM from magnetite nanoparticles, which would be then used for immobilizing thymine PNA monomer on their surface.

A EBiB/CuBr/$Me_6$Tren molar ratio of 1/1/1 has successfully been used in our group to synthesize well-defined (co)polymers based on VDM in solution [34]. Therefore, in this work, poly(PEGMA-*stat*-VDM) was synthesized *via* ATRP of PEGMA and VDM monomers using the same catalytic/initiator system and similar catalyst/ligand ratios. Table 1 shows the summary of the statistical copolymerizations of 50/50/1 molar ratio of PEGMA/VDM/EBiB at various CuBr/$Me_6$Tren ratios.

**Table 1.** ATRP of mixtures of PEGMA and VDM using various molar ratios of EBiB initiator and CuBr/$Me_6$Tren catalytic complexes in toluene.

| entry | EBiB/CuBr /$Me_6$Tren | Temp ($^oC$) | time (min) | conv[a] (%) | | $\overline{M_n}_{,th}$[b] (g/mol) | $\overline{M_n}_{,SEC}$[c] (g/mol) | $PDI$[c] |
|---|---|---|---|---|---|---|---|---|
| | | | | PEGMA | VDM | | | |
| 1 | 1/1/1 | 50 | 30 | 83 | 90 | 18705 | 29400 | 2.17 |
| 2 | 1/0.5/0.5 | 30 | 90 | 70 | 82 | 16199 | 18600 | 1.72 |
| 3 | 1/0.2/0.2 | 30 | 90 | 52 | 61 | 12039 | 14400 | 1.35 |

[a] Calculated *via* $^1$H NMR spectroscopy.

[b] $\overline{M_n}_{,th}$ = ([PEGMA]$_0$/[EBiB]$_0$ × conv.$_{PEGMA}$ × $M_{PEGMA}$) + ([VDM]$_0$/[EBiB]$_0$ × conv.$_{VDM}$ × $M_{VDM}$).

[c] Measured *via* SEC (calibrated with polystyrene standard).

A preliminary experiment was performed in toluene at 50$^o$C using [EBiB]$_0$/ [CuBr]$_0$/[$Me_6$Tren]$_0$ ratio of 1/1/1 (entry 1, Table 1). Figure 1 shows that conversions of PEGMA and VDM reached 83% and 90%, respectively, after 30 min of polymerization time. Moreover, the ln([M]$_0$/[M]) *vs* time plot shows a curvature and reaches a plateau after 30 min of the reaction, indicating the presence of irreversible terminations. This phenomenon is confirmed by the relative broad polydispersity indices obtained (PDIs = 2.17) (Figure 2). A decrease of [EBiB]$_0$/[CuBr]$_0$/[$Me_6$Tren]$_0$ ratio to 1/0.5/0.5 and a decrease of the reaction temperature to 30$^o$C resulted in a decrease of PEGMA and VDM conversion to 70 % and 82 %, respectively (after 90 min, entry 2, Table 1 and Figure 3). However, the polydispersity indices were still high (PDIs = 1.40-2.19) for a controlled radical polymerization (Figure 4). In addition, the ln([M]$_0$/[M]) *vs* time plot again shows a decrease of active species concentration, which is compatible with the presence of irreversible terminations (Figure 3).

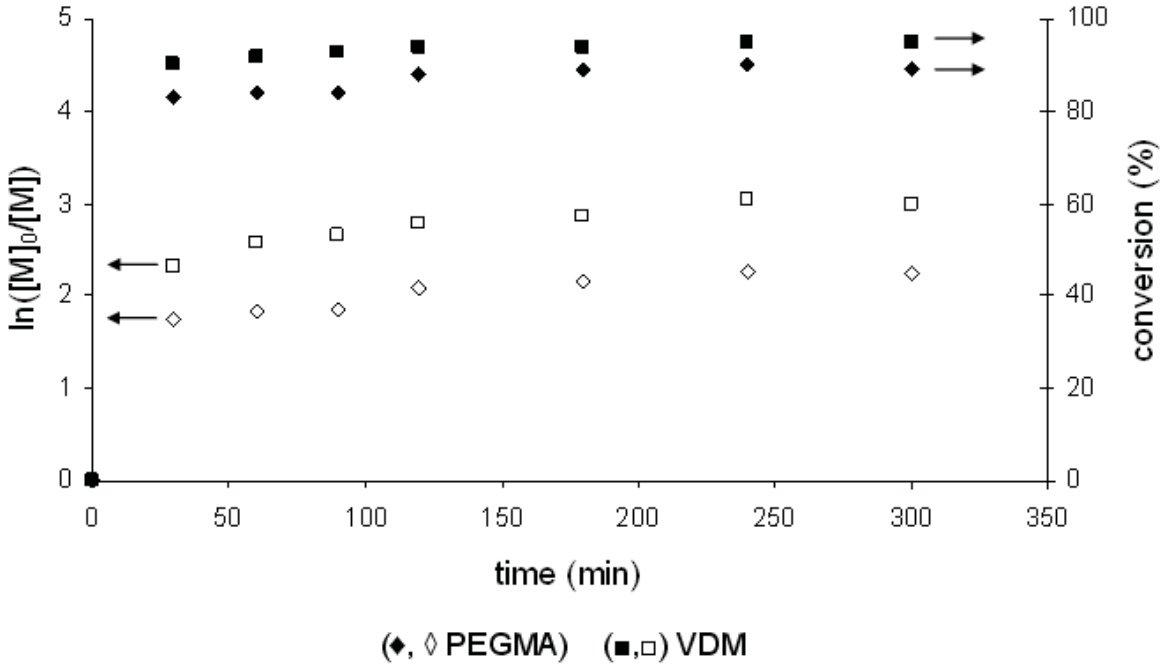


**Figure 1.** The $\ln([M]_0/[M])$ *vs* time plot and monomers conversions *vs* time plot of ATRP of PEGMA and VDM using $[PEGMA]_0/[VDM]_0/[EBiB]_0/[CuBr]_0/[Me_6Tren]_0$ molar ratio = 50/50/1/1/1, in toluene at 50°C.

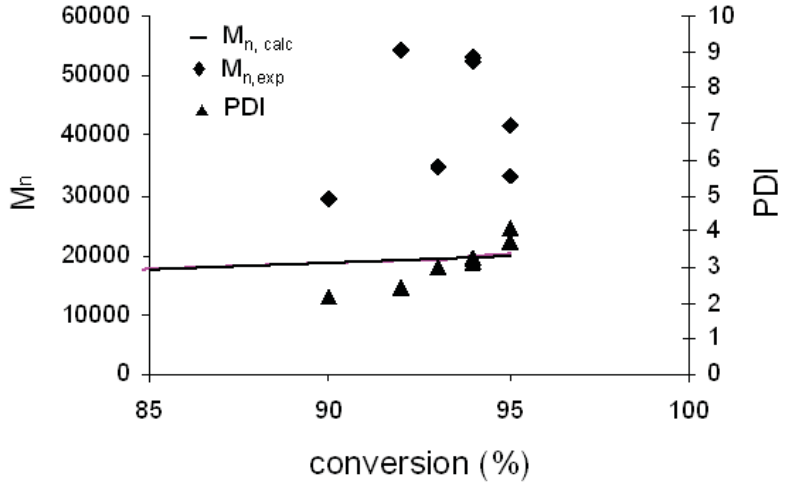


**Figure 2.** Dependence of $\overline{M_n}$ and $\overline{M_w}/\overline{M_n}$ (PDI) with monomer conversion of ATRP of PEGMA and VDM using $[PEGMA]_0/[VDM]_0/[EBiB]_0/[CuBr]_0/[Me_6Tren]_0$ molar ratio = 50/50/1/1/1, in toluene at 50°C.

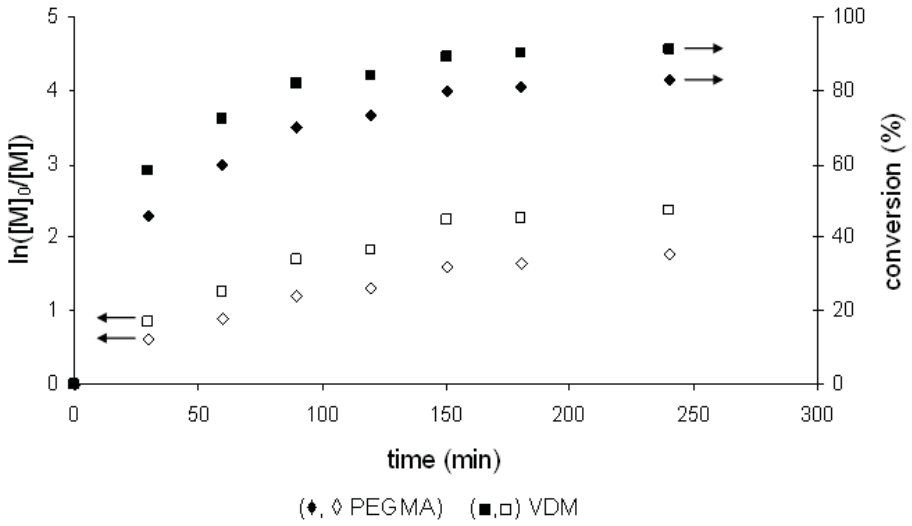


**Figure 3.** The ln([M]$_0$/[M]) *vs* time plot and monomers conversions *vs* time plot of ATRP of PEGMA and VDM using [PEGMA]$_0$/[VDM]$_0$/[EBiB]$_0$/[CuBr]$_0$/[Me$_6$Tren]$_0$ molar ratio = 50/50/1/0.5/0.5, in toluene at 30$^o$C.

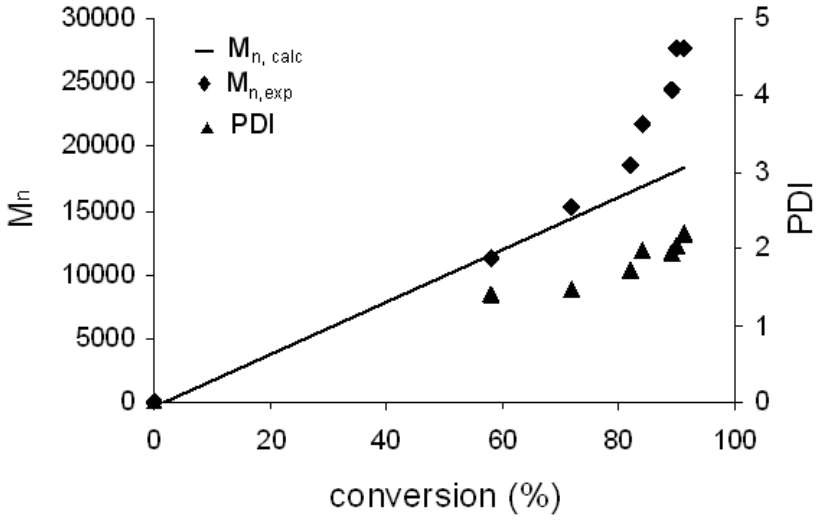


**Figure 4.** Dependence of $\overline{M_n}$ and $\overline{M_w}/\overline{M_n}$ (PDI) with monomer conversion of ATRP of PEGMA and VDM using [PEGMA]$_0$/[VDM]$_0$/[EBiB]$_0$/[CuBr]$_0$/[Me$_6$Tren]$_0$ molar ratio = 50/50/1/0.5/0.5, in toluene at 30$^o$C

When a 1/0.2/0.2 molar ratio of [EBiB]$_0$/[CuBr]$_0$/[Me$_6$Tren]$_0$ was used, the ln([M]$_0$/[M]) *vs* time plot was linear at the beginning, indicating that the concentration of active species was constant in the first step of the polymerization (Figure 5). At 90 min, 52 %

of PEGMA conversion and 61% of VDM conversion were reached (entry 3, Table 1). The polydispersity index in this case decreased to 1.35 and the $\overline{M_n}$ values increased with the monomer conversion, and they are somewhat closed to the theoretical values (Figure 6). This experiment clearly shows that a decrease of the catalytic complex-to-initiator ratio allows a better control of the ATRP of PEGMA and VDM in toluene.

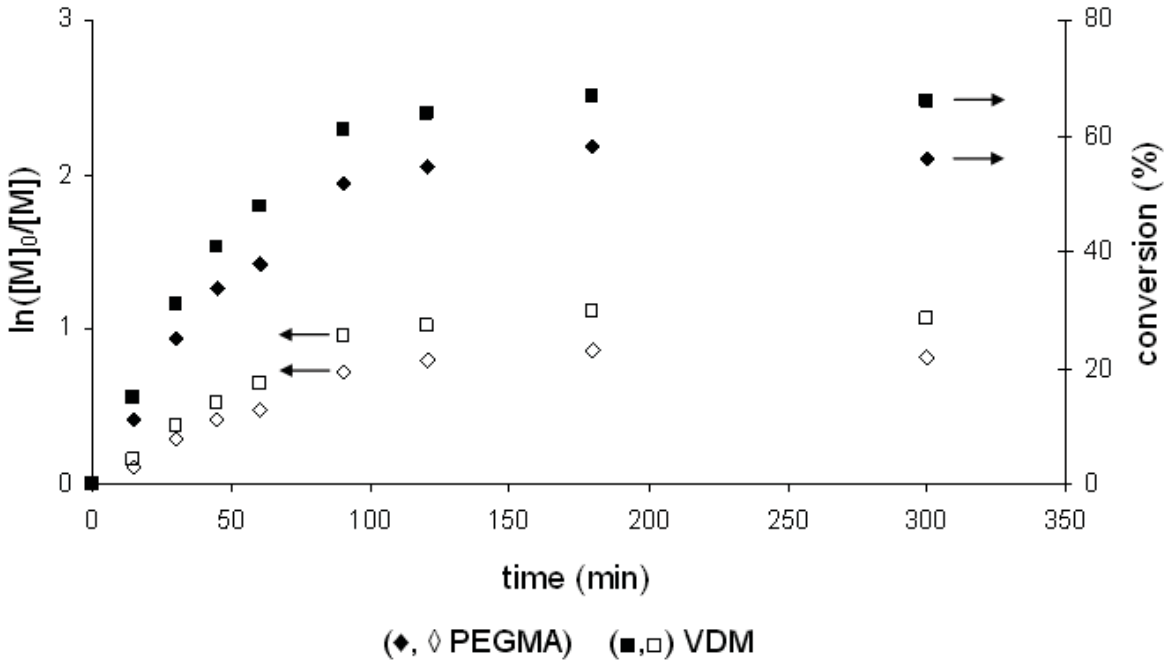


**Figure 5.** The ln([M]$_0$/[M]) *vs* time plot and monomers conversion *vs* time plot of ATRP of PEGMA and VDM using [PEGMA]$_0$/[VDM]$_0$/[EBiB]$_0$/[CuBr]$_0$/[Me$_6$Tren]$_0$ molar ratio = 50/50/1/0.2/0.2, in toluene at 30°C.

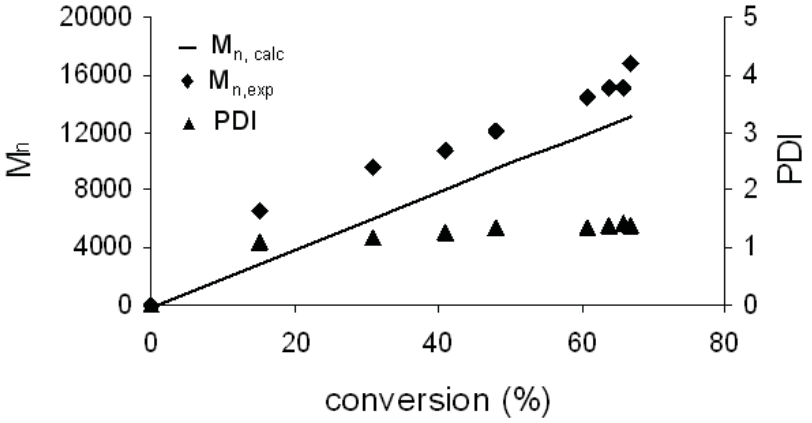


**Figure 6.** Dependence of $\overline{M_n}$ and $\overline{M_w}/\overline{M_n}$ (PDI) with monomer conversion of ATRP of PEGMA and VDM using $[PEGMA]_0/[VDM]_0/[EBiB]_0/[CuBr]_0/[Me_6Tren]_0$ molar ratio = 50/50/1/0.2/0.2, in toluene at 30°C.

**Preparation of poly(PEGMA-*stat*-VDM)-coated MNP *via* ATRP**

To perform ATRP from MNP surface, 2-bromo-2-methyl-*N*-(3-(triethoxysilyl)propyl)propanamide (BTPAm), a molecule containing an ATRP initiating site, was first immobilized onto the particle surface *via* silanization reaction using the triethoxy silane group of BTPAm. FTIR spectrum of BTPAm-coated MNP shows characteristic absorption signals of BTPAm: C-O (1111-1109 $cm^{-1}$), N-H (3346 $cm^{-1}$), NH-CO (1643 $cm^{-1}$), indicating the anchorage of BTPAm (Figure 7B). Elemental analysis indicated the presence of 0.71% Br in the MNP, corresponding to $8.89 \times 10^{-2}$ mmol Br per gram of MNP.

Then, to prepare statistical copolymers based on PEGMA and VDM grafted onto MNP surface, the optimal condition established previously for ATRP in solution were used. Because the MNP-supported copolymers were undetectable in NMR technique, the free initiator EBiB (also called "sacrificial" initiator) was added to the reaction to easily monitor the reaction progress. Such a strategy was previously applied to VDM monomer by our group [24]. Therefore, monomer conversions and copolymer compositions, discussed in the latter section, were investigated from the free copolymers *via* NMR spectroscopy. The reaction was carried out in toluene at 30°C using $[PEGMA]_0/[VDM]_0/[EBiB]_0/[BTPAm\text{-coated MNP}]_0/[CuBr]_0/[Me_6Tren]_0$ in a 100/100/1/1/0.4/0.4 molar ratio. This molar ratio was adjusted in accordance with the fact that there were both ATRP initiating sites (BTPAm)

grafted on particle surface and a free initiator (EBiB) in this system. After the ATRP reactions, the particles in the dispersion were magnetically separated from the mixture. The aggregate was used in FTIR and VSM characterizations, and the supernatant containing the free copolymers was used in SEC and NMR analyses.

Figure 7C shows FTIR spectrum of poly(PEGMA-*stat*-VDM)-coated MNP compared with those of bare MNP (Figure 7A) and BTPAm-coated MNP (Figure 7B). Poly(PEGMA-*stat*-VDM)-coated MNP exhibited a characteristic signal of azlactone rings of VDM units at 1816 $cm^{-1}$ (-C=O stretching), 1203 $cm^{-1}$ (C-O-C stretching) and that of PEGMA at 1722 $cm^{-1}$ (-C=O stretching) (Figure 7C), indicating the presence of the copolymer in the complex. A broad and strong band of Fe-O from MNP cores was also observed at 578 $cm^{-1}$.

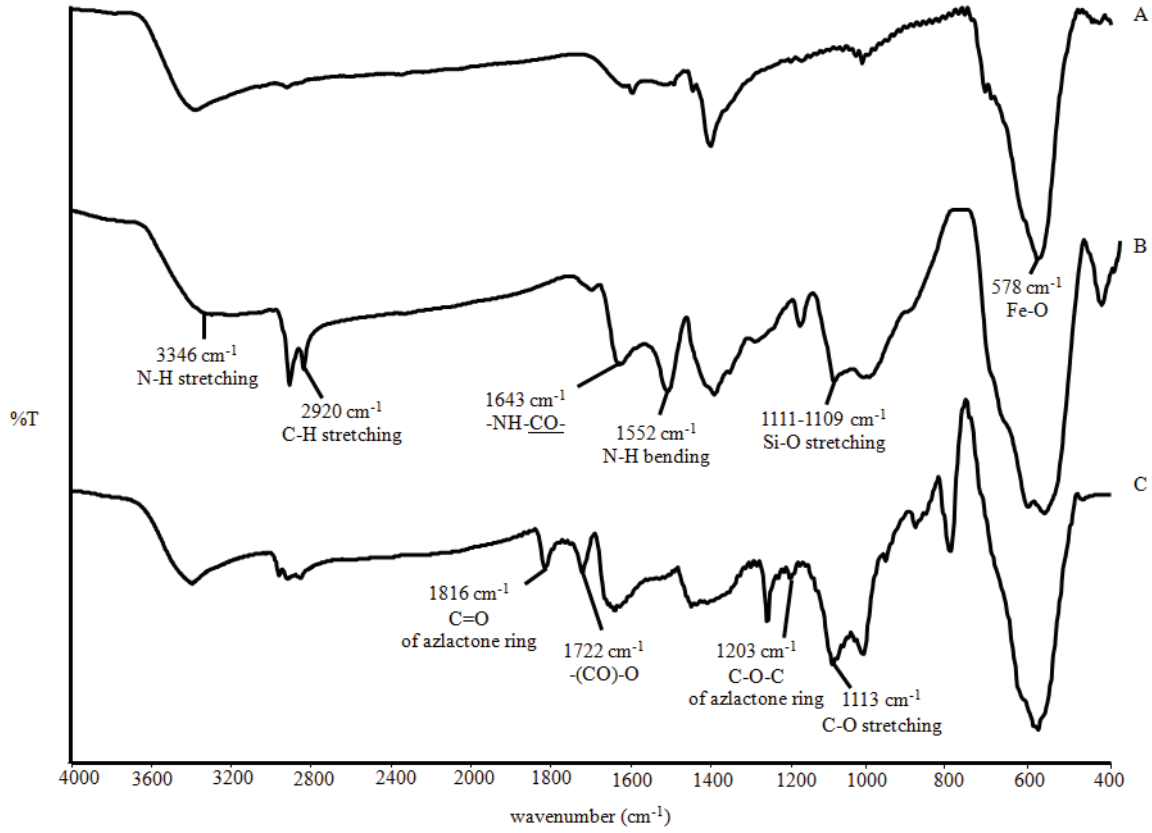


**Figure 7.** FTIR spectra of (A) bare MNP, (B) BTPAm-coated MNP and (C) poly(PEGMA-*stat*-VDM)-coated MNP

Table 2 shows the monomer conversion, $\overline{M_n}$ and polydispersity indices (PDI) of poly(PEGMA-*stat*-VDM) produced by the free initiator. It was found that the monomer conversions of PEGMA and VDM in BTPAm-coated MNP reached 24% and 29%,

respectively, after 24 h of reaction, while those in the solution system with the same reaction conditions proceeded in a much shorter time (25% and 31%, respectively, in 30 min reaction) (see Table S3 in the supporting information). This phenomenon has been previously observed in the surface-initiated ATRP of VDM from the Wang resin solid support [24]. $\overline{M_n}$ gradually increased when the reaction conversions increased, indicating the growth of the copolymer chains. In all cases, the $\overline{M_{n,SEC}}$ values were higher than the theoretical ones and their distributions were narrow (PDIs = 1.09-1.21) throughout the reaction (Table 2).

**Table 2.** Summary of monomers conversions, $\overline{M_n}$, and PDIs of poly(PEGMA-*stat*-VDM) copolymers using 100/100/1/0.4/0.4 molar ratio of $[PEGMA]_0/[VDM]_0/[EBiB]_0/[CuBr]_0/[Me_6Tren]_0$, respectively, in toluene at 30°C

| time (min) | conv[a] (%) | | $\overline{M_{n,th}}$[b] (g/mol) | $\overline{M_{n,SEC}}$[c] (g/mol) | $PDI$[c] |
|---|---|---|---|---|---|
| | PEGMA | VDM | | | |
| 0 | 0 | 0 | 0 | 0 | 0 |
| 30 | 13 | 16 | 3062 | 3800 | 1.20 |
| 45 | 14 | 17 | 3282 | 4100 | 1.21 |
| 60 | 15 | 20 | 3640 | 5400 | 1.19 |
| 90 | 18 | 22 | 4229 | 7700 | 1.14 |
| 120 | 18 | 25 | 4438 | 7900 | 1.13 |
| 150 | 20 | 24 | 4668 | 8000 | 1.13 |
| 180 | 22 | 28 | 5246 | 8100 | 1.13 |
| 1440 | 24 | 29 | 5616 | 8300 | 1.09 |

[a] Determined *via* $^1$H NMR spectroscopy (monomer depletion monitored relative to DMF used as an internal standard). [b] $\overline{M_{n,th}} = ([PEGMA]_0/[EBiB]_0 \times conv._{PEGMA} \times M_{PEGMA}) + ([VDM]_0/[EBiB]_0 \times conv._{VDM} \times M_{VDM})$. [c] Measured by SEC (calibrated with polystyrene standard).

**Immobilization of thymine PNA monomer on poly(PEGMA-*stat*-VDM)-coated MNP**

The as-synthesized poly(PEGMA-*stat*-VDM)-coated MNP containing active azlactone functional groups were then used as a magnetically guidable-nanoscale amine support. In this study, thymine PNA monomer was selected as a model compound for grafting onto the particle surface. It is anticipated that these novel copolymer-coated MNPs can be used as a nanosolid support for PNA oligomer immobilization. Because precedents have reported the utilization of PNA oligomer as a probe for detection of DNA sequences [35-38], the attachment of PNA oligomers on these copolymer-coated MNP is warrant for further studies.

The immobilization process of thymine PNA monomer on the particle surface was performed in anhydrous DMF at room temperature for 6 h (Scheme 2). Figure 8C shows the disappearance of cyclic carbonyl of azlactone rings at 1816 $cm^{-1}$ [24] and the appearance of a signal at 1159 $cm^{-1}$ corresponding to a C-H stretching of thymine [39], indicating the presence of thymine PNA monomer in the complex.

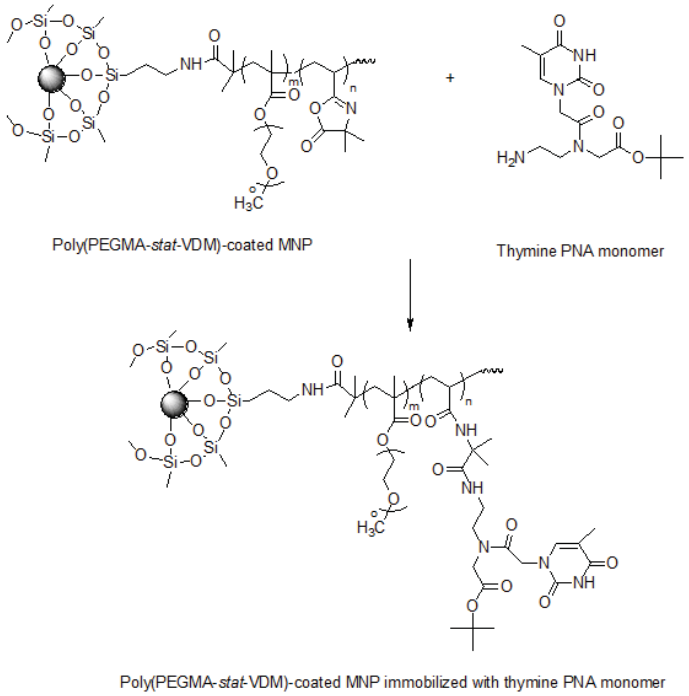


**Scheme 2** Immobilization of thymine PNA monomer onto poly(PEGMA-*stat*-VDM)-coated MNP

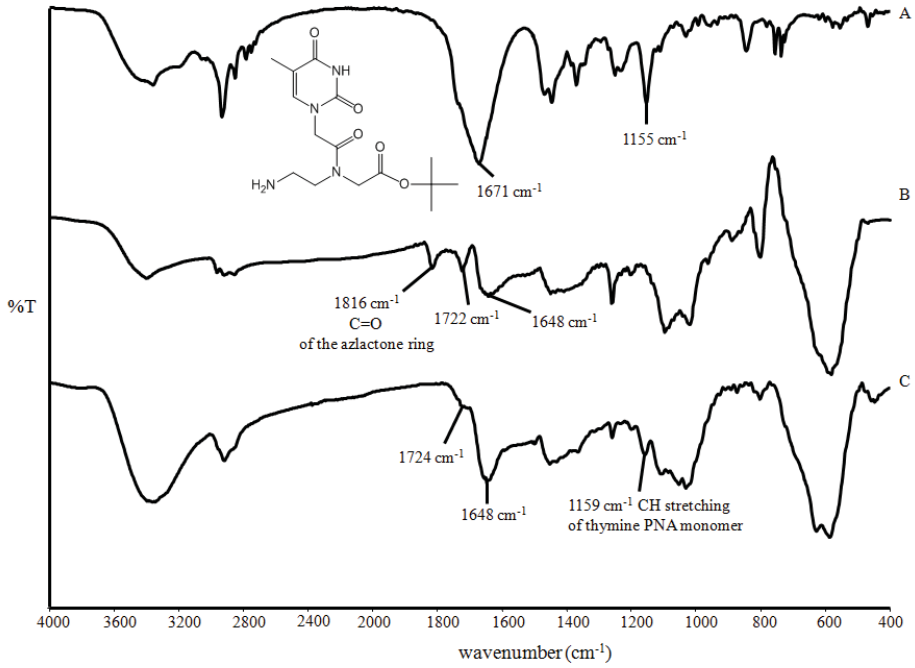


**Figure 8.** FTIR spectra of (A) thymine PNA monomer, (B) poly(PEGMA-*stat*-VDM)-coated MNP and (C) poly(PEGMA-*stat*-VDM)-coated MNP immobilized with thymine PNA monomer

TEM images of MNP complexes at each step of the reaction are shown in Figure 9. Bare MNP was not well dispersible in any solvent due to the lack of polymer coating; TEM experiments were not performed on bare MNP sample. After coating with oleic acid, the particles were well dispersible in toluene. Therefore, the TEM image shown in Figure 9A was prepared from the particle dispersion in toluene. The particle size was in the range of 7-14 nm with the average diameter of 9 nm. After surface modification of the particle with poly(PEGMA-*stat*-VDM) in DMF, there was some nanoscale aggregation of about 30-50 particles/cluster (Figure 9B). After immobilization of thymine PNA monomer on their surface, more aggregation of the particles was observed (about 100 particles/cluster) (Figure 9C). The presence of hydrophobic thymine PNA monomer units on surface of the complexes might promote the particle aggregation in DMF. Although there was some nano-aggregation observed in TEM, these complexes were still visually re-dispersible in various solvents, such as THF, DMF and toluene, probably due to the presence of the polymeric thin film on their surface. A TEM image showing the presence of polymeric thin films on the particle surface was illustrated in the supporting information.

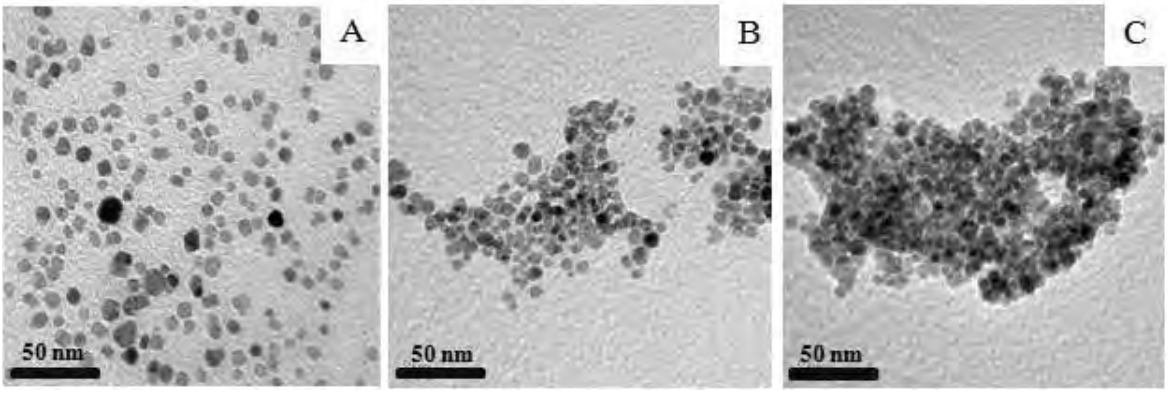


**Figure 9**. TEM images of (A) oleic acid-coated MNP (prepared from toluene dispersion), (B) poly(PEGMA-*stat*-VDM)-coated MNP (prepared from DMF dispersion) and (C) poly(PEGMA-*stat*-VDM)-coated MNP immobilized with thymine PNA monomer (prepared from DMF dispersion)

TGA studies were carried out to determine the mass loss of the organic components in the grafted-MNP. The MNP complexes in each step of the reaction showed their distinctive TGA curves, giving rise to the information of the amount of BTPAm, poly(PEGMA-*stat*-VDM) and thymine PNA monomer in the grafted-MNP (Figure 10). The slight loss in mass of bare MNP was attributed to the residual benzyl alcohol used as the reaction solvent in the MNP preparation step. According to the TGA results, there were about 6 wt% of BTPAm and 17 wt% of poly(PEGMA-*stat*-VDM) copolymer in the complexes. After the immobilization step of thymine PNA monomer, an increase in weight loss as compared to the one before the grafting reaction was observed (Figure 10D), indicating that there were about 4 wt% thymine PNA monomer grafted to the grafted-MNP. This number corresponds to about 1.2 μmol of thymine PNA monomer per gram of the grafted-MNP (An example of the calculation is show in the supporting information). This was a supportive result to FTIR that thymine PNA monomer existed in the copolymer-coated MNP.

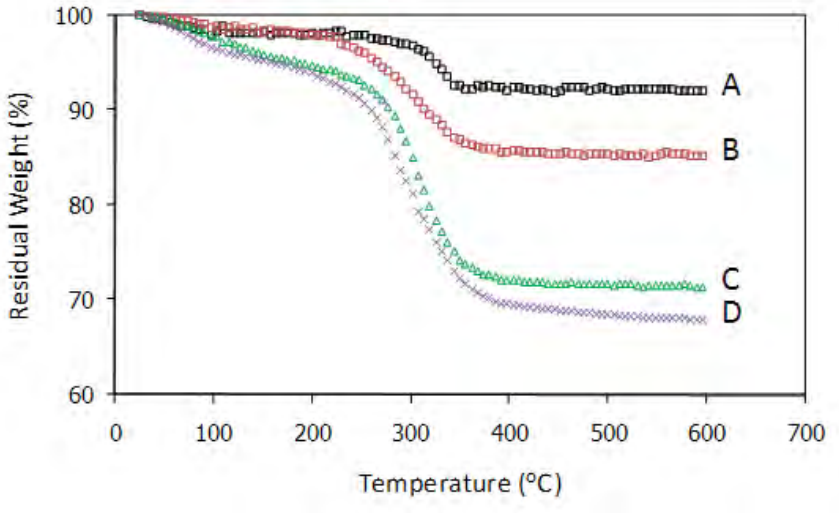


**Figure 10**. TGA curves of (A) bare MNP, (B) BTPAm-coated MNP, (C) poly(PEGMA-*stat*-VDM)-coated MNP and (D) poly(PEGMA-*stat*-VDM)-coated MNP immobilized with thymine PNA monomer

The *M-H* curves measured at room temperature of the particles in each step of the reaction are illustrated in Figure 11. As illustrated in the inset, all samples showed no hysteresis at room temperature. The decrease of saturation magnetization ($M_s$) from 56 emu/g of bare MNP to 49 emu/g of BTPAm-coated MNP was attributable to the presence of BTPAm thin layer on the particle surface, resulting in the decrease of the percentage of MNP core in the complex (Figure 11). Likewise, the $M_s$ values of poly(PEGMA-*stat*-VDM)-coated MNP (36 emu/g) and poly(PEGMA-*stat*-VDM)-coated MNP immobilized with thymine PNA monomer (34 emu/g) were significantly lower than those of the BTPAm-coated MNP, which was again devoted to the decrease of MNP content in the complexes owing to the copolymer/thymine coating. This was in good agreement with the FTIR result indicating the presence of the copolymer in the complex. When taking the percentage of magnetite in the complex into account, the $M_s$ values in emu/g magnetite basis were in the range of 46-56 emu/g magnetite (see Table S4 in the supporting information). The slight drop in the $M_s$ values in emu/g magnetite basis was attributed to the use of organic solvents, e.g. DMF, in surface modification reactions, which might, to some extent, affect the magnetic properties of MNP core.

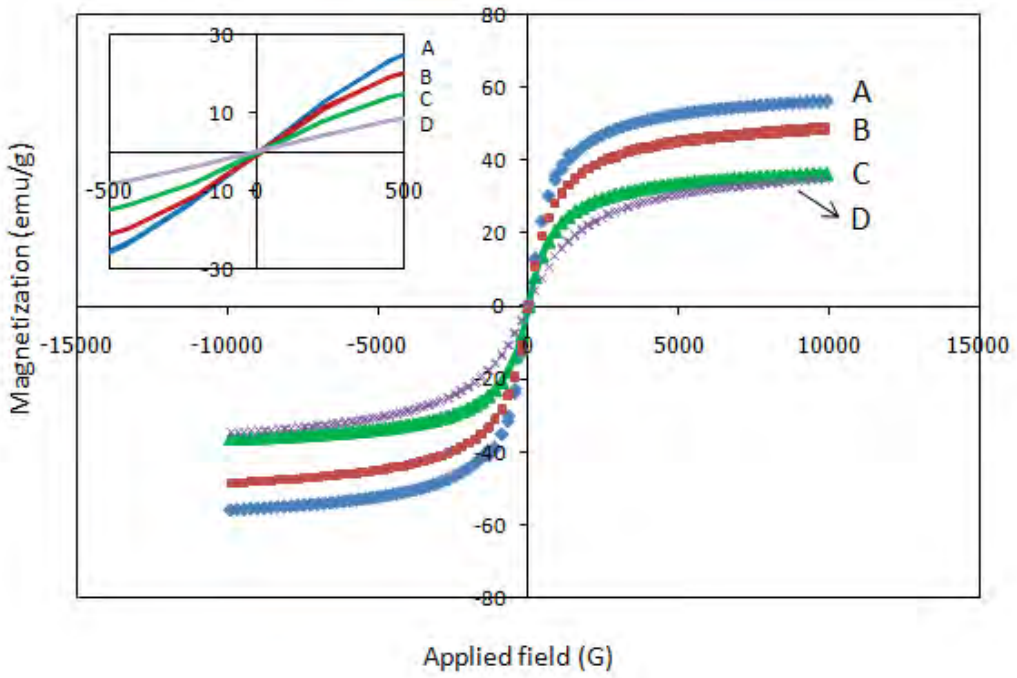


**Figure 11.** *M-H* curves of A) bare MNP, B) BTPAm-coated MNP, C) poly(PEGMA-*stat*-VDM)-coated MNP and (D) poly(PEGMA-*stat*-VDM)-coated MNP immobilized with thymine PNA monomer. The expansion in the range of ±500 G of applied filed is shown in the inset.

The crystal structures of each complex were also investigated. From XRD studies, the position and relative intensities of all diffraction signals of bare MNP and poly(PEGMA-*stat*-VDM)-coated MNP matched well with the characteristic peaks of magnetite crystal [40] (2θ = 30.2°, 35.6°, 43.3°, 53.7°, 57.2° and 62.7°) obtained from the standard $Fe_3O_4$ powder diffraction data (see Figure S10 in the supporting information). Due to the limited amount of the as-synthesized poly(PEGMA-*stat*-VDM)-coated MNP immobilized with thymine PNA monomer, determination of its crystal structure *via* the XRD technique was not possible. Selected area electron diffraction (SAED) was thus performed to study the crystal structure information of the MNP immobilized with thymine PNA monomer (see Figure S11 in the supporting information). Its SAED pattern revealed that the particles were crystalline and the *d*-values of the SAED were in good agreement with those observed in $Fe_3O_4$ [41].

## Conclusions

This work presented the surface modification of MNP with the statistical copolymer between PEGMA and VDM *via* ATRP to obtain the particles containing active functional groups on its surface. Hydrophilic PEGMA promoted good dispersibility to the particle in polar solvents and azlactone rings served as active functional groups for further chemical attachment with nucleophiles of interest. Surface-initiated ATRP of the copolymer *vi*a a "grafting from" strategy from the particle produced the active polymer layer with a predicable and controllable fashion. The nanosolid supports were successfully used for immobilization of thymine PNA monomers on its surface. The results signified the feasibility to functionalize the surface of these novel azlactone-based nanoparticles with a broad range of other nucleophilic scavengers such as hydroxyl- and thiol-containing compounds.

## Acknowledgement

The authors thank the Thailand Research Fund (TRF) and Naresuan University (DBG5380001) for financial funding. We also thank the Franco-Thai Cooperation Program in Higher Education and Research 2009-2010, supported by the Ministry of Foreign Affairs, Ministry of Higher Education and Research of France and the Commission on Higher Education of Thailand and PHC grant (PHC 2009-2010 n° 20609UF**)**. YP specially acknowledges the Royal Golden Jubilee for the scholarship (PHD/0207/2551). The Center of Excellence for Innovation in Chemistry (PERCH-CIC), Commission on Higher Education, Ministry of Education is also gratefully acknowledged for financial support.

**References**

[1] Singh A, Dilnawaz F, Mewar S, Sharma U, Jagannathan NR, Sahoo SK. ACS Appl Mater 2011;3:842-56.

[2] Chen HH, Josephson L, Josephson DE. WIREs Nanomed Nanobiotechnol 2011;3: 86-99.

[3] Valero E, Tambalo S, Marzola P, Ortega-Muñoz M, López-Jaramillo FJ, Sanoyo-González F, López J, Delgado JJ, Calvino JJ, Cuesta R, Domínguez-Vera JM, Gálvez N. J Am Chem Soc 2011;133:4889-95.

[4] Yu C, YunPeng B, Bao T, ZhaoLong L. Chin Sci Bull 2009;54:1190-6.

[5] Ruiz-Hernández E, Baeza A, Vallet-Regı´ M. ACS Nano 2011;5:1259-66.

[6] Ponvel KM, Lee DG, Woo EJ, Ahn IS, Lee CH. Korean J Chem Eng; 2009;26:127-130.

[7] Johnson AK, Zawadzka AM, Deobald LA, Crawford RL, Paszczynski AJ. J Nanopart Res 2008;10:1009-25.

[8] Park HJ, McConnell JT, Boddohi S, Kipper MJ, Johnson PA. Colloids Surf B 2011;83:198-203.

[9] Sarkar TR, Irudayaraj J. Anal Biochem 2008; 379:130-2.

[10] Kang K, Choi J, Nam JH, Lee SC, Kim KJ, Lee SW, Chang JH. J Phys Chem B 2009;113:536-43.

[11] Park ME, Chang JH. Mater Sci Eng C 2007;27:1232-5.

[12] Ito A, Matsuoka F, Honda H, Kobayashi T. Cancer Gene Ther 2003;10:918-25.

[13] Morishita N, Nakagami H, Morishita R, Takeda S, Mishima F, Terazono B, Nishijima S, Kaneda Y, Tanaka N. Biochem Biophys Res Commun 2005;334:1121-6.

[14] Hayashi K, Moriya M, Sakamoto W, Yogo T. Chem Mater 2009;21: 1318-25.

[15] Beyaz S, Tanrisever T, Kockar H. Macromol Res 2010; 18:1154-9.

[16] Ko SW, Hong MK, Choi HJ, Ryu BH. IEEE Trans Magn 2009;45: 2503-6.

[17] Cai J, Guo J, Ji M, Yang W, Wang C, Fu S. Colloid Polym Sci 2007;285:1607-15.

[18] Wan S, Huang J, Yan H, Liu K. J Mater Chem 2006;16:298-303.

[19] Marutani1 E, Yamamoto S, Ninjbadgar T, Tsujii Y, Fukuda T, Takano M. Polymer 2004;45:2231-5.

[20] Zhou Y, Wang S, Ding B, Yang Z. Chem Eng J 2008;138:578-85.

[21] Sun Y, Ding X, Zheng Z, Cheng X, Hu X, Peng Y. Eur Polym J 2007;43:762-72.

[22] Heilmann SM, Rasmussen JK, Krepski LR, J. Polym. Sci. Part A. Polym. Chem 2001; 39: 3655-77.

[23] Guyomard A, Fournier D, Pascual S, Fontaine L, Bardeau J-F. Eur. Polym. J 2004;40: 2343-48.

[24] Fournier D, Pascual S, Montembault V, Haddleton DM, Fontaine L. J Comb Chem 2006;8:522-30.

[25] Lucchesi C, Pascual S, Dujardin G, Fontaine L. React Funct Polym 2008; 68: 97-102.

[26] Drtina G J, Heilmann S M, Moren D M, Rasmussen J K, Krespski L R, Smith H K, Pranis R A, Turek T C. Macromolecules 1996; 29: 4486-89.

[27] Tripp JA, Stein JA, Svec F, Fréchet J M J. Org. Lett 2000; 2: 195-8.

[28] Tripp JA, Svec F, Fréchet J M J. J. Comb. Chem 2001; 3:216-223.

[29] Messman JM, Lokitz BS, Pickel JM, Kilbey II SM. Macromolecules 2009; 42: 3933-41.

[30] Cullen SP, Mandel IC, Gopalan P. Langmuir 2008;24:13701-9.

[31] Coleman PL, Walker MW, Milbrath DS, Stauffer DM, Rasmussen JK, Krepski LR, Heilmann SM. J Chromatogr A 1190;512:345-63.

[32] Ciampolini M, Nardi N. Inorg Chem 1966; 5: 41.

[33] Rutnakornpituk M, Puangsin N, Theamdee P, Rutnakornpituk B, Wichai U. Polymer 2011;52:987-95.

[34] Fournier D, Pascual S, Fontaine L. Macromolecules 2004;37:330-5.

[35] Ananthanawat C, Vilaivan T, Hoven VP, Su X. Biosens Bioelectron 2010;25:1064-9.

[36] Huang B, Hou J, Lin S, Chen J, Hong H. Harmful Algae 2008;7:495-503.

[37] Masuko M. Nucleic Acids Res 2003;3:145-6.

[38] Perry-O'Keefe H, Rigby S, Oliveira K, Sørensen D, Stender H, Coull J, Hyldig-Nielsen J.J. J Microbiol Methods 2001;47: 281-92.

[39] Singh JS. J Mol Struct 2008;876: 127-133.

[40] Bomat-Miguel O, Tartaj P, Morales MP, Bonville P, Golla-Schindler U, Zhao XQ, Veintemillas-Verdaguer S. Small 2006;2:1476-83.

[41] Moisescu C, Bonneville S, Tobler D, Ardelean I, Benning LG. Mineral Mag 2008;72:333–336.

## Supporting Information

### Part 1. Synthesis of tris-[2-(dimethylamino)ethyl]amine ($Me_6$Tren) and 2-bromo-2-methyl-*N*-(3-(triethoxysilyl)propyl)propanamide (BTPAm)

### (A) Synthesis of tris-[2-(dimethylamino)ethyl]amine ($Me_6$Tren) (Figure S1)

Tris-(2-aminoethyl)amine (Tren) (10 mL, 0.33 mol, 1 equiv.) was slowly dropped into the mixture of formic acid (64 mL, 6.67 mol, 20 equiv.) and formaldehyde (54 ml, 3.34 mol, 10 equiv.) at 0$^o$C in an ice bath. The mixture was heated to 120$^o$C and stirred under reflux overnight. Unreacted formic acid and formaldehyde were removed by rotary evaporation. Then, the resulting orange oil was adjusted to pH 10 with saturated sodium hydroxide solution. The oil layer was extracted into diethyl methyl ether (four times), and the volatiles removed by rotary evaporation to leave a yellow oil. The resulting oil was distilled under reduced pressure (69$^o$C, 0.5 mmHg) to give a colorless liquid. Yield 84%.

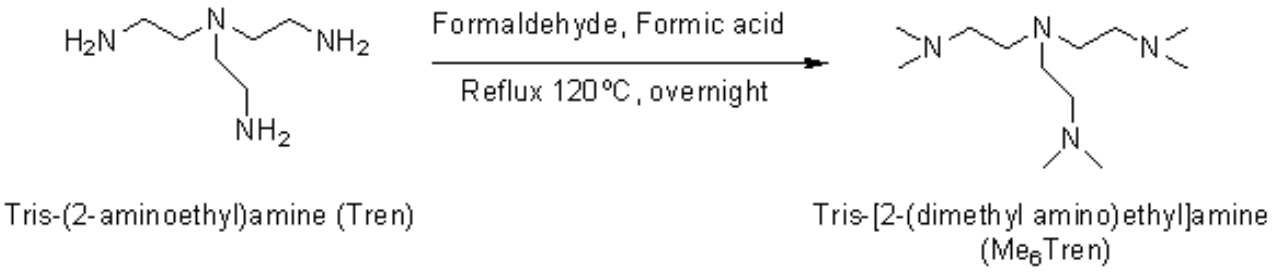


**Figure S1.** Synthesis of tris-(2-(dimethylamino)ethyl)amine ($Me_6$Tren)

Figure S2B showed a $^1$H NMR spectrum of $Me_6$Tren in comparison with that of Tren starting reagent (Figure S2A), the formation of $Me_6$Tren was identified by the presence of the methyl protons at 2.14 ppm (signal *a*). Also, the methylene protons of signal *b* (2.52 ppm) and signal *c* (2.28 ppm) confirmed the formation of $Me_6$Tren.

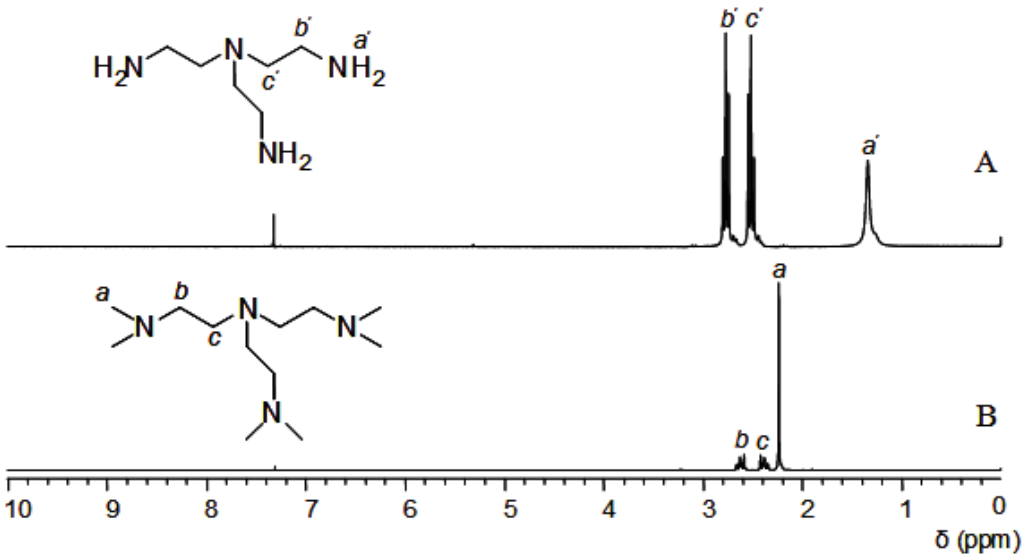


**Figure S2.** $^{1}$H NMR spectra of (A) tris-(2-aminoethyl)amine (Tren) (solvent:$CDCl_3$), and tris-(2-(dimethylamino)ethyl)amine ($Me_6$Tren) (solvent: $CDCl_3$).

**(B) Synthesis of 2-bromo-2-methyl-*N*-(3-(triethoxysilyl)propyl)propanamide (BTPAm) (Figure S3)**

To a stirred solution of 3-aminopropyl triethoxysilane (APS) (0.18 mL, 0.8 mmol) and triethylamine (TEA) (0.12 ml, 0.8 mmol) in dried toluene (10 ml), 2-bromoisobutyryl bromide (BIBB) (0.1 mL, 0.8 mmol) in dried toluene (10 ml) was added dropwise at 0°C for 2 h under nitrogen. The reaction mixture was warmed to room temperature and stirred for 24 h. The mixture was passed through a filter paper to remove salts and the filtrate was evaporated to remove the unreacted TEA under reduced pressure. The resulting product, BTPAm, was yellowish thick liquid (78% yield).

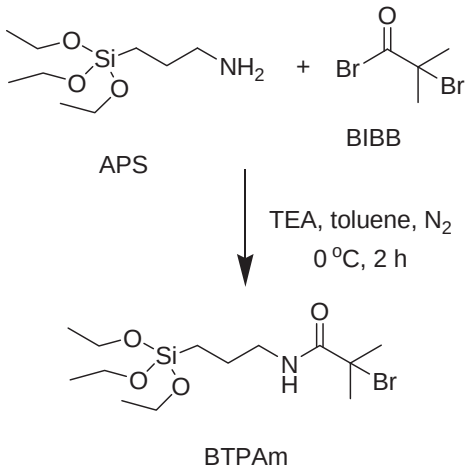


**Figure S3.** Reaction between APS and BIBB to obtain BTPAm

BTPAm was prepared through an amidization reaction between APS and BIBB. Comparing with the FTIR spectra of APS and BIBB, Figure S4C showed FTIR characteristic absorption peaks of BTPAm (1658 $cm^{-1}$ of -NH-CO- carbonyl stretching, 1112-1026 $cm^{-1}$ of Si-O stretching, 1532 $cm^{-1}$ of N-H bending and 3345 $cm^{-1}$ of N-H- stretching). The signal at 1738 $cm^{-1}$ belonging to -(CO)-Br carbonyl stretching indicated the slight remaining of unreacted BIBB after the reaction.

Figure S5C showed a $^{1}H$ NMR spectrum of BTPAm in comparison with APS and BIBB starting reagents. In good agreement with FTIR results, a distinctive shift of the $^{1}H$ NMR signal corresponding to methylene protons adjacent to NH group (from 2.50 ppm, signal *a*, to 3.22 ppm, signal *a'*) indicated the formation of BTPAm. In addition, slight shifts of other signals such as methylene protons of signal *b* (1.45 ppm) to signal *b'* (1.62 ppm), and methyl protons of signal *f* (2.50 ppm) to signal *f'* (2.40 ppm) also confirmed the formation of BTPAm.

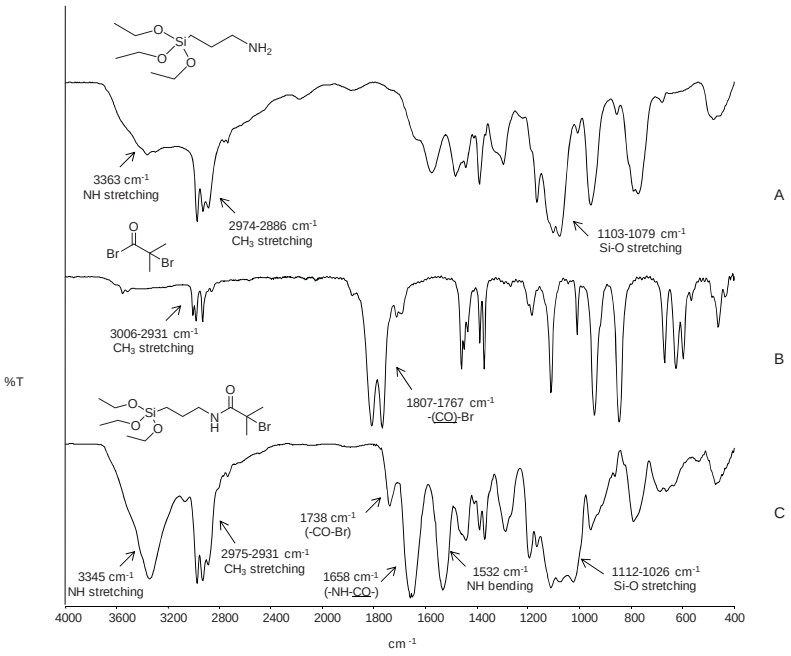


**Figure S4.** FTIR spectra of A) 3-aminopropyl triethoxysilane (APS), B) 2-bromoiso-butyryl bromide (BIBB) and C) (2-bromo-2-methyl-*N*-(3- (triethoxysilyl) propanamide (BTPAm)

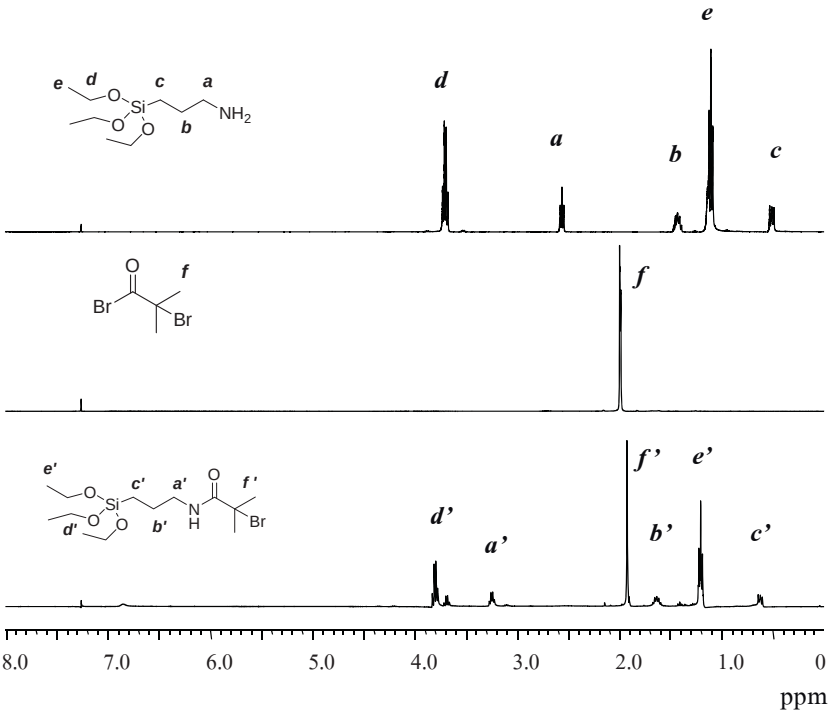


**Figure S5.** $^{1}$H NMR spectra of A) 3-aminopropyl triethoxysilane (APS) (solvent: $CDCl_3$), B) 2-bromoisobutyryl bromide (BIBB) (solvent: $CDCl_3$) and C) (2-bromo-2-methyl-*N*-(3-(triethoxysilyl) propanamide (BTPAm) (solvent: $CDCl_3$)

**Part 2. Synthesis of poly(PEGMA-*stat*-VDM) by ATRP in solution in different reaction conditions**

**(A) Synthesis of poly(PEGMA-*stat*-VDM) by ATRP in solution**

Conditions: $[PEGMA]_0/[VDM]_0/[EBiB]_0/[CuBr]_0/[Me_6Tren]_0$ = 50/50/1/1/1

Temperature: 50°C

Solvent: 70% v/v toluene

Internal standard: 5% v/v DMF

**Table S1** Summary of monomer conversion, molecular weight and PDI of statistical copolymers poly(PEGMA-*stat*-VDM) obtained by ATRP using $[EBiB]_0/[CuBr]_0/[Me_6Tren]_0$ molar ratio = 1/1/1 in toluene (70% v/v) at 50°C.

| time (min) | conv[a] (%) | | $\overline{M_n}_{,th}$[b] (g/mol) | $\overline{M_n}_{,SEC}$[c] (g/mol) | $PDI$[c] |
|---|---|---|---|---|---|
| | PEGMA | VDM | | | |
| 0 | 0 | 0 | 0 | 0 | 0 |
| 30 | 83 | 90 | 18705 | 29400 | 2.17 |
| 60 | 84 | 92 | 18994 | 54200 | 2.44 |
| 90 | 84 | 93 | 19064 | 34800 | 3.00 |
| 120 | 88 | 94 | 19733 | 52200 | 3.12 |
| 180 | 89 | 94 | 53122 | 19900 | 3.28 |
| 240 | 90 | 95 | 33327 | 20100 | 4.09 |
| 300 | 89 | 95 | 41552 | 20000 | 3.71 |

[a] Determined by $^1$H NMR spectroscopy (monomer depletion monitored relative to DMF, which was used as an internal standard). [b] $\overline{M_n}_{,th}$ = ($[PEGMA]_0/[EBiB]_0 \times conv._{PEGMA} \times M_{PEGMA}] + [VDM]_0/[EBiB]_0 \times conv._{VDM} \times M_{VDM}$]). [c] Measured by SEC (calibrated with polystyrene standards).

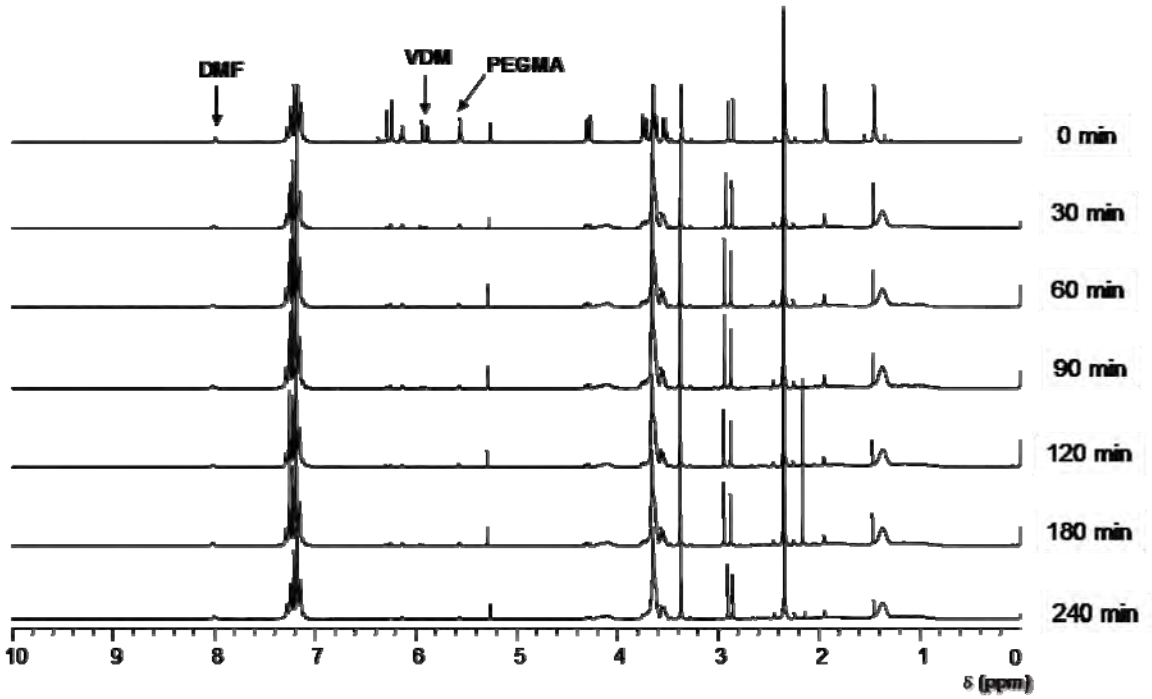


**Figure S6**. Monitoring of monomers conversions by $^{1}$H NMR spectroscopy during atom transfer radical polymerization of PEGMA and VDM using DMF as an internal standard

**(B) Synthesis of poly(PEGMA-*stat*-VDM) by ATRP in solution**

Conditions: $[PEGMA]_0/[VDM]_0/[EBiB]_0/[CuBr]_0/[Me_6Tren]_0$ = 50/50/1/0.5/0.5

Temperature: 30°C

Solvent: 70% v/v toluene

Internal standard: 5% v/v DMF

**Table S2** Summary of monomer conversion, molecular weight, and PDI of statistical copolymers poly(PEGMA-*stat*-VDM) obtained by ATRP using $[EBiB]_0/[CuBr]_0/[Me_6Tren]_0$ ratio = 1/0.5/0.5 in toluene (70% v/v) at 30°C.

| time (min) | conv[a] (%) | | $\overline{M_n}_{,th}$[b] (g/mol) | $\overline{M_n}_{,SEC}$[c] (g/mol) | *PDI*[c] |
|---|---|---|---|---|---|
| | PEGMA | VDM | | | |
| 0 | 0 | 0 | 0 | 0 | 0 |
| 30 | 46 | 58 | 10931 | 11244 | 1.40 |
| 60 | 60 | 72 | 14004 | 15281 | 1.48 |
| 90 | 70 | 82 | 16199 | 18604 | 1.72 |
| 120 | 88 | 94 | 16788 | 21743 | 1.96 |
| 180 | 89 | 94 | 18186 | 24390 | 1.95 |
| 240 | 90 | 95 | 18405 | 27781 | 2.04 |
| 300 | 89 | 95 | 18775 | 27799 | 2.19 |

[a] Determined *via* $^1$H NMR spectroscopy (monomer depletion monitored relative to DMF, which was used as an internal standard). [b] $\overline{M_n}_{,th}$ = ([PEGMA]$_0$/[EBiB]$_0$ × conv.$_{PEGMA}$ × $M_{PEGMA}$] + [VDM]$_0$/[EBiB]$_0$ × conv.$_{VDM}$ × $M_{VDM}$]). [c] Measured by SEC (calibrated with polystyrene standard).

**(C) Synthesis of poly(PEGMA-*stat*-VDM) by ATRP in solution**

Conditions: $[PEGMA]_0/[VDM]_0/[EBiB]_0/[CuBr]_0/[Me_6Tren]_0$ = 50/50/1/0.2/0.2

Temperature: 30°C

Solvent: 70% v/v toluene

Internal standard: 5% v/v DMF

**Table S3** Summary of monomer conversion, molecular weight, and PDI of statistical copolymers poly(PEGMA-*stat*-VDM) obtained by ATRP using $[EBiB]_0/[CuBr]_0/[Me_6Tren]_0$ molar ratio = 1/0.2/0.2 in toluene (70% v/v) at 30°C.

| time (min) | conv[a] (%) | | $\overline{M}_{n,th}$[b] (g/mol) | $\overline{M}_{n,SEC}$[c] (g/mol) | $PDI$[c] |
|---|---|---|---|---|---|
| | PEGMA | VDM | | | |
| 0 | 0 | 0 | 0 | 0 | 0 |
| 15 | 11 | 15 | 2693 | 6500 | 1.11 |
| 30 | 25 | 31 | 5905 | 9500 | 1.17 |
| 45 | 34 | 41 | 7950 | 10800 | 1.24 |
| 60 | 38 | 48 | 9036 | 12200 | 1.33 |
| 90 | 52 | 61 | 12040 | 14400 | 1.35 |
| 120 | 55 | 64 | 12698 | 15200 | 1.40 |
| 180 | 58 | 67 | 13357 | 16700 | 1.39 |
| 300 | 56 | 66 | 12987 | 15100 | 1.43 |

[a] Determined by $^1$H NMR spectroscopy (monomer depletion monitored relative to DMF, which was used as an internal standard). [b] $\overline{M}_{n,th} = ([PEGMA]_0/[EBiB]_0 \times conv._{PEGMA} \times M_{PEGMA}] + [VDM]_0/[EBiB]_0 \times conv._{VDM} \times M_{VDM})$. [c] Measured by SEC (calibrated with polystyrene standard).

**Part 3. Synthesis of thymine PNA monomer and the determination of the grafting density on MNP surface**

**(A) Synthesis of *aeg*PNA backbone**

*(A1) Synthesis of tert-butyl-N-[2-(N-9-fluorenylmethoxycarbonyl)aminoethyl] glycinate hydrochloride **(5)***

To a vigorously stirred solution of ethylenediamine **(1)** (20.38 mL, $3.26\times10^{-1}$ mol) in anh.$CH_2Cl_2$ (130 mL) cooling down to 0 °C with ice bath, *tert*-butyl bromoacetate **(2)** (6.00 mL, $4.08\times10^{-2}$ mol) in anh.$CH_2CI_2$ (70 mL) was added dropwise over a period of 5 h at $0^oC$. The resulting mixture was allowed to warm up and then stirred overnight. The reaction mixture was washed with distilled water (5×60 mL), and the combined aqueous layers were back-extracted with $CH_2CI_2$ (120 mL) and were dried ($Na_2SO_4$) and filtered. Solvent was removed under reduced pressure and then co-evaporated with toluene and was dried *in vacuo* to give *tert*-butyl-*N*-(2-aminoethyl)glycinate **(3)** as a crude product. It was then used for the next step without further purification.

To a solution of **(3)** (3.56 g, $2.04x10^{-2}$mol) in anh.$CH_2CI_2$ (150 mL), diisopropylethylamine (DIEA) (3.22 mL, $1.95 \times 10^{-2}$ mol) was added and stirred 1 h. A solution of *N*-(9-fluorenylmethoxycarbonyloxy)succinimide **(4)** (6.58 g, $4.59\times10^{-2}$ mol) in anh.$CH_2CI_2$ (50 mL) was added dropwise over 5 h. The resulting solution was stirred *ca*. 12 h, and then washed with 1 N aq. HCl (5 × 50 mL) and brine (50 mL). The organic layer was dried ($Na_2SO_4$) and partially concentrated *in vacuo* (*ca*. 1 L). Cooling (*ca*. $-20^oC$) overnight resulted in a precipitate which was collected by filtration and washed with cooled $CH_2Cl_2$ until the filtrate was colorless. The solids were purified by recrystallization in 40% acetone: $CH_2Cl_2$ and drying *in vacuo* to give the HCI salt of **(5)** as a white solid in 30% yield over two steps : $R_f$ = 0.44 (9:1 $CH_2Cl_2$/MeOH) $^1$H NMR 400 MHz (DMSO-$d_6$) δ 9.13 (br s, 2H, NH), 7.90 (d, 2H, *J*=7.5 Hz, Ar), 7.69 (d, 2H, *J*=7.3 Hz, Ar), 7.51 (t, 1H, *J*=5.6 Hz, ), 7.42 (t, 2H, *J*=7.4 Hz, Ar), 7.34 (t, 2H, *J*=7.0 Hz, Ar), 4.35 (d, 2H, *J*=6.7 Hz), 4.23 (t, 1H, *J*=6.6 Hz), 3.87 (s, 2H), 3.29 (m, 2H), 2.99 (t, 2H, *J*=6.0 Hz), 1.46 (s, 9H, $C(CH_3)_3$); $^{13}$C NMR 400 MHz (DMSO-$d_6$) δ 165.7, 156.3, 143.7, 140.7, 127.6, 127.0, 125.1, 120.1, 83.0, 65.6, 54.9, 47.2, 46.6, 36.6, 27.6; HRMS: Calcd. For $C_{23}H_{29}N_2O_4$: *m/z* 397.2127, found *m/z* 397.2120 [M+H]

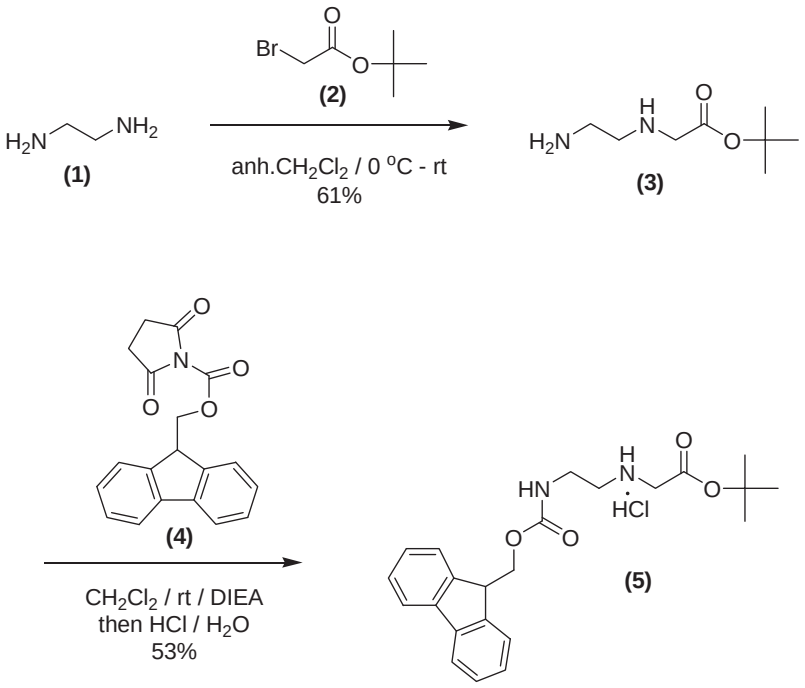


**Figure S7.** Synthesis of *tert*-Butyl *N*-[2-(*N*-9-fluorenylmethoxycarbonyl)aminoethyl] glycinate hydrochloride, *aeg*PNA backbone **(5)**

*(A2) Synthesis of thymine acetic acid*

To a suspension of (**6**) (2.00 g, 15.8 mmol) and potassium *tert*-butoxide (2.13 g, 19.0 mmol) in dry DMF (40 mL) was added methyl bromoacetate (7) (1.74 mL, 19.0 mmol), and the mixture was vigorously stirred overnight under $N_2$. The mixture was filtered and evaporated to dryness *in vacuo*. The solid residue was cooled to 0ºC, treated with water (15 mL) and 2 M HCl (aqueous, 3 mL), and stirred for 30 min. The precipitate was collected by filtration and washed with water (3×10 mL). The precipitate was treated with 4 M NaOH (aqueous, 5 mL) and the mixture was cooled to 0 ºC, treated with 2 M HCl (pH = 2), and stirred for 30 min. The title compound was collected by filtration, washed with water (3×10 mL) and dried *in vacuo* to give of **(8)** as a white solid in 56%yield. $^{1}$H NMR 400 MHz (DMSO-$d_6$) δ 11.33 (s, lH, NH), 7.49 (s, lH, CH), 4.36 (s, 2H, $CH_2$), 1.74 (s, 3H, $CH_3$); $^{13}$C NMR 400 MHz (DMSO-$d_6$) δ 169.5, 164.3, 150.9, 141.8, 108.3, 48.4, 11.8.

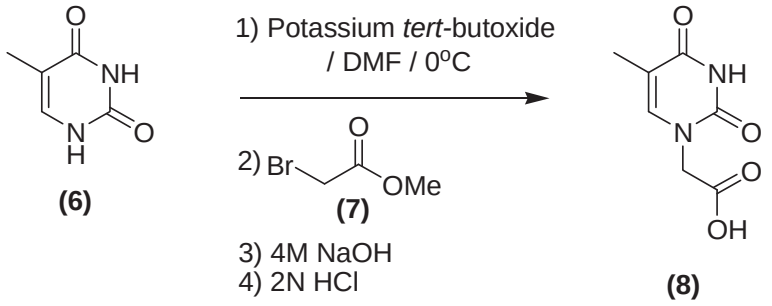


**Figure S8**. Synthesis of thymine acetic acid **(8)**

*(A3) Synthesis of tert-butyl-N-(2-(N-9-fluororenylmrthoxycarbonyl)amino ethyl)-N-((thymin-1-yl)acetyl)glycinate **(9)***

To a solution of **(5)** (1.00 g, 2.3 mmol) in anh. DMF (10 mL) was added the DIEA (0.59 mL, 4.6 mmol) and the mixture was stirred 1 h. After that, thymine acetic acid (8) (0.51 g, 2.76 mmol) was added and stirred until most of acid dissolved. Then, 2,6-lutidine (0.79 mL, 6.90 mmol) and HATU (1.39 g, 3.68 mmol) were added and the mixture was stirred for 4 h. The solution was concentrated *in vacuo*, and brought up with $CH_2Cl_2$, then extracted with saturated $NaHCO_3$ and brine and back extracted water layer with $CH_2Cl_2$ (2×25 mL). Combined organic layers were dried ($Na_2SO_4$) and filtered. The solution was concentrated and triturated with ethyl acetate:diethyl ether, filtered and washed with diethyl ether several times and dried *in vacuo* gave **(9)** 69% yield. $R_f$ = 0.58 (9:1 $CH_2Cl_2$/MeOH); $^1$H NMR 400 MHz ($CDCl_3$) (two rotomers) δ 8.54 (s, lH, NH), 7.75-7.73 (d, *J*=8.1 Hz, 2H, Ar), 7.59 (t, *J*=8.1 Hz, 2H, Ar), 7.38 (t, *J*=8.0 Hz, 2H, Ar), 7.27 (t, *J*=8.0Hz, 2H, Ar), 6.96/6.83 (rotomer s, 1H) 5.98/5.39 (rotomer br, 1H, NH), 4.45-4.35 (m, 3H), 4.20 (t, *J*=7.0 Hz, 1H), 4.06/3.93 (rotomer s, 1H), 3.54-2.94 (m, 4H), 1.86 (s, 3H), 1.46/1.49 (rotomer s, 9H); $^{13}$C NMR 400 MHz ($CDCl_3$) δ 168.8, 168.6, 144.1, 143.9, 141.4, 141.2, 141.0, 127.9, 127.8, 127.2, 127.1, 125.3, 125.1, 120.1, 110.9, 110.7, 83.9, 82.8, 66.9, 51.4, 50.0, 49.1, 47.7, 47.4, 39.4, 39.1, 28.2, 12.4; HRMS: Calcd. For $C_{30}H_{34}N_4O_7$: *m/z* 562.61, found *m/z* 563.58 (M+H)

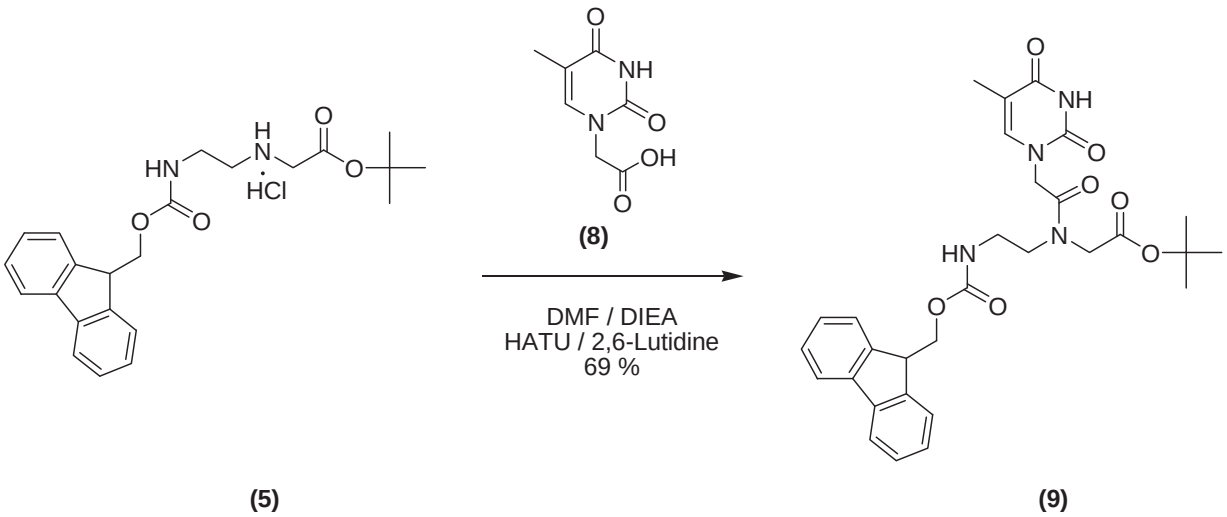


**Figure S9.** Synthesis of *tert*-butyl *N*-(2-(*N*-9-fluorenylmrthoxycarbonyl)aminoethyl)-*N*-((thymin-1-yl)acetyl)glycinate **(9)**

**(B) Calculation of the grafting density of thymine PNA monomer on the MNP surface**

From TGA result, the MNP complex exhibited about 4.1 wt% of thymine PNA monomer. Weight of poly(PEGMA-*stat*-VDM)-coated MNP used was 10 mg; weight of thymine PNA monomer per gram of the complex;

$$= \left(\frac{4.1 g \times 10 \times 10^{3} g}{100 g}\right)$$

$$= 4.1 \times 10^{-4} \text{ g / g of the complex}$$

Because molecular weight of thymine PNA monomer = 338 g/mol, mole of thymine PNA monomer per gram of the complex;

$$= \left(\frac{4.1 \times 10^{4} g}{338 g / mol}\right)$$

$$= 1.2 \text{ μmol/g of the complex}$$

**Part 4. Determination of crystal structure of magnetite nanoparticles**

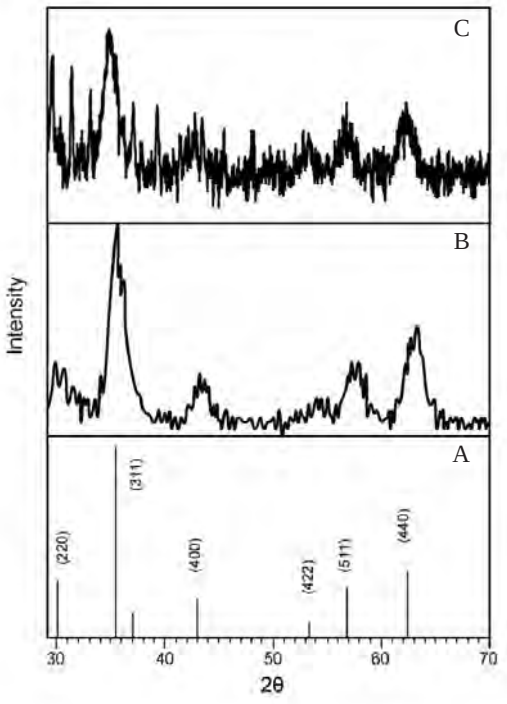


**Figure S10.** X-ray diffraction patterns of (A) standard magnetite powder (ICSD No. 01-075-0449), (B) bare MNP and (C) poly(PEGMA-*stat*-VDM)-coated MNP

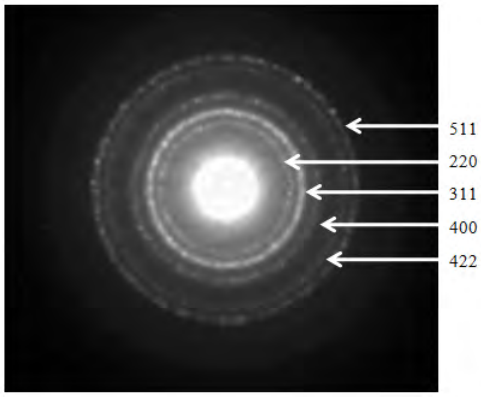


**Figure S11.** Selected area electron diffraction (SAED) pattern of poly(PEGMA-*stat*-VDM)-coated MNP immobilized with thymine PNA monomer

## Part 5. Percentage of magnetite in the complex and their magnetic properties

**Table S4** Composition and magnetic properties of the each complex

| Type of complex | % Char yield [a] | % in the complex [a] | | | | emu/g of complex [b] | emu/g of $Fe_3O_4$ [a,b] |
|---|---|---|---|---|---|---|---|
| | | $Fe_3O_4$ | BTPAm | Poly(PEGMA-*stat*-VDM)- | Thymine | | |
| Bare MNP | 92 | 100 | - | - | - | 56 | 56 |
| BTPAm-coated MNP | 85 | 92 | 8 | - | - | 49 | 53 |
| Poly(PEGMA-*stat*-VDM)-coated MNP | 71 | 77 | 6 | 17 | - | 36 | 47 |
| Thymine-poly(PEGMA-*stat*-VDM)-coated MNP | 68 | 74 | 6 | 16 | 4 | 34 | 46 |

[a] Estimated from % char yield at 600ºC *via* TGA technique

[b] Estimated from $M_s$ values at 10,000 G *via* VSM technique

## Part 6. A TEM image of poly(PEGMA-*stat*-VDM)-coated MNP

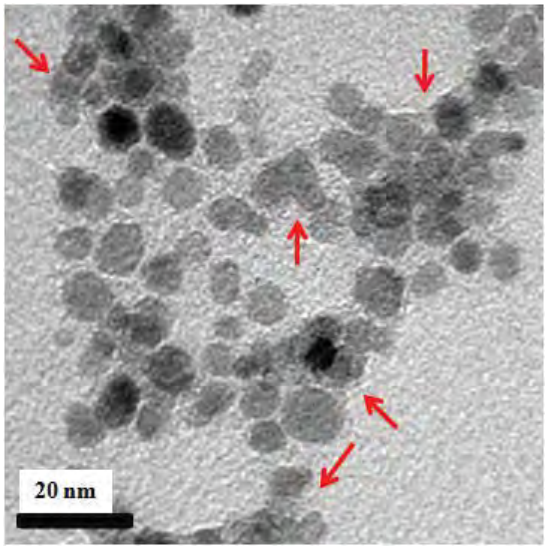


**Figure S12.** A TEM image of poly(PEGMA-*stat*-VDM)-coated MNP showing the presence of polymeric thin film on the particle surface (indicated by arrows)

# Surface modification of magnetite nanoparticle with azobenzene-containing water dispersible polymer

*Pawinee Theamdee, Rakchart Traiphol, Boonjira Rutnakornpituk, Uthai Wichai and Metha Rutnakornpituk**

**Abstract**: We here report the synthesis of magnetite nanoparticle (MNP) grafted with poly (ethylene glycol) methyl ether methacrylate (PEGMA)-azobenzene acrylate (ABA) statistical copolymer *via* atom transfer radical polymerization (ATRP) for drug entrapment and photocontrolled release. MNP was synthesized *via* thermal decomposition of iron (III) acetylacetonate in benzyl alcohol and surface functionalized to obtain ATRP initiating sites. Molar compositions of the copolymer on MNP surface were systematically varied (100:0, 90:10, 70:30 and 50:50 of PEGMA:ABA, respectively) to obtain water dispersible particles with various amounts of azobenzene. The presence of polymeric shell on MNP core was evidenced by transmission electron microscopy (TEM). Drug loading and entrapment efficiencies as well as drug release behavior of the copolymer-MNP complexes were investigated. It was found that when percent of ABA in the copolymers was increased, entrapment and loading efficiencies of prednisolone model drug were enhanced. Releasing rate and percent of the released prednisolone of the complex exposed in UV light were slightly enhanced as compared to the system without UV irradiation. This copolymer-MNP complex with photocontrollable drug release and magnetic field-directed properties is warranted for further studies for potential uses as a novel drug delivery vehicle.

KEYWORDS. Atom transfer radical polymerization; magnetite; nanoparticle; azobenzene

## 1. Introduction

In recent years, magnetite nanoparticle (MNP) coated with water dispersible polymeric surfactants have been intensively studied because it offers intriguing new opportunities for many biomedical applications such as magnetic resonance imaging (MRI) contrast enhancing agents [Pei et al., 2007; Sun et al., 2000; Teng et al., 2003; Sellmyer et al., 2002; Anders et al., 2002; Woo et al., 2004], hyperthermia treatment of tumors [Laurent et al., 2008], magnetic field-guided drug delivery [Zhang et al., 2007] and biomolecular

magnetic separation and diagnosis [Pinna et al., 2005]. Surface coating of MNP is necessary when expected for use in vivo because it protects the particles from agglomeration, provides surface functionality for conjugation of biomolecules and prevents non-specific cell interaction [Veiseh et al., 2010]. Therefore, surface modification of MNP is an important and challenging step for controlling chemical composition and function of the polymer on its surface.

A number of chemical approaches have been reported for coatings polymers on MNP surface such as physical adsorption, emulsion polymerization, and "grafting to" and "grafting from" methods [Fan et al., 2007; Hu et al., 2006; Marutani et al., 2004]. Among these approaches, surface-initiated atom transfer radical polymerization (ATRP) has recently become a method of choice for coating organic polymeric shell on MNP core [Zhoua et al., 2008; Fischer et al., 2001; Sun et al., 2007]. ATRP from the silanized surface of MNP has also been reported as an effective "grafting-from" method for surface modification. ATRP is a recently developed living/controlled radical polymerization method, which does not require stringent experimental conditions. It enables for the polymerization and block copolymerization of various functional monomers such as styrene [Zhao et al., 2003; Liu et al., 2005], methacrylate [Hermann et al., 2007] and methacrylamide [Teodorescu et al., 1999] in a controlled condition, resulting in polymers with narrowly dispersed molecular weights. However, most of the researches on surface-initiated ATRP of MNP focused on the formation of hydrophobic polymeric shell on magnetite core, which limited its potential in biomedical applications [Moineau et al., 1998; Fischer et al., 1999; Monteiro et al., 2005; Zhou et al., 2008].

In this work, we adopted a "grafting from" method to modify MNP surfaces with poly (ethylene glycol) methyl ether methacrylate (PEGMA)-azobenzeneacrylate (ABA) statistical copolymer *via* ATRP reaction (Figure 1). Hydrophilic PEGMA allows the particles to well disperse in water, which is a requirement for biomedical uses. ABA was of particular interest in this work because azobenzene moiety can be switched from *trans* to *cis* forms by UV irradiation [Dokic et al., 2009; Maria et al., 2009; Yager et al., 2006; Nishimura et al., 1984]. Isomerization from *trans* to *cis* of azobenzene moiety involves a structural rearrangement, resulting in a decrease in size from 9 to 5 Å (a distance between the para carbon atoms of azobenzene) and an increase in its dipole moment from 0 to 3.0 D [Archut et al., 1998]. Taking advantage of the drastic change in its polarity, it was hypothesized that photocontrollable drug release should be gained due to *trans*-to-*cis* isomerizations of

azobenzene units upon UV irradiation [Sin et al., 2005; Bucio et al., 2005; Liu et al., 2000; Sharma et al., 2003; Li et al., 2006; Aruna et al., 2009; Kim et al., 2005; Park et al., 2001], resulting in an increase in polarity of the copolymer and acceleration of the expelling rate of the entrapped hydrophobic model drug from the complex (Figure 2). It has been reported that azobenzene-modified mesoporous silica enhanced the releasing rate of molecules from inside to outside of the mesopore upon irradiated under UV and visible light [Fujiwara et al., 2008; Wang et al., 2009].

Hence, the primary aim of this work is to synthesize a well defined PEGMA-ABA statistical copolymer *via* surface-initiated ATRP of MNP. Molar ratio of PEGMA to ABA on MNP surface was systematically varied to obtain water dispersible MNP with photoresponsive properties. The existence of ABA in the structure was characterized by fourier transform infrared (FTIR) and UV-Visible spectrophotometry. Transmission electron microscopy (TEM) was studied to investigate the particle size and the presence of polymeric shell coated on MNP core. Magnetic properties of the complexes were determined *via* a vibrating sample magnetometer (VSM). Entrapment efficiency, loading efficiency and releasing behavior of prednisolone model drug from the MNP complexes were also reported.

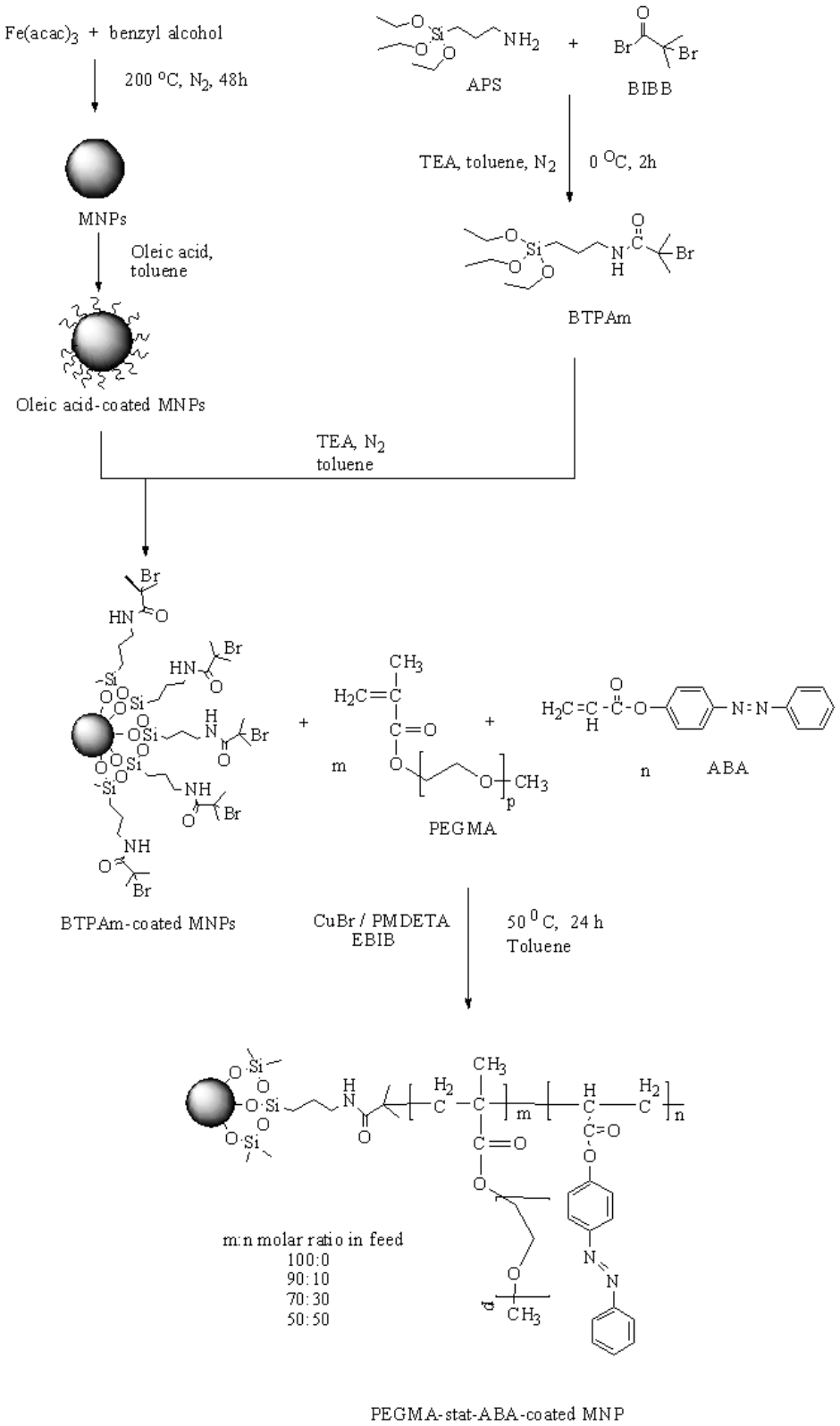


Figure 1 An experimental overview

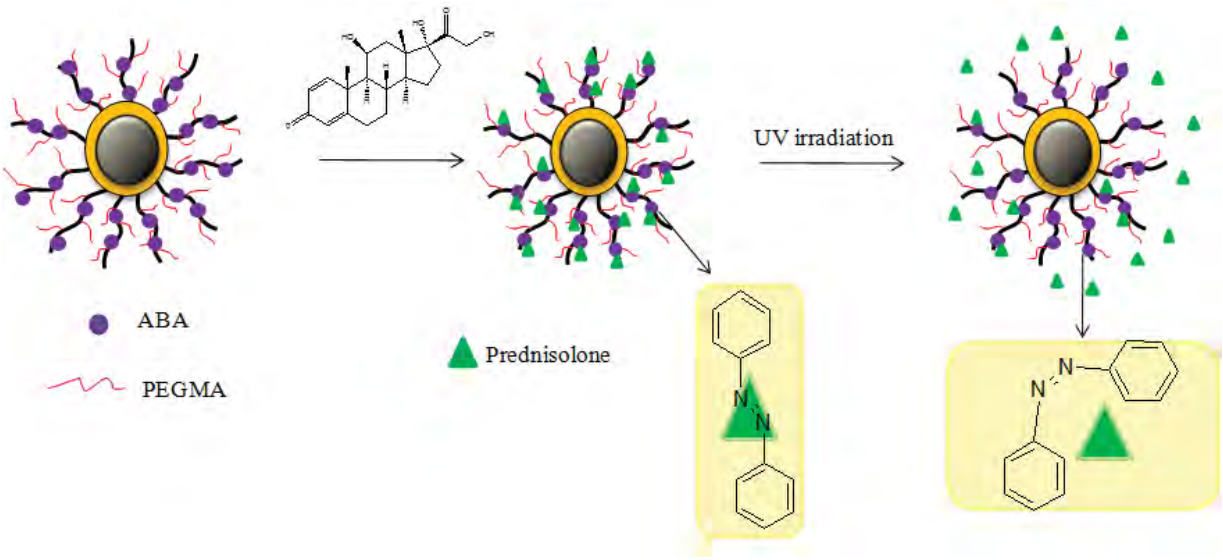


Figure 2 Proposed mechanism of prednisolone-controlled release from PEGMA-ABA-magnetite complex

## 2. Experimental Section

### 2.1 Materials

Unless stated otherwise, all reagents and solvents were used without further purification. Inhibitor-free PEGMA macromonomer ($\overline{M_n}$ ~ 300 g/mol) was stored under $N_2$ at -5 $^{o}$C until used. The following reagents were used as received: iron (III) acetylacetonate ($Fe(acac)_3$), 99+% (Acros), benzyl alcohol, 98% (Unilab), 3-aminopropyl triethoxysilane, 99% (Acros), 2-bromoisobutyryl bromide, 98% (Acros), copper (I) bromide, 98% (Acros), pentamethyldiethylenetriamine (PMDETA), 99% (Acros), dicyclohexyl carbodiimide (DCC), 99% (Acros), 4-phenylazophenol, 97% (Acros), acrylic acid 99.5% (Acros), ethyl-α-bromoisobutyrate (Aldrich) and oleic acid (Fluka). Triethylamine, 97% (Carto Erba) and toluene were stirred under $CaH_2$ and distilled prior to use. Cellulose dialysis tubing (Sigma-Aldrich) with molecular weight cutoff (MWCO) 12,400 was immersed in running water for 24 h before used.

### 2.2 Synthesis

#### 2.2.1 Synthesis of oleic acid-coated MNP

MNP was prepared following the method previously reported by Nicola [Pinna et al., 2005]. In a typical synthesis, iron (III) $(acac)_3$ (5.0 g, 14.05 mmol) was dissolved in benzyl alcohol (90 ml) in a three-neck round bottom flask. It was stirred at 200 $^{o}$C for 48 h under nitrogen blanket. The precipitant was removed from the dispersion using an external magnet

and washed with ethanol and $CH_2Cl_2$. This procedure was repeated three times and the particles were dried *in vacuo*. The dried particles (0.8 g) were re-suspended in dried toluene (30 ml) and sonicated for 1 h. Oleic acid (4 ml) was then added in the dispersion, followed by sonication for 3 h under nitrogen atmosphere. Finally, the aggregate was separated from the dispersion by centrifugation at 5000 rpm for 15 min.

2.2.2 Synthesis of 2-bromo-2-methyl-N-(3-(triethoxysilyl) propanamide, (BTPAm)

BTPAm was synthesized following the method previously reported by Yabin [Sun et al., 2007]. The solution of 2-bromoisobutyrylbromide (BIBB) (0.1 ml, 0.8 mmol) in toluene (10 ml) was added dropwise to a cold solution of 3-aminopropyl triethoxysilane (APS) (0.18 ml, 0.8 mmol) in 10 ml of toluene containing triethoxylamine (TEA) (0.11 ml, 0.8 mmol) at 0 $^oC$. The mixture was magnetically stirred for 2 h at 0 $^oC$ under nitrogen atmosphere. The reaction mixture was stirred for 24 h at room temperature. The mixture was filtered to remove salts, evaporated to remove the unreacted TEA and dried under reduced pressure. The resulting product, BTPAm, was yellowish thick liquid.

2.2.3 Synthesis of MNP coated with BTPAm, an ATRP initiator

To immobilize BTPAm on the oleic acid-coated MNP surfaces, the MNP-toluene dispersion (0.1 g of MNPs in 5 ml toluene) (30 ml), BTPAm (0.30 ml) and 2 M TEA in toluene (5 ml) were added into a round bottom flask. The mixture was stirred for 24 h at room temperature under nitrogen blanket. The particles were subsequently precipitated in methanol, following by magnet separation to obtain the BTPAm-coated MNP. Then, the MNP was re-dispersed in toluene and re-precipitated again in methanol. This procedure was repeated several times to completely remove unreacted BTPAm. The particles were finally dried *in vacuo*.

2.2.4 Synthesis of azobenzeneacrylate (ABA) monomer

ABA was prepared by a coupling reaction of 4-phenylazophenol and acrylic acid. To a 100 ml round-bottom flask containing an excess of 4-phenylazophenol (1.21 g, 0.0061 mol), acrylic acid (0.38 ml, 0.0054 mol) and dicyclohexylcarbodiimide (DCC) (1.24 g, 0.0061 mol) in distilled $CH_2Cl_2$ (20 ml) were slowly added. The solution was stirred at room temperature for 24 h under $N_2$ gas. The solution was filtered and $CH_2Cl_2$ was then evaporated. The mixture was dissolved in diethyl ether, extracted with saturated $NaHCO_3$ (3 x 20 ml), dried with anh.$MgSO_4$, and then the solvent was evaporated until dryness.

2.2.5 (Co)polymerization of PEGMA and/or ABA *via* ATRP from MNP surface

Three different molar ratios of PEGMA-ABA copolymer (50:50, 70:30 and 90:10, respectively) and PEGMA homopolymer (100:0 of PEGMA-ABA molar ratio) grafted on MNP surface were prepared. An example for synthesizing 50:50 PEGMA-ABA-coated MNP was described herein. Other copolymer-MNP complexes were prepared in a similar fashion with proper amounts of reagents used. In a typical procedure, BTPAm-immobilized MNP (0.1 g) were sonicated in toluene (0.381 ml, 60% w/v) in a Schlenk tube. A solution of PEGMA (0.64 g, 2.13 mmol), ABA (0.56 g, 2.22 mmol) and ethyl-α-bromoisobutyrate (EBiB) as a sacrificial initiator (0.007 g, 0.35 mmol) were then syringed to the above Schlenk tube. The solution was degassed by three freeze-pump-thaw cycles before adding a solution of CuBr (0.064 g, 0.44 mmol) and PMDETA (0.009 g, 0.05 mmol) in DMF (0.032 ml, 5% v/v) filled with nitrogen. ATRP reaction was set at 50 °C for 24 h. The dispersions were removed periodically *via* a degassed syringe for determining reaction conversion and GPC analyses.

2.3 Characterization

2.3.1 Characterization of polymer and MNP

$^{1}$H NMR was performed on a 400 MHz Bruker NMR spectrometer using $CDCl_3$ as a solvent. FTIR was performed on a Perkin-Elmer Model 1600 Series FTIR Spectrophotometer. The solid samples were mixed with KBr to form pellets. Gel permeation chromatography (GPC) data was conducted on PLgel 10 μm mixed B2 columns and a refractive index detector. Tetrahydrofuran (THF) was used as a solvent with a flow rate of 1 ml/min at 30$^{o}$C. Magnetite concentrations in dispersions were analyzed *via* atomic absorption spectroscopy (AAS) and calculated from sample responses relative to those of standard and blank. Particles size and its distribution were observed from transmission electron microscopy (TEM). TEM images were taken using a Philips Tecnai 12 operated at 120 kV equipped with Gatan model 782 CCD camera. The particles were re-suspended in water with sonication before deposition on a TEM grid. Magnetic properties of the particles were measured at room temperature using a Standard 7403 Series, Lakeshore vibrating sample magnetometer (VSM). Magnetic moment of each sample was investigated over a range of ±10000 G of applied magnetic fields using 30 min sweep time. Prednisolone concentrations were determined using Specord S100 UV-Visible spectrophotometer (Analytikjena AG) coupled with a photo diode array detector. A standard curve at λmax = 320 nm UV absorbance was established using identical conditions to calculate the amount of the drug entrapped on and released from the particles.

2.3.2 Studies on drug entrapping and loading efficiencies of the surface-modified MNPs

Prednisolone was used as a model drug in the current studies. To incorporate the drug to the complex, the drug solution (6 ml, 0.375 mg/ml in THF) was added dropwise with sonication to the copolymer-magnetite complex dispersed in water (5 ml, 0.2-0.5 mg/ml MNP). The mixture was sonicated for 30 min to fully aggregate the drug in the hydrophobic ABA units presenting on the particle surface. The excess drug was precipitated out from the mixture and was removed by centrifugation at 2000 rpm. Drug-loaded MNP was then separated using an external magnet. Due to a good solubility of prednisolone in a THF:ethanol solution (50:50 %v/v), it was used to repeatedly extract the entrapped drug from the particle. After centrifugation to remove aggregated particle, the drug concentration in the supernatant, reflecting the amount of the entrapped drug in the complex, was determined using UV-Visible spectrophotometer. Entrapment efficiency (%EE) and drug loading efficiency (%DLE) were determined as following:

$$\%EE = \frac{\text{Weight of the entrapped drug in nanoparticle}}{\text{Weight of the loaded drug}} \times 100$$

$$\%DLE = \frac{\text{Weight of the entrapped drug in nanoparticle}}{\text{Weight of the magnetite nanoparticle}} \times 100$$

Each experiment was repeated three times to obtain average values.

2.3.3 In vitro releasing studies of the entrapped prednisolone in the copolymer-magnetite complex

Prednisolone-loaded magnetite dispersions (5 ml) were dialyzed against 250 ml-phosphate buffer solution releasing media (pH 7.45) with consistently stirring at room temperature. Two experiments were performed simultaneously; under UV light irradiation and in the dark place as a control. At a given time, 5 ml aliquots of the aqueous solution were withdrawn from the releasing media and 5 ml of phosphate buffer solution was replaced into the releasing media. Concentrations of the released prednisolone were determined *via* UV–Visible spectrophotometer at 297 nm wavelength

3. Results and discussion

MNPs were first synthesized *via* a thermal decomposition reaction of $Fe(acac)_3$ to obtain narrow-size distribution nanoparticles. To functionalize the particles surfaces, the initiator for ATRP was first covalently bonded onto the surface of the particles through the combination of ligand exchange reaction and condensation of triethoxysilane.

3.1 Synthesis of MNPs coated with BTPAm, an ATRP initiator

Figure 3 shows an FTIR spectrum of BTPAm-coated MNP (Figure 3C) in comparison with those of bare magnetite (Figure 3A) and BTPAm (Figure 3B). In addition to a strong and broad signal of Fe-O bonds (578 $cm^{-1}$) observed in BTPAm-modified MNP, it also exhibited characteristic absorption signals of BTPAm; 1643 $cm^{-1}$ (-NH-CO- carbonyl stretching), 2920 $cm^{-1}$ (C-H stretching), 1111-1109 $cm^{-1}$ (Si-O stretching), 1532 $cm^{-1}$ (N-H bending) and 3346 $cm^{-1}$(N-H stretching) (Figure 3C). It should be noted that an excess of BTPAm or unbound BTPAm was repeatedly removed from the particles.

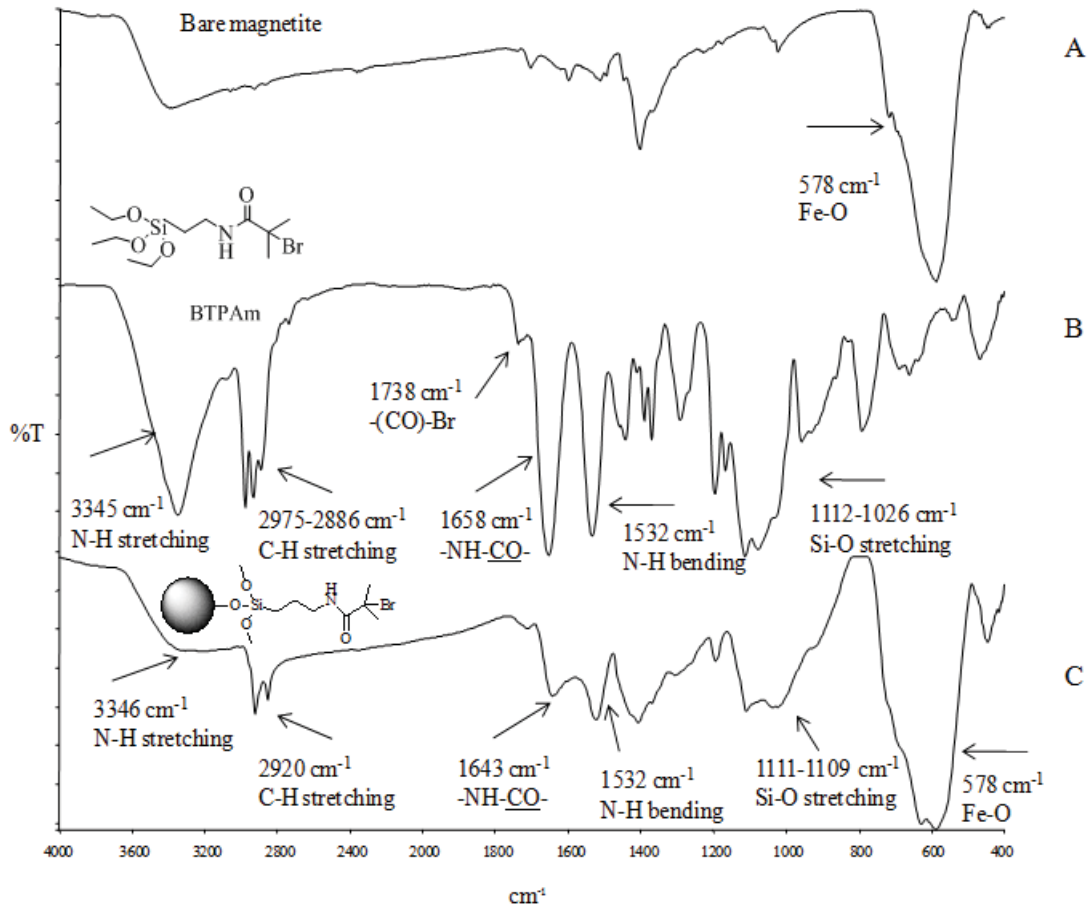


Figure 3 FTIR spectra of A) bare magnetite, B) BTPAm and C) BTPAm-coated MNPs

3.2 Copolymerization of PEGMA and ABA *via* ATRP from MNP surface

3.2.1 Synthesis of azobenzeneacrylate (ABA)

ABA is a resultant product from a coupling reaction between 4-phenylazophenol and acrylic acid (Figure 4A). The presence of sharp and strong signals of carbonyl group (1736 $cm^{-1}$) and acrylate group (987, 900 $cm^{-1}$) indicated the coupling reaction between carboxylic acid of acrylic acid and hydroxyl group of 4-phenylazophenol. It should be noted once again that unreacted acrylic acid and 4-phenylazobenzene were removed from the final product. According to the $^{1}H$ NMR spectrum in Figure 4B, characteristic signals of ABA were found as following: $^{1}H$-NMR ($CDCl_3$, ppm): δ 7.98 (m, 4H (a), Ar*H*), 7.52 (d, 2H (b), Ar*H*), 7.30 (d, 2H (c), Ar*H* ), 6.67 (d, *J*=17.3 Hz, 1H (d), C*H*H=CH), 6.36 (dd, 1H, J=17.3 and 10.50 Hz (e), C*H*=$CH_2$), 6.07 (d, 1H, J=10.46 Hz (f), CH*H*=CH).

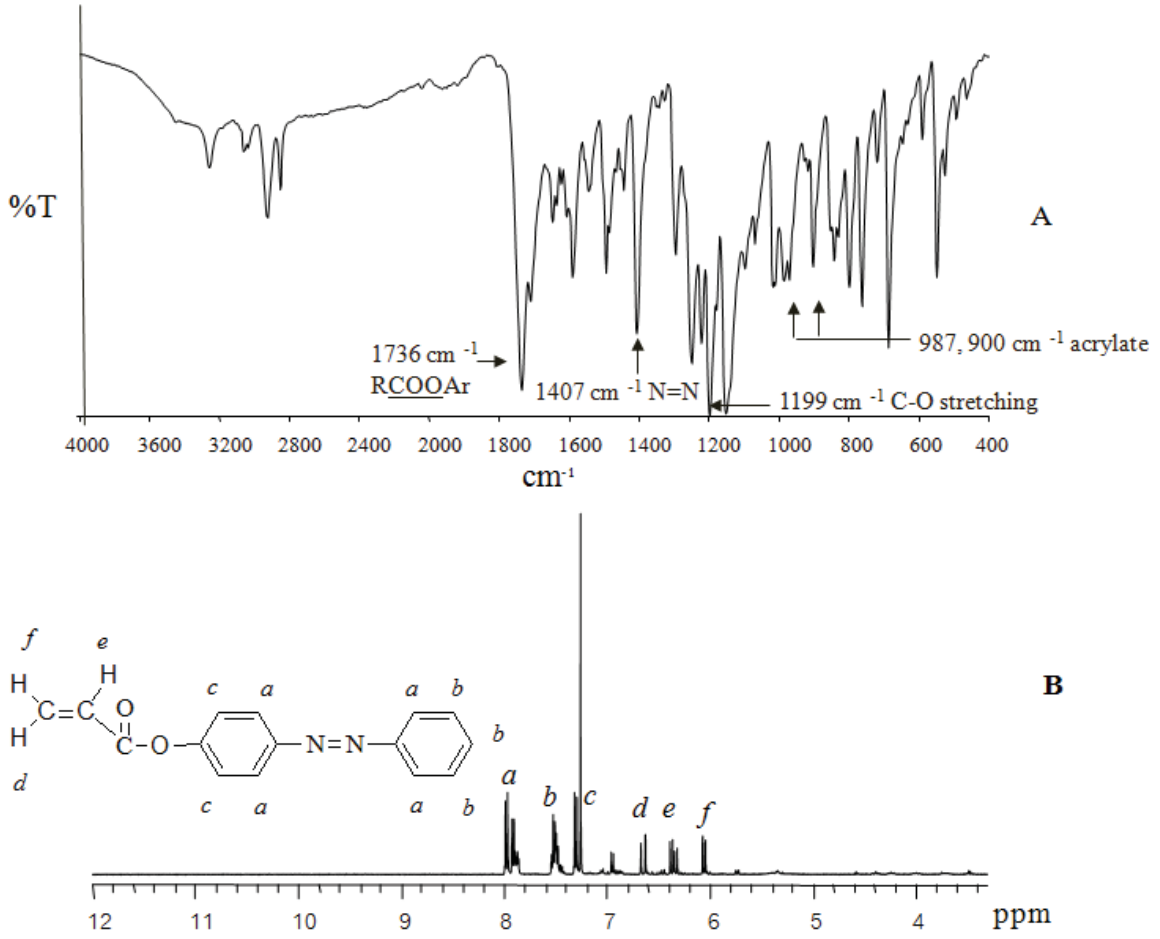


Figure 4 (A) FTIR and (B) $^{1}H$-NMR spectra of ABA

Figure 5 shows the representative UV-Visible absorption spectra of ABA solution in chloroform (0.01 mg/ml). The maximum absorption at 329 nm corresponds to the π-π* transition of *trans* azobenzene chromophore and a weak band at 425 nm corresponds to the n-

π* transition of *cis* isomer [Sin et al., 2005; Bucio et al., 2005; Liu et al., 2000; Sharma et al., 2003; Li et al., 2006; Aruna et al., 2009; Kim et al., 2005; Park et al., 2001]. *Trans* form of ABA, the energetically preferred ground state, can switch to the *cis* form *via* a photochemical isomerization process. Upon UV irradiation, the intensity of the *trans* peak at 329 nm decreased and broadened and, at the same time, the broad *cis* absorption band around 425 nm increased. This phenomenon was observed during the first 3 min of UV irradiation. When the time for UV exposure was extended, there was no significant change in UV spectra. Since the decrease of absorbance at 329 nm is a direct result of the *trans* to *cis* isomer conversion, the fraction of the *cis* isomer is estimated to be about 25 mol%.

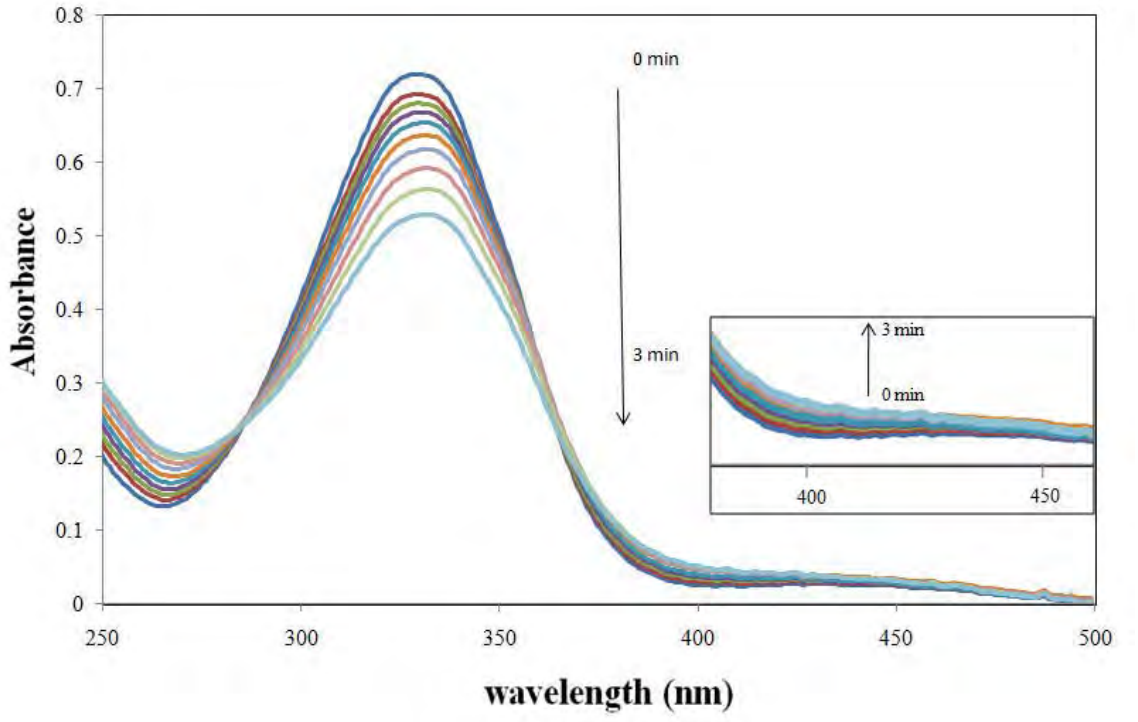


Figure 5 Changes in UV-Visible spectra of ABA at different UV irradiation times, indicating the change from *trans* to *cis* forms

3.2.2 Copolymerization of PEGMA and ABA from MNP surface *via* ATRP

In this work, PEGMA and ABA with various molar compositions (100:0, 90:10, 70:30 and 50:50, respectively) were statistically copolymerized on MNP surface *via* ATRP reaction. PEGMA on MNP surface allows the particles to well suspend in water, while ABA possesses photoisomerization upon UV light irradiation. Optimization of molar ratio of these two components was necessary to obtain dispersible particles in water with maximum UV light responsive properties.

In the ATRP reaction, a CuBr/PMDETA catalytic complex was used because it has been reported to be an effective copper-mediated complex for a controlled living ATRP reaction of PEGMA [Neugebauer et al., 2007]. Ethyl-α-bromoisobutyrate (EBiB) was also added in the reaction solution as a "sacrificial" initiator. EBiB in the MNP dispersion can initiate free PEGMA-ABA copolymer in the solution. Because the MNP-supported copolymers were undetectable in NMR technique, therefore, the reaction conversions and copolymer compositions, discussed in the latter section, were investigated from the free copolymers *via* NMR spectrometry.

Figure 6 illustrates FTIR spectra of MNPs modified with various copolymer compositions (Figure 6C-F) compared with those of PEGMA macromonomer and ABA (Figure 6A and B, respectively). The spectra of PEGMA-ABA-coated MNPs exhibited characteristic absorption signals of PEGMA; 1095 $cm^{-1}$ (C-O-C stretching) and 1720 $cm^{-1}$ (O(C=O) stretching), and also those of azobenzene; 1407 $cm^{-1}$ (*trans* N=N). The drop of the intensity of ester (-O(C=O)- stretching, 1720 $cm^{-1}$) and ether linkage signals (C-O-C stretching, 1095 $cm^{-1}$) of PEGMA in relative to those of Fe-O bonds from MNP cores (~ 589 $cm^{-1}$) correspond to the decreased PEGMA compositions in the copolymer (Figure 6C-F). In addition to that, the gradual increase of N=N signal of azobenzene (1407 $cm^{-1}$) was also observed as percentage of ABA in the copolymer was increased. It should be noted that the signal corresponding to Fe-O bonds (578 $cm^{-1}$) from MNP cores were observed throughout the reactions without significant change in its intensity. The drastic decreases of the aliphatic signal around 3000 $cm^{-1}$ and the ester signal around 1720 $cm^{-1}$ upon addition only 10% of ABA into the copolymer (from Figure 6C to 6D) were attributed to the low copolymer content in the complexes. PEGMA-ABA copolymerization having other copolymer compositions also exhibited similar FTIR patterns. TGA experiments showed a supportive result to FTIR results. Namely, the percent weight loss of the copolymer-coated MNPs, corresponding to the copolymer content in the complexes, was significantly lower than those of the PEGMA-coated MNP. Representative TGA thermograms of MNPs coated with PEGMA homopolymer and PEGMA-ABA copolymer were available in the supporting information.

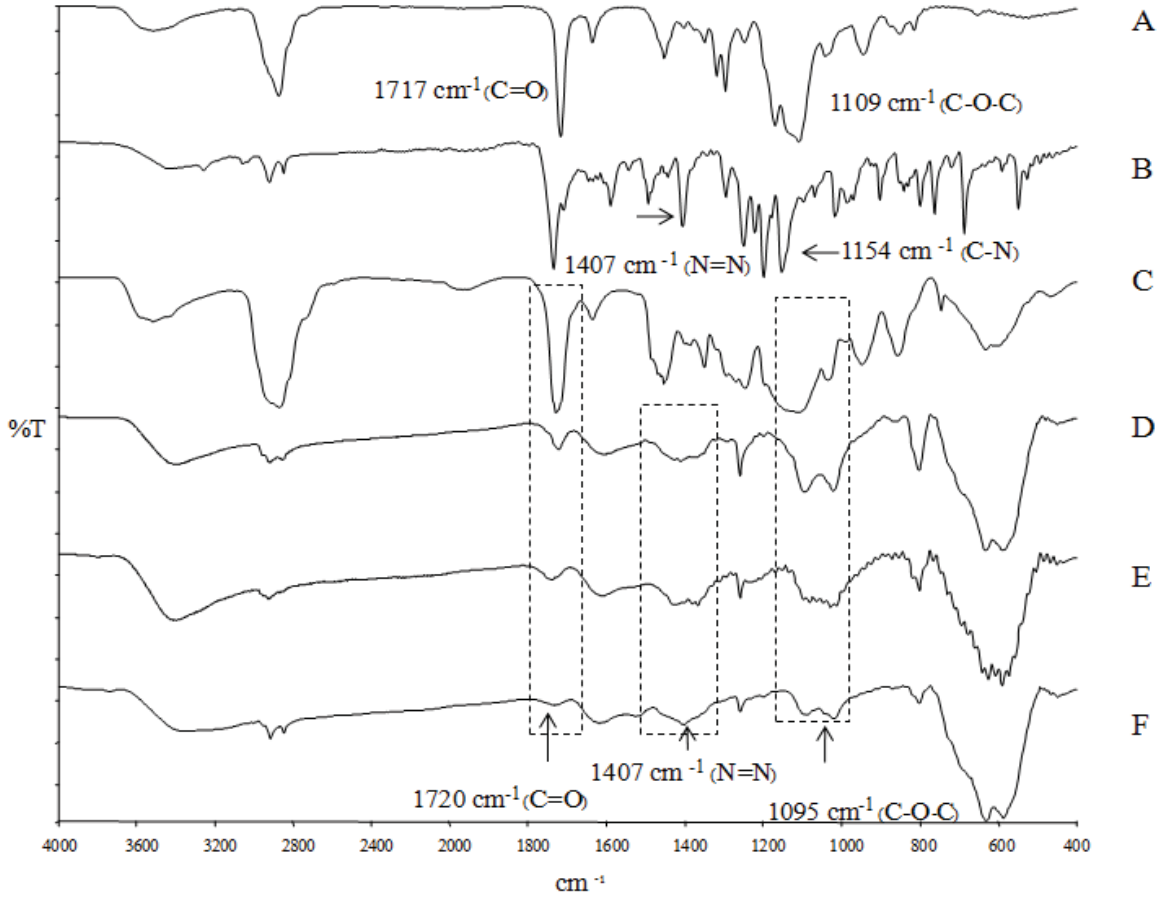


Figure 6 FTIR spectra of A) PEGMA macromonomer, B) ABA, C) 100:0, D) 90:10, E) 70:30 and F) 50:50 PEGMA-ABA-coated MNPs

Kinetic studies of the polymerization of PEGMA homopolymer (100:0 PEGMA-ABA) were first performed and followed by those of PEGMA-ABA copolymerization. In the PEGMA homopolymerization, the reaction rate was rapid at the beginning and dropped after 4 h (240 min) of the reaction (Figure 7A). This was attributed to a decrease of radical concentration probably due to irreversible recombination of the active species. The first order plot reveals a linear relationship during the course of first 4 h reaction, indicating a constant concentration of active radical species (supporting information). The rate of monomer conversion started to deviate from linearity at higher monomer conversion (after 4 h reaction).

Figure 7B illustrates a conversion plot of 50:50 PEGMA-ABA copolymerization during 24 h of ATRP reaction. Conversion plots of the copolymerization having different PEGMA-ABA compositions (90:10 and 70:30, respectively) showed similar results to Figure 7B (supporting information). Kinetic experiments indicate that the reaction rates of the PEGMA-ABA copolymerization gradually increased at the beginning and they were slower

than that of PEGMA homopolymerization. This was attributed to the presence of ABA in the reaction, which essentially influenced the change in polarity of the system. Decreasing ABA molar ratio in the copolymer seemed to promote rate of the reaction. When the reactions further proceeded, the rate of polymerization decreased and ended at about 30-50% monomer conversion, suggesting feasible premature chain termination (Table 1). It was also found that ABA reacted more rapidly than PEGMA as indicated by the higher monomer conversion in all cases.

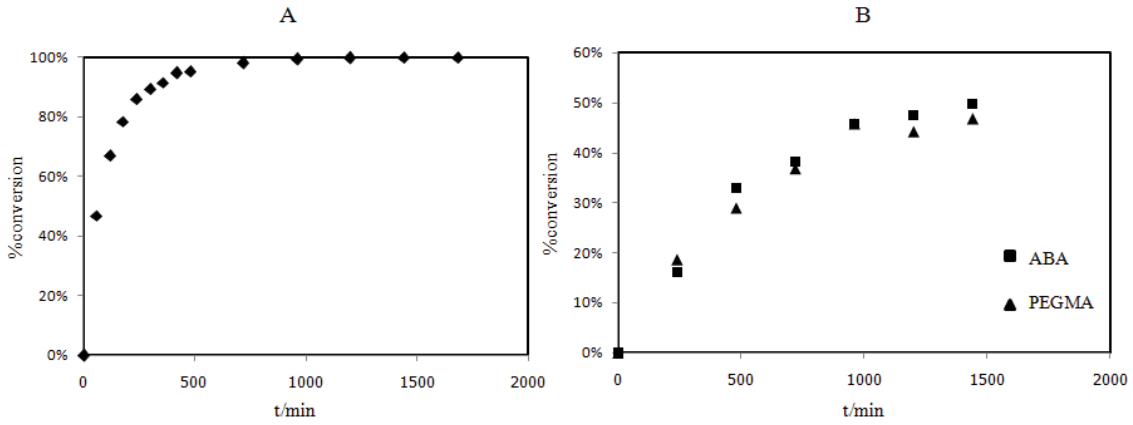


Figure 7 Conversion *vs* time plots of the polymerization of (A) PEGMA homopolymer and (B) 50:50 PEGMA-ABA copolymer

Table 1 summarizes % conversion and copolymer composition of PEGMA and ABA having various molar ratios. Copolymer compositions were estimated from the feed composition of the monomer and taking percent conversion into account. Percent ABA in the copolymer was calculated in a similar fashion. It was found that PEGMA-ABA molar ratio in the copolymer were comparable to the feed compositions. Interestingly, percentage of ABA in the copolymer was found to be slightly higher than percent feeding in every composition. This result agrees well with the conversion *vs* time plots indicating higher reaction reactivity of ABA than that of PEGMA. In addition, the relatively low percent monomer conversions in the copolymerization as compared to the PEGMA homopolymerization (100:0 PEGMA-ABA) were in good agreement with the FTIR and TGA results, which indicated that the polymer contents in the complexes in the case of the copolymerizations were lower than that of the PEGMA homopolymerization.

Table 1 A summary of reaction conversions and copolymer compositions of PEGMA-ABA copolymer at 24 h of ATRP reaction

| Type of copolymer | % conversion[a] of | | % in the copolymer[b] of | |
|---|---|---|---|---|
| | PEGMA | ABA | PEGMA | ABA |
| 50:50 PEGMA-ABA | 47 | 50 | 48 | 52 |
| 70:30 PEGMA-ABA | 52 | 53 | 69 | 31 |
| 90:10 PEGMA-ABA | 32 | 42 | 89 | 11 |
| 100:0 PEGMA-ABA | 95 | - | 100 | 0 |

[a] Reaction conversions were calculated from $^{1}$H NMR, [b] % PEGMA in the copolymer = [% $Conv._{PEGMA}$ x % $feed_{PEGMA}$] / [(% $Conv._{PEGMA}$ x % $feed_{PEGMA}$) + (% $Conv._{ABA}$ x % $feed_{ABA}$)]. % ABA in the copolymer was calculated in a similar fashion

3.3 Characterization of PEGMA-ABA-coated MNP

According to TEM experiments, particles size and particle distribution of PEGMA-ABA-coated MNPs with various copolymer molar ratios were not significantly different from each other (Figure 8). The particle size was in the range of 6-12 nm with the average diameter of 9.0 nm. In addition, the images also showed nanoscale agglomeration of multiple nanoparticles. This was attributed to *in situ* aggregation of hydrophilic PEGMA grafted on MNP surface during the ATRP copolymerizations in toluene. Even though nanoscale agglomeration was apparent, these particles were well re-suspended in water due to the presence of polymeric thin film on their surface (indicated by arrows). Furthermore, it was also observed that increasing PEGMA-to-ABA ratio in the copolymer enhanced dispersibility of the particles in water. Namely, 100:0 PEGMA-ABA-coated MNPs exhibited a good dispersibility in water without any aggregation observed, while 50:50 PEGMA-ABA-coated MNPs showed more aggregate than that of other copolymers after centrifugation. These complexes were stable in aqueous dispersions with insignificant aggregation after one month of preparation, indicating that these stable magnetite dispersions might be applicable for long-term uses.

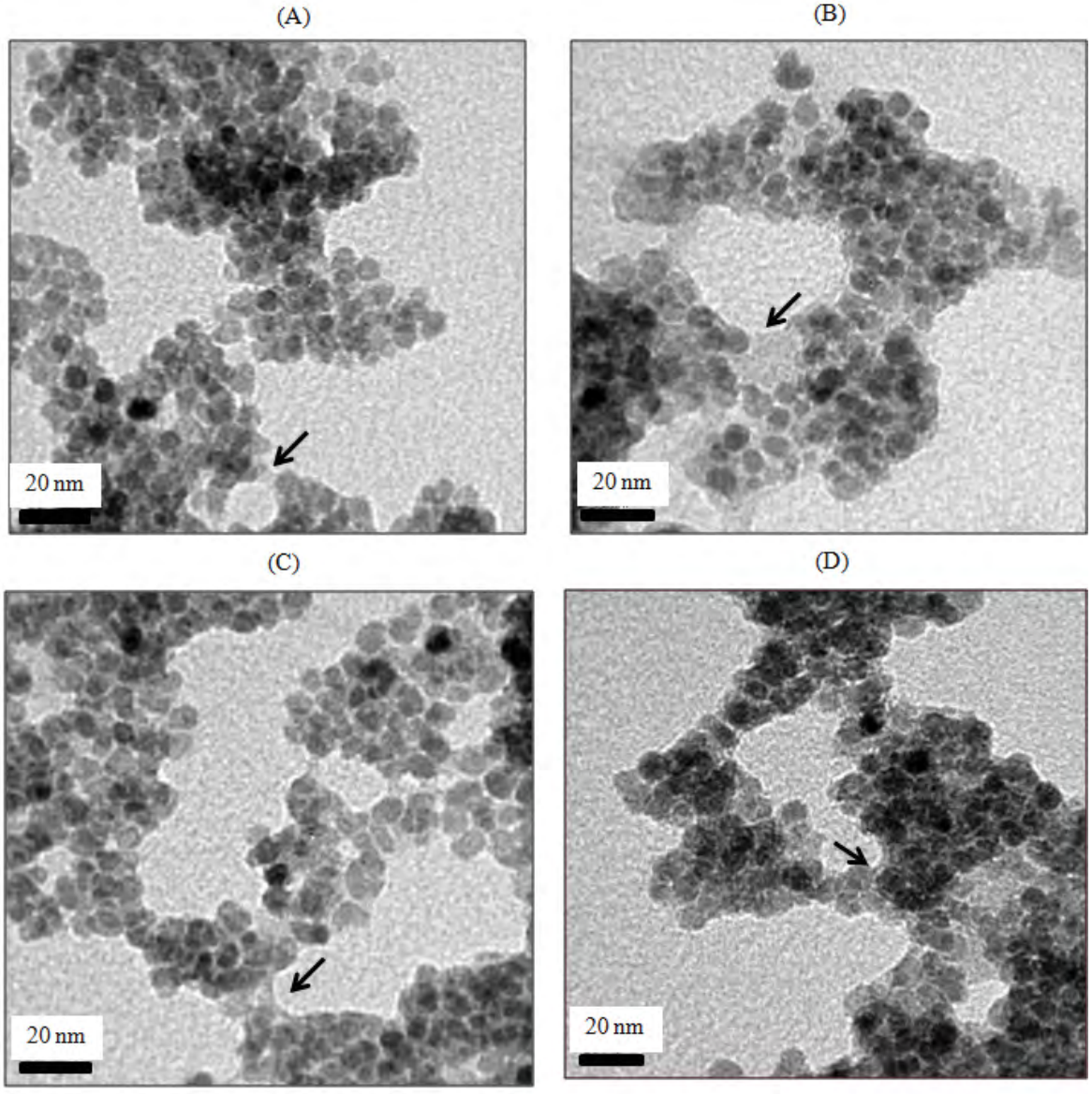


Figure 8 TEM images of (A) 50:50, (B) 70:30, (C) 90:10 and (D) 100:0 PEGMA-ABA-coated MNPs

Hysteresis curves of bare MNP, BTPAm-coated MNP and PEGMA-ABA-coated MNP were illustrated in Figure 9. The particles showed superparamagnetic behavior at room temperature as indicated by the absence of remanence and coercitivity. Bare MNP and BTPAm-coated MNP showed relatively high saturation magnetization ($M_s$) (54-55 emu/g) due to a trace amount of organic component in the complexes (Figure 9A and B). A slight decrease of Ms of PEGMA-ABA-coated MNP (39-45 emu/g) as compared to its precursors was attributed to the presence of the copolymers on MNP surface, reflecting a drop of magnetite content in the complex (Figure 9C-E). Further decrease of $M_s$ value was observed in PEGMA-coated MNP (31 emu/g) due to high content of PEGMA homopolymer in the

complex (Figure 9F). These results were in good agreement with the percent conversions of ATRP reactions shown in Table 1; high percent monomer conversions correspond to high amounts of the polymer in the complex.

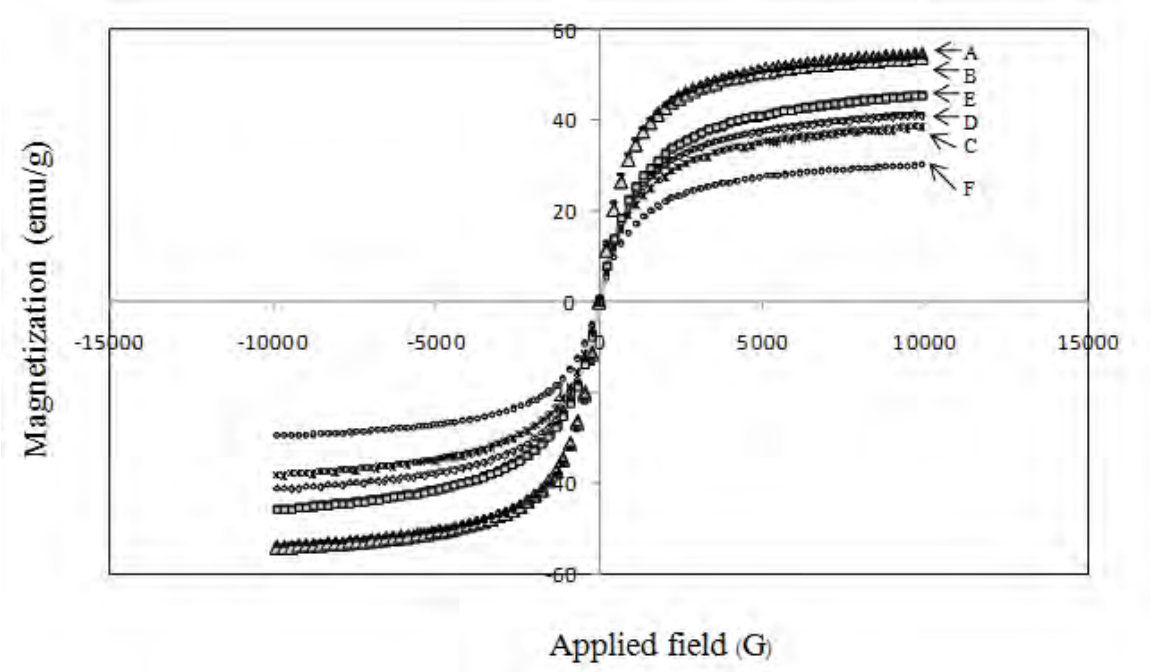


Figure 9 Hysteresis curves of A) bare MNP, B) BTPAm-coated MNP, C) 50:50, D) 70:30, E) 90:10 and F) 100:0 PEGMA-ABA-coated MNPs

3.4 Study in the configuration change of azobenzene moiety in PEGMA-ABA-coated MNP

Direct investigation of the isomerization of azobenzene grafted on the MNP was not detectable *via* UV-Visible spectrophotometry as performed in ABA monomer because the MNP blocked UV signals in the range of interest. In the present study, pyrene was thus used to investigate configuration change from *trans* to *cis* forms of azobenzene when it was exposed under UV light. Pyrene is typically used as a fluorescent probe to monitor the change in system polarity because its vibrational structure is sensitive to polarity of its environment [Winnik et al., 1987; Lee et al., 2004]. Fluorescence of pyrene monomer possesses five predominant signals resulting from different vibrational levels, some of which are sensitive to the molecular solvent environment [Winnik et al., 1987]. For instance, the $I_1/I_3$ ratio of pyrene is mostly dependent on solvent polarity as measured by the dielectric constant [Kalyanasundaram et al., 1977]. In this work, we used 50:50 PEGMA-ABA-coated MNP coupled with pyrene as a probe to investigate polarity change of surrounding environment because it possessed high amount of azobenzene moieties in the complex. Figure 10 shows

the fluorescence spectra of pyrene in the copolymer-coated MNP in DMSO excited at 330 nm before and after UV irradiations for 10-180 min. The change in fluorescence emission intensity ratio of pyrene ($I_1/I_3$) at 370 nm ($I_1$) and 376 nm ($I_3$) indicates the change in polarities of the surrounding environment. Namely, the increase in $I_1/I_3$ value indicates the increase in polarity of the system, implying the change from *trans* to *cis* forms of azobenzene moiety. From the result shown in Figure 10, $I_1/I_3$ values continuously increased when UV irradiation time was prolonged, indicating the increase of solvent polarity due to the change from *trans* to *cis* forms of azobenzene moiety. Since the *trans* to *cis* isomer conversion may also cause the reorientation of neighboring moieties, which additionally affects the polarity of pyrene local surrounding, it is not trivial to estimate the fraction of *cis* isomer from the change of $I_1/I_3$ value. The relatively long irradiation time of the copolymer-coated MNP (~180 min) as compared to that of the free ABA in solution (~3 min) was attributed to the restricted mobility of ABA grafted on the nanosolid support combined with the presence of PEGMA randomly copolymerized in the polymer chains, which might sterically inhibit the transformation from *trans* to *cis* forms of azobenzene on its surface.

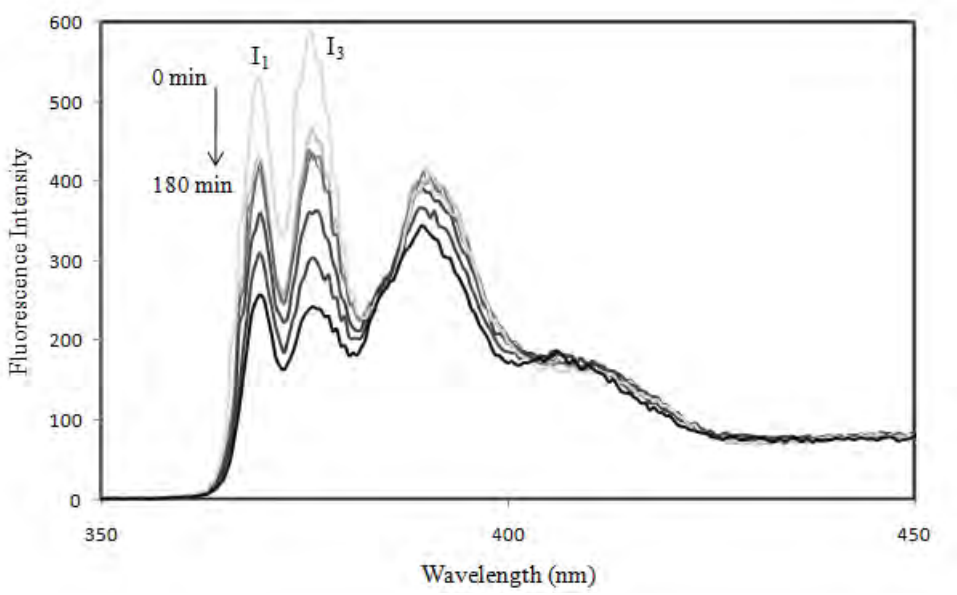


Figure 10 Fluorescence spectra of pyrene in 50:50 PEGMA-ABA-coated MNP excited at 330 nm at various UV irradiation times

3.5 Studies in prednisolone entrapment and loading efficiencies and releasing profile

It is known that UV irradiation of azobenzene groups enables to induce the switching of its *trans* to *cis* forms, resulting in an increase of its polarity. In the current work, drug control release application is of particular interest because we can take an advantage of this

photoisomerization of azobenzene groups. It was envisioned that, once a hydrophobic model drug was added to the copolymer-coated MNP dispersion, it would somewhat partition to *trans*-azobenzene grafted on MNP surface due to similarity in their polarity. UV irradiation of the drug-loaded MNP complexes was thought to accelerate the releasing rate of the entrapped drug from their surface due to the switching from *trans* to *cis* forms of azobenzene moiety, resulting in the increase in the system polarity and repelling the drug from the MNP surface.

Prednisolone was selected as a model drug in the current studies because its λmax in UV-Visible absorbance peaks did not overlap with those of ABA presenting in the copolymer-MNP complex. In addition, it shows fair solubility in phosphate buffer solution (PBS) which was used as a dialysis releasing media. It was hence hypothesized that prednisolone would partially precipitate in azobenzene grafted on MNP surface and was gradually expelled from the complex through dialysis membrane to PBS releasing media. Prednisolone releasing rate was thus expected to be accelerated upon UV irradiation due to photoisomerization of azobenzene moiety on MNP surface. To prepare prednisolone-entrapped copolymer-MNP complex, prednisolone solution in THF (0.375 mg/ml) was slowly added to the MNP complex resuspended in water with ultrasonicating. It is necessary to resuspend the particles in aqueous base because a potential application of this complex is biomedical use, which essentially involves with aqueous base system.

3.5.1 Determination of prednisolone entrapment efficiency (%EE) and loading efficiency (%DLE)

%EE and %DLE of PEGMA-ABA-coated MNPs having various molar ratios of PEGMA to ABA were investigated (Figure 11). Increasing ABA moiety in the copolymer seemed to promote both %EE and %DLE in every copolymer composition. This was rationalized that high percent of *trans*-azobenzene, reflecting high hydrophobic moiety, might enhance degrees of prednisolone aggregation in ABA, resulting in the increase in entrapment and loading capacities of the complex.

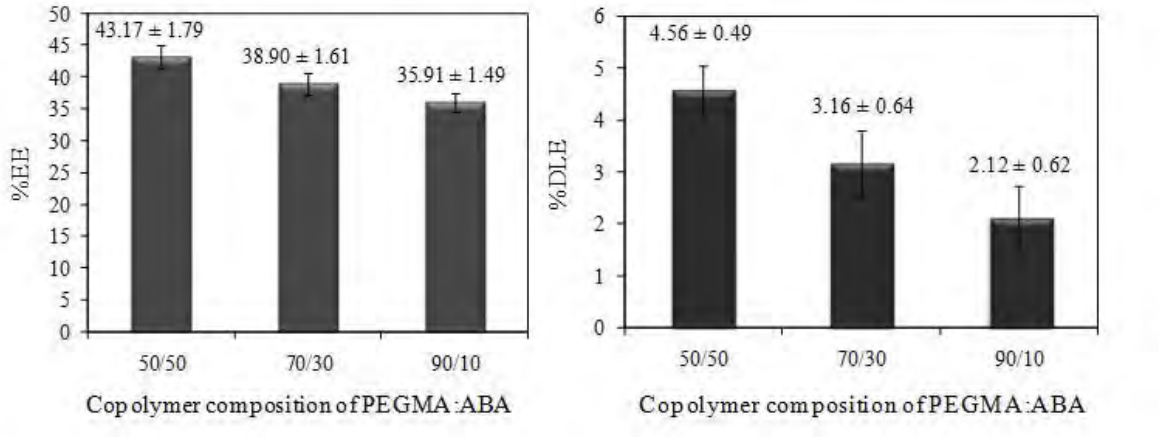


Figure 11 Prednisolone entrapment efficiency (% EE) and loading efficiency (% DLE) of PEGMA-ABA-coated MNP in water

3.5.2 Investigation of prednisolone releasing behavior

Drug releasing profiles of the drug-entrapped particles exposed under UV light was established and compared with that of a control experiment (the sample was kept in the dark place). The percentage of the released drug was calculated based on the amount of the entrapped drug in each complex. It was found that the drug concentration released at equilibrium in the case of exposure under UV light was slightly higher than those without UV irradiation (Figure 12). Prednisolone released from the complex was primarily attributed to desorption of the hydrophobic drug from azobenzene moiety in the copolymer. Under UV irradiation, photoisomerization from *trans* to *cis* forms of azobenzene moiety led to an additional driving force to expel the drug from the particle surface due to the increase in its polarity. The slight enhancement of the drug-released amounts at equilibrium of the samples exposed under UV light was attributed to the statistical architecture of the copolymer, which might inhibit the *trans*-to-*cis* transformation of azobenzene moiety. Formation of block structure having ABA inner block and PEGMA outer shell on the particle surface might improve the transformation efficiency and percent drug loading of this complex. Synthesis of the PEGMA-ABA block copolymer grafted on MNP surface and its photocontrolled drug release are warranted for a future studies. In addition, it was also found that increasing percentage of PEGMA in the copolymer seemed to slightly enhance % prednisolone released at equilibrium. This was attributed to the good dispersibility in water of the particles with high loading of PEGMA, which thus promoted releasing competency of the entrapped drug from the particle surface.

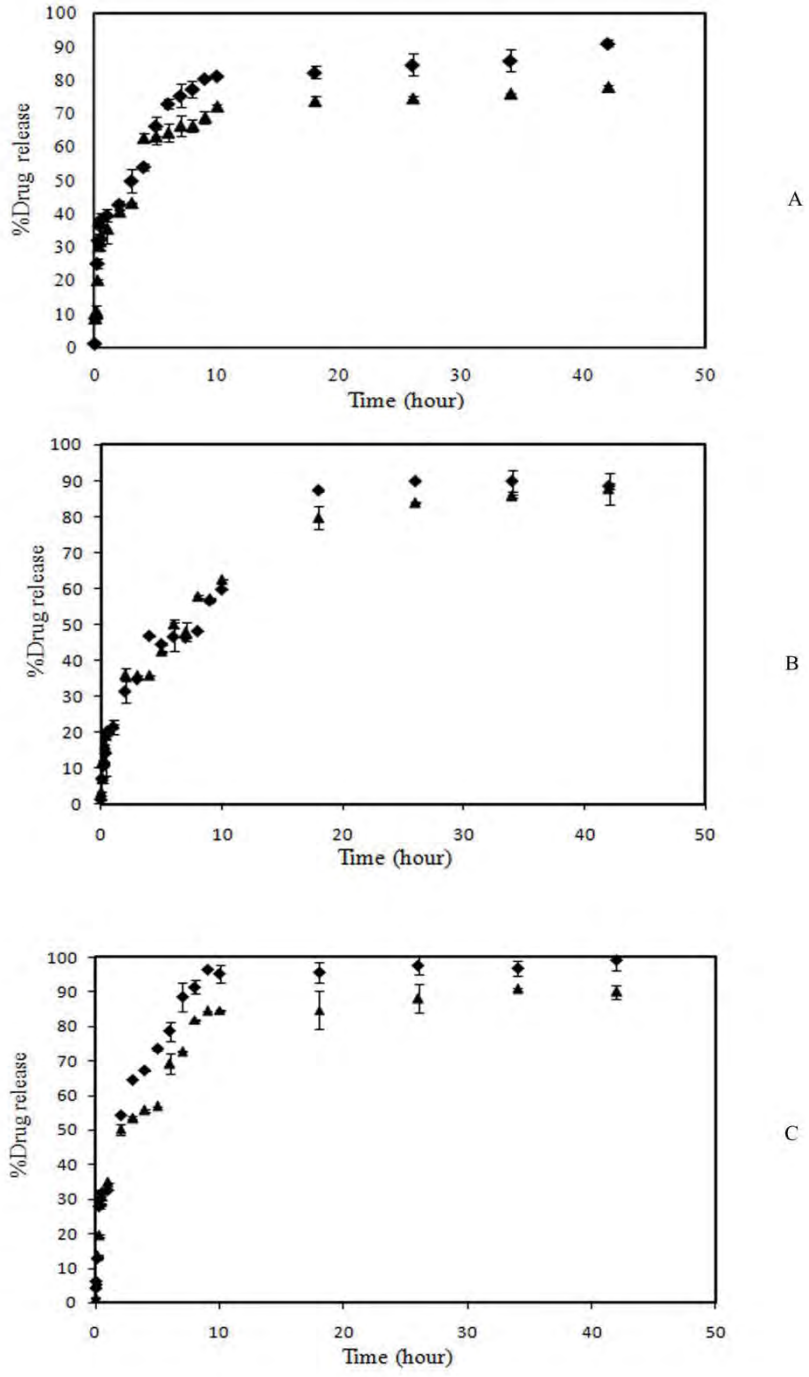


Figure 12 Prednisolone-releasing profiles of (A) 50:50, (B) 70:30 and (C) 90:10 PEGMA-ABA-coated MNPs in PBS releasing media, (◆) under UV and (▲) without UV irradiation

## 4. Conclusions

This work presented a “grafting-from” method to modify MNP surfaces with PEGMA and ABA statistical copolymer *via* ATRP reaction and a study on its application for photocontrolled drug release. The originality of this work is that this is the first report on conjugating photoresponsive azobenzene on MNP surface. It was hypothesized that the change in configuration from *trans* to *cis* in azobenzene moiety renders the system more polar, resulting in acceleration of the repelling rate of prednisolone, the hydrophobic model drug, entrapped in azobenzene in the particle surface. Increasing percentage of azobenzene in the copolymer seemed to promote %EE and %DLE of the complex. Under UV irradiation, the percentage of the released drug was slightly higher than the system without UV irradiation. This complex was hypothetically applicable to load any other hydrophobic drug by partitioning to azobenzene moiety on the particle surfaces. Improvement of drug loading efficiency and releasing behavior of the complex is warranted for future studies for potential uses as magnetic field-directed drug delivery vehicle with photocontrollable drug release.

Acknowledgement. The authors thank the Thailand Research Fund (TRF) (DBG5380001) and Naresuan University for financial funding. The National Research Council of Thailand (NRCT) is also acknowledged. The Center of Excellence for Innovation in Chemistry (PERCH-CIC), Commission on Higher Education, Ministry of Education is gratefully acknowledged for financial supports.

Supporting Information Available: TGA thermograms of PEGMA-coated MNP and 90:10 PEGMA-ABA-coated MNP. A first-order plot of 100:0 PEGMA-ABA polymer and conversion plots of 70:30 PEGMA-ABA copolymer and 90:10 PEGMA-ABA copolymer.

## REFERENCES

Anders S, Sun S, Murray CB, Rettner CT, Best ME, Thomson T, Albrecht M, Thiele J-U, Fullerton EE, Terris BD (2002) Lithography and self-assembly for nanometer scale magnetism .Microelectron Eng 61-62:569-575

Archut A, Azzellini GC, Balzani V, Cola LD, Vgtle F (1998) Toward photoswitchable dendritic hosts Interaction between azobenzene-functionalized dendrimers and erosin. J Am Chem Soc 120:12187-12191

Aruna P, Rao BS (2009) Ionomeric poly(urethane semicarbazides) with azobenzene groups in the main chain-studies on photoswitching behavior and mechanical properties. React Funct Polym 69:20-26

Bucio E, Skewes P, Burillo G (2005) Synthesis and characterization of azo acrylates grafted onto polyethylene terephthalate by gamma irradiation. Nucl Instrum Methods Phys Res 236:301-306

Dokic J, Gothe M, Wirth J, Peters MV, Schwarz J, Hecht S, Saalfrank P (2009) Quantum chemical investigation of thermal cis-to-trans isomerization of azobenzene derivatives: Substituent effects, solvent effects, and comparison to experimental data. J Phys Chem A 113:6763-6773

Fan QL, Neoh KG, Kang ET, Shuter B, Wang SC (2007) Solvent- free atom transfer radical polymerization for the preparation of poly (poly(ethyleneglycol) monomethacrylate)-grafted Fe3O4 nanoparticles: Synthesis, characterization and cellular uptake. Biomaterials 28:5426-5436

Fischer H (1999) The persistent radical effect in controlled radical polymerizations. J Polym Sci., Part A: Polym Chem 37:1885-1901

Fischer H (2001) The Persistent radical effect: A principle for selective radical reactions and living radical polymerizations. Chem Rev 101:3581-3610

Fujiwara M, Akiyama M, Hata M, Shiokawa K, Nomura R (2008) Photoinduced acceleration of the effluent rate of developing solvents in azobenzene-tethered silica gel. ACS Nano 2:1671-1681

Hermann High LR, Holder SJ, Penfold HV (2007) Synthesis of star polymers of styrene and alkyl (Meth)acrylates from a porphyrin initiator core via ATRP. Macromolecules 40:7157-7165

Hu F, Neoh KG, Cen L, Kang ET (2006) Cellular response to magnetic nanoparticles “PEGylated” via surface-initiated atom transfer radical polymerization. Biomacromolecules 7:809-816

Kalyanasundaram K, Thomas JK (1977) Environmental effects on vibronic band intensities in pyrene monomer fluorescence and their application in studies of micellar systems. J Am Chem Soc 99:2039-2044.

Kim SY, Lee YM, Kang JS (2005) Indomethacin-loaded methoxy poly(ethylene glycol)/poly(D,L-lactide) amphiphilic diblock copolymericnanospheres: Pharmacokinetic and toxicity studies in rodents. J Biomed Mater Res Part A 74A:581-590

Laurent S, Forge D, Port M, Roch A, Robic C, Elst LV, Muller RN (2008) Magnetic iron oxide nanoparticles: synthesis, stabilization, vectorization, physicochemical characterizations, and biological applications. Chem Rev 108:2064-2110

Lee JH, Carraway ER, Schlautman MA, Yim S, Herbert BE (2004) Characterizing pyrene-Ag+ exciplex formation in aqueous and ethanolic solutions. J Photochem Photobiol A 167:141-148

Li Y, Deng Y, Tong X, Wang X (2006) Formation of photoresponsive uniform colloidal spheres from an amphiphilic azobenzene-containing random copolymer. Macromolecules 39:1108-1115

Liu G, Yan X, Lu Z, Curda SA, Lal J (2005) One-Pot synthesis of block copolymer coated cobalt nanocrystals. Chem Mater 17:4985-4991

Liu KW, Bian S, Li L, Samuelson L, Kumar J, Tripathy S (2000) Enzymatic synthesis of photoactive poly(4-phenylazophenol). Chem Mater 12:1577-1584

Maria PD, Fontana A, Gasbarri C, Siani G, Zaniratob P (2009) Kinetics of the Z-E isomerization of monosubstituted azobenzenes in polar organic and aqueous micellar solvents. Arkivoc 8:16-29

Marutani E, Yamamoto S, Ninjbadgar T, Tsujii Y, Fukuda T, Takano M (2004) Surface-initiated atom transfer radical polymerization of methyl methacrylate on magnetite nanoparticles. Polymer 45:2231-2235

Moineau G, Granel C, Dubois Ph, Jerome R, Teyssie P (1998) Controlled radical polymerization of methyl methacrylate initiated by an alkyl halide in the presence of the wilkinson catalyst. Macromolecules 31:542-544

Monteiro MJ, Adamy MM, Leeuwen BJ, Herk AM, Destarac M. (2005) “Living” radical ab initio emulsion polymerization of styrene using a fluorinated xanthate agent. Macromolecules 38:1538-1541

Neugebauer D (2007) Graft copolymers with hydrophilic and hydrophobic polyether side chains. Polymer 48:4966-4973

Nishimura N, Kosako S, Sueishi Y (1984) The thermal isomerization of azobenzenes. III. Substituent, solvent, and pressure effect on the thermal isomerization of push-pull azobenzenes. Bull Chem Soc Jpn 57:1617-1625

Park EK, Lee SB, Lee YM (2001) Preparation and characterization of methoxy poly(ethylene glycol)/poly(e-caprolactone) amphiphilic block copolymeric nanospheres for tumor-specific folate-mediated targeting of anticancer drugs. Biomaterials 26:1053-1061

Pei W, Kumada H, Natusma T, Saito H, Ishio S (2007) Study on magnetite nanoparticles synthesized by chemical method. J Mag Magn Mater 310:2375-2377

Pinna N, Grancharov S, Beato P, Bonville P, Antonietti M, Niederberger M (2005) Magnetite nanocrystals: Nonaqueous synthesis characterization and solubility. Chem Mater 17:3044-3049

Sellmyer DJ (2002) Strong magnets by self-assembly. Nature 420:374-375

Sharma L, Kimura T (2003) FT-IR investigation into the miscible interactions in new materials for optical devices. Polym Adv Technol 14:392-399

Sin SL, Gan LH, Hu X, Tam KC, Gan YY (2005) Photochemical and thermal isomerizations of azobenzene-containing amphiphilic diblock copolymers in aqueous micellar aggregates and in film. Macromolecules 38:3943-3948

Sun S, Murray CB, Weller D, Folks L, Moser A (2000) Monodisperse FePt Nanoparticles and Ferromagnetic FePt Nanocrystal Superlattices. Science287:1989-1992

Sun Y, Ding X, Zheng Z, Cheng X, Hu X, Peng Y (2007) Surface initiated ATRP in the synthesis of iron oxide/polystyrene core/shell nanoparticles. Eur Polym J 43:762-772

Teng X, Yang H (2003) Synthesis of Face-Centered Tetragonal FePt Nanoparticles and Granular Films from Pt@Fe2O3 Core-Shell Nanoparticles. J Am Chem Soc 125:14559-14563

Teodorescu M, Matyjaszewski K (1999) Atom rransfer radical polymerization of (Meth)acrylamides. Macromolecules 32:4826-4831

Veiseh O, Gunn JW, Zhang M (2010) Design and fabrication of magnetic nanoparticles for targeted drug delivery and imaging. Adv Drug Delivery Rev 62:284-304

Wang Y, Zhang M, Moers C, Chen S, Xu H, Wang Z, Zhang X, Li Z (2009) Block copolymer aggregates with photo-responsive switches:Towards a controllable supramolecular container. Polymer 50:4821-4828

Winnik FM, Winnik MA, Tazuke S (1987) Interaction of hydroxypropylcellulose with aqueous surfactants: Fluorescence probe studles and a look at pyrene-labeled polymer. J Phys Chem 91:594-597

Woo K, Hong J, Choi S, Lee HW, Ahn JP, Kim CS, Lee SW (2004) Easy synthesis and magnetic properties of iron oxide nanoparticles. Chem Mater 16:2814-2818

Yager KG, Barrett CJ (2006) Novel photo-switching using azobenzene functional materials. J Photochem Photobiol, A 182:250-261

Zhang J, Misra RDK (2007) Magnetic drug-targeting carrier encapsulated with thermo sensitive smart polymer: Core–shell nanoparticle carrier and drug release response. Acta Biomater 3:838-850

Zhao H, Shipp DA (2003) Preparation of Poly(styrene-block-butyl acrylate) block copolymer-silicate nanocomposites. Chem Mater 15:2693-2695

Zhou Y, Wang S, Ding B, Yang Z (2008) Modification of magnetite nanoparticles via surface-initiated atom transfer radical polymerization (ATRP). Chem Eng J 138:578-585

**Supporting Information**

TGA thermograms of PEGMA-coated MNP and 90:10 PEGMA-ABA-coated MNP.

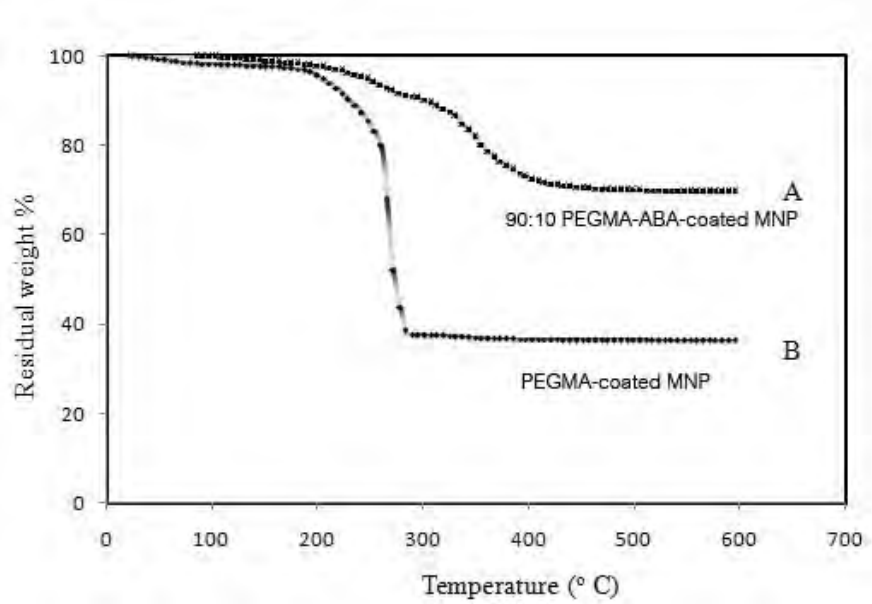


A first-order plot of 100:0 PEGMA-ABA polymer

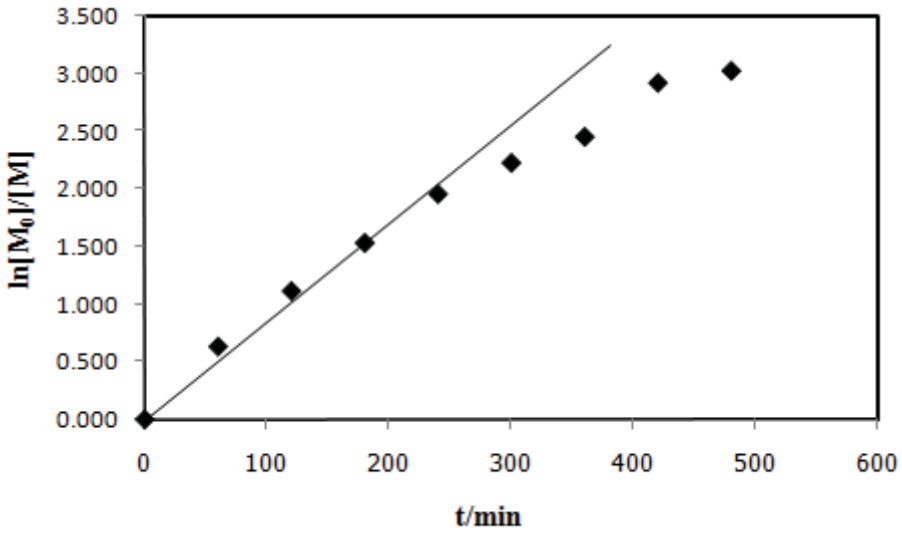

Conversion plots of 70:30 PEGMA-ABA copolymer

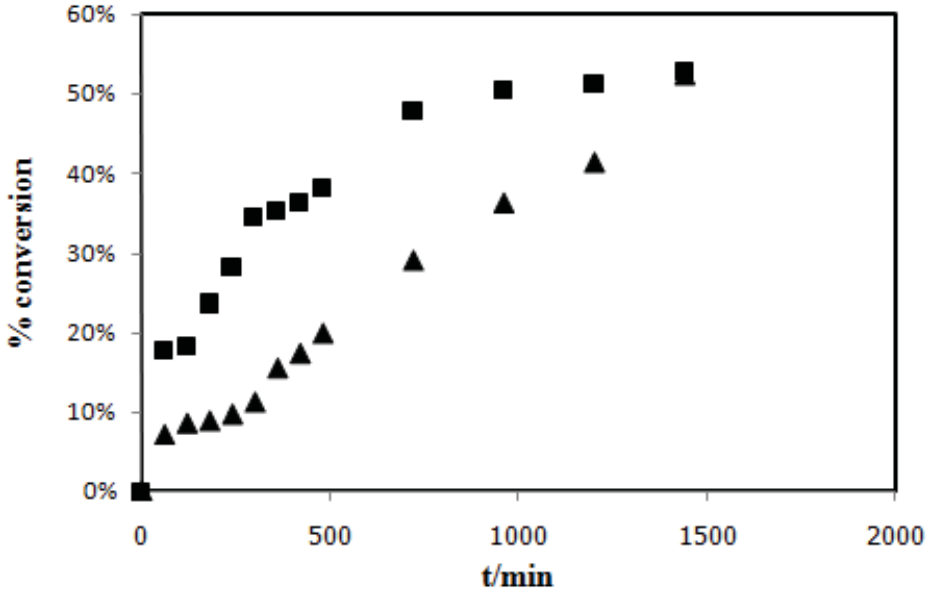


Conversion plots of 90:10 PEGMA-ABA copolymer.

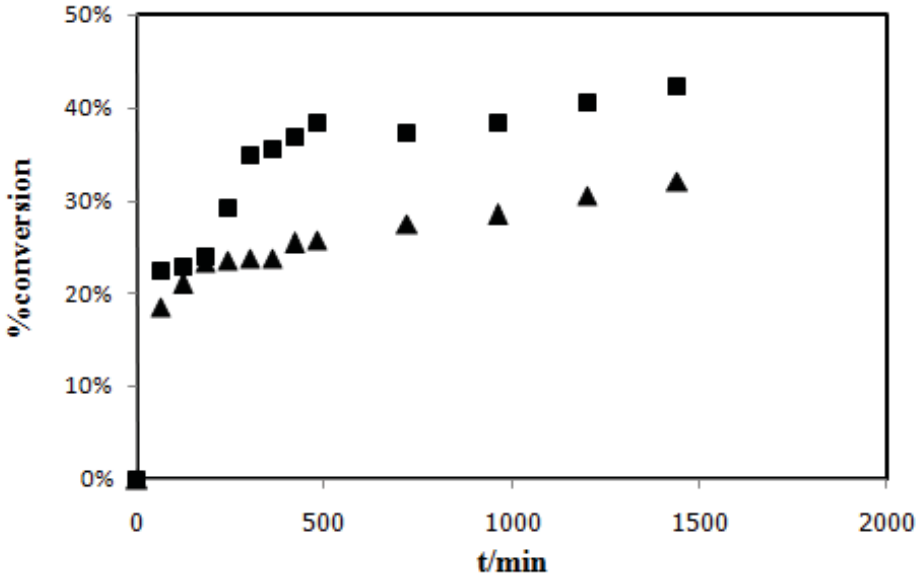

# Magnetite nanoparticle coated with amphiphilic bilayer surfactant of polysiloxane and poly(poly(ethylene glycol) mathacrylate)

*Bandit Thong-On, Boonjira Rutnakornpituk, Uthai Wichai and Metha Rutnakornpituk**

**Abstract:** We are here reporting the surface modification of magnetite nanoparticle (MNP) with amphiphilic steric stabilizer of polydimethylsiloxane (PDMS) and poly(poly(ethylene glycol) methacrylate) (PPEGMA). The main purpose of this work is to obtain the polymeric bilayer surfactant of hydrophobic PDMS inner shell and hydrophilic PPEGMA brush corona on MNP core. Functionalized PDMS was first synthesized and then covalently grafted on the functionalized MNP surface. The PDMS-coated MNP served as a reactive macroinitiator for ATRP of PPEGMA. Kinetics studies indicated the constant consumption of PEGMA during first 7 h of the ATRP. Transmission electron microscopy (TEM) showed the average particle size of 7 nm in diameter. Fourier transform infrared spectrophotometry (FTIR), thermogravimetric analysis (TGA) and vibrating sample magnetometry (VSM) indicated the increase of the percentage of the copolymer in the complex when the ATRP was prolonged. The decrease in its hydrodynamic size from 446 nm to 162 nm when the ATRP was extended indicated the improvement in its dispersibility in water. In addition, it was found that percent entrapment efficiency and loading efficiency of indomethacin model drug in the PPEGMA-coated MNP was 62% and 27 %, respectively.

*Keywords*: magnetite; bilayer; ATRP

## 1. Introduction

During these recent years, magnetite nanoparticle (MNP) ($Fe_3O_4$) has widely been of scientific and technological interest because of its magnetically guidable and nanoscale-related properties. The broad applications of MNP include magnetic resonance imaging (MRI) enhancement [Lee et al., 2009; Park et al., 2003; Pei et al., 2007; Hong et al., 2008; Jaffer et al., 2006], drug delivery [Jain et al., 2009; Meerod et al., 2008; Rutnakornpituk et al., 2010], magnetic separation and diagnosis of biological molecules such as DNA and antibodies [Pich et al., 2004; Öisjöen et al., 2009; Brestovac et al., 2005]. MNP is usually stabilized either by charge repulsion of electrical surface or steric repulsion of long-chain polymeric surfactants [Chorny et al., 2010; Storm et al., 2002; Zhang et al., 2005] grafted on

their surfaces to prevent particle aggregation. Several methods have been investigated to prepare polymer-coated MNP, such as physical adsorption of polymers on the particle surfaces, emulsion polymerization in the presence of nanoparticles and the so-called “grafting to” and “grafting from” strategies [Fan et al., 2007; Galeotti et al., 2011; Kralj et al., 2010; Cao et al., 2009].

Many attempts have recently been made on preparing core/shell MNP that possessed polymer-coated surfaces. Atom transfer radical polymerization (ATRP) has been successfully applied to surface-initiated grafting polymerization in order to prepare a dense polymeric layer with controlled structure on the surface of MNP [Galeotti et al., 2011; Rutnakornpituk et al., 2011; Neugebauer, 2007; Sun et al., 2007]. ATRP is one of a controlled radical polymerization method that has widely applied for (co)polymerization of homo- and block (co)polymers because it allows for a good control in the molecular weight and polydispersity of the (co)polymers. ATRP has been used for polymerizations of a wide range of functional monomers such as styrene [Brown and Price., 2001; Yi et al., 2007; Reining, 2002; Qiang et al., 2006], (meth)acrylates [Semsarzadeh et al., 2003; Yin et al., 2005; Wootthikanokkhan et al., 2001] and (meth)acrylamides [Monge and Haddleton., 2004; Jiang et al., 2008]. It was found that reasonable $\overline{M_n}$ and narrow polydispersity indice (PDI) of the polymers were obtained.

The primary aim of this work was to coat MNP surface with amphiphilic surfactant of PPEGMA and PDMS to obtain the particles with bilayer surface of hydrophobic PDMS inner shell and hydrophilic PPEGMA corona. Precedents have reported the stabilization of MNP with a variety of amphiphilic copolymers, such as poly(ethylene oxide) (PEO)-poly(propylene oxide) (PPO) copolymer [Jain et al., 2009], poly(ethylene glycol) methyl ether (mPEG)-poly(ε-caprolactone) (PCL) copolymer [Meerod et al., 2008; Rutnakornpituk et al., 2010], polyurethane (PU)-PEO copolymer [Harris et al., 2003] and PDMS-poly(lactide) (PLA) copolymer [Ragheb and Riffle., 2008], to obtain stable MNP dispersions in water. Physical adsorption [Jain et al., 2009; Meerod et al., 2008; Rutnakornpituk et al., 2010] or ionic interactions[Harris et al., 2003; Ragheb and Riffle., 2008] of one block of the copolymers to MNP surface was mostly proposed for the particle stabilization mechanism. Because of their weak interactions, dissolution of the copolymers from MNP surface when used for a long period of time was concerned. The advantage of our present work is that the PDMS hydrophobic block was covalently bound onto the MNP surface, which might diminish the stabilization limitation for long-term applications. In addition, the hydrophobic

PDMS inner layer can be used as a reservoir for entrapment of hydrophobic compounds, while the hydrophilic PPEGMA provides steric repulsion and water dispersibility to the particles.

In this report, PDMS was first synthesized *via* an acid-catalyzed ring-opening copolymerization of $D_4$ and $D_4H$, followed by ATRP of PPEGMA brush from the polysiloxane macroinitiator. Kinetic studies of the ATRP of PEGMA from the PDMS macrointiator were investigated *via* nuclear magnetic resonance spectroscopy ($^1$H NMR). TEM was conducted to determine the particle size and its distribution and photocorrelation spectroscopy (PCS) was performed to determine hydrodynamic size of the copolymer-MNP complex. Magnetic properties of the complex were investigated *via* VSM. The percentages of the composition in the copolymer-MNP complex were also determined *via* TGA. In addition, the preliminary studies on the entrapment and loading efficiencies of indomethacin as a model drug in this complex are also reported.

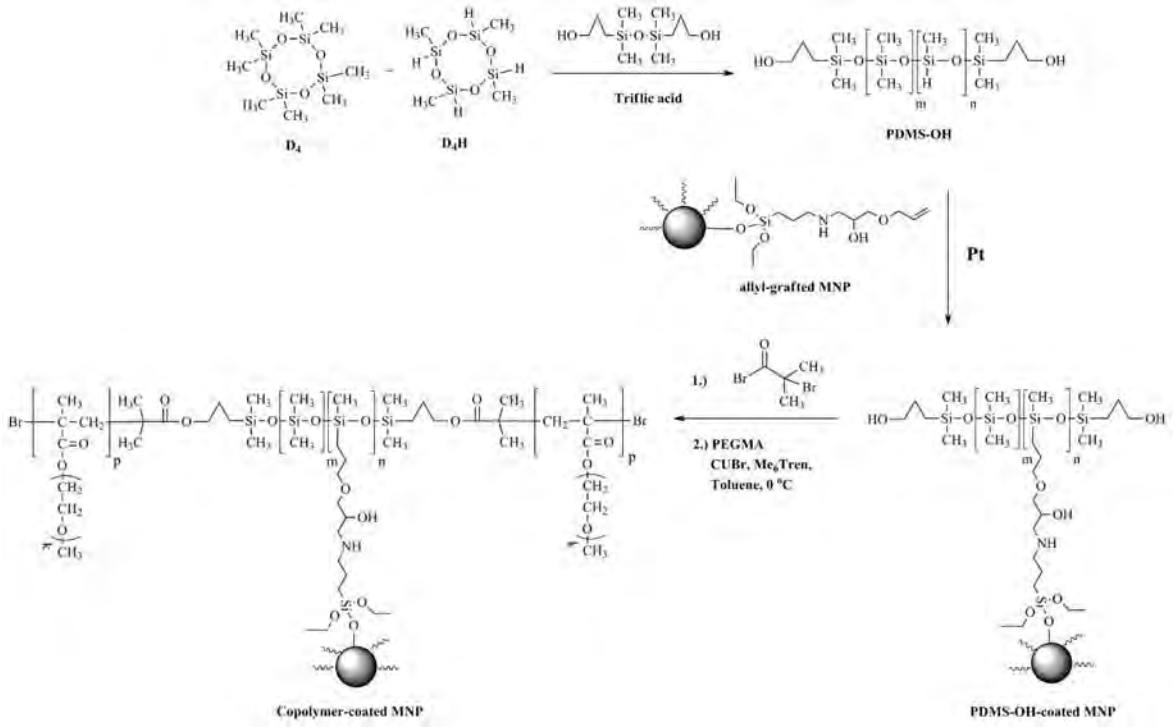


**Figure 1** Surface modification of MNP with amphiphilic steric surfactant of PDMS and PPEGMA

## 2. Experimental

### 2.1 Materials

Unless otherwise stated, all reagents were used without further purification: iron (III) acetylacetonate ($Fe(acac)_3$), 99.9% (Acros), benzyl alcohol, 98% (Unilab), oleic acid (Fluka), CuBr, 99.999% (Aldrich), triethylamine, 97% (Carto Erba), 3-aminopropyl triethoxysilane, 99% (Acros), 2-bromoisobutyryl bromide (BIBB), 98% (Acros) and allyl glycidyl ether, 99% (Acros). $D_4$, 99% (Fluka) and *$D_4H$*, 95% (Fluka) were stirred in $CaH_2$ and distilled prior to use. 1,1,3,3-Tetramethyldisiloxane, 97% (Acros) and allyl alcohol, 99C% (Acros) were fractionally distilled and stored under $N_2$ until used. Poly(ethylene glycol) methacrylate (PEGMA) (Aldrich) with average $\overline{M_n}$ of 300 g.mol$^{-1}$ was purified by passing through basic and neutral alumina, respectively and stored at -4 $^{o}$C after purification. $Me_6$Tren was prepared according to the previously reported procedure and the details of the syntheses have been provided in the supporting information. *N*,*N*-dimethyl formamide (Acros), toluene (Acros) and $CDCl_3$ (Euriso-Top) were used as received.

### 2.2 Syntheses

*2.2.1. Synthesis of PDMS via acid-catalyzed ring-opening polymerization*

*2.2.1.1. Synthesis of 3-dihydroxypropyl tetramethyl disiloxane (disiloxane diol) as an endcapper*

Allyl alcohol (4.2 ml, 0.06 mole), toluene (15 ml) and platinum (0)-1,3-divinyl-1,1,3,3-tetramethyldisiloxane complex (0.046 ml, 0.5%v/v) were charged into a reaction flask with consistently stirring at 50 $^{o}$C. 1,1,3,3-Tetramethyldisiloxane (5 ml, 0.025 mole) was then slowly introduced into the reaction flask *via* a dropping funnel. The reaction temperature was set at 65 $^{o}$C for 4 h. After the reaction was complete, an excess of allyl alcohol was removed from the mixture under reduced pressure at 65 $^{o}$C for at least 3 h.

*2.2.1.2. Synthesis of hydroxyl-terminated polydimethylsiloxane (PDMS-OH)*

PDMS-OH was prepared through an equilibrium acid-catalyzed ring-opening copolymerization of $D_4$ and $D_4H$. 1:1 Molar ratio of $D_4$ to $D_4H$ ($D_4$, 1 g, 3.4 mmole and $D_4H$, 0.81 g, 3.4 mole) was used in the reaction with the use of the disiloxane diol (0.19 g, 0.722 mmole) end capping agent. After the reaction temperature was raised to 50 $^{o}$C, trifluoromethane sulfonic acid (triflic acid) (0.001 ml, 0.65%v/v) was slowly added into the solution *via* a syringe. The reaction was equilibrated at 55 $^{o}$C for 48 h. The acidic mixture was cooled to room temperature, dissolved in diethyl ether and neutralized by extraction with

water. The mixture was dried over sufficient anhydrous magnesium sulfate with continuously stirring for 30 min and subsequently filtered through a filter paper. Diethyl ether was evaporated *via* a rotary evaporator and monomers remaining from the equilibration were removed under reduced pressure at 60 $^{o}$C overnight.

*2.2.2. Synthesis of allyl-grafted MNP*

APS (2.734 ml, 0.012 mole) was slowly introduced into a mixture of sulfamic acid (SA) (0.1 g, 1.03 mmol) and allyl glycidyl ether (1.175 g, 0.010 mol) under nitrogen atmosphere. The reaction was set at room temperature for 12 h with stirring. After reaction was complete, SA was removed by filtration and the product was washed with diethyl ether (3×10 ml) and evaporated until dryness. The as-synthesized allyl-containing silane compound (0.1 ml) and 2 M TEA in toluene (1 ml) were added into the dispersion of oleic acid-coated MNP (0.1 g oleic acid-coated MNP in 5 ml toluene) and the details of the synthesis of oleic acid-coated MNP have been provided in the supporting information. The mixture was stirred at room temperature for 24 h under nitrogen blanket. The particles were precipitated in ethanol, following by external magnet separation to obtain the allyl-grafted MNP. Then, the MNP were re-dispersed in toluene and re-precipitated in ethanol. This procedure was repeated three times to remove unreacted species from the particles.

*2.2.3. Immobilization of the PDMS onto surface of the allyl-grafted MNP and ATRP of PPEGMA from the particle surface*

The PDMS-OH (1 g, 0.476 mmole) was slowly introduced into the reaction mixture of the allyl-grafted MNP dispersion (0.1 g of the MNP in 10 ml toluene) and Pt catalyst (Platinum (0)-1,3-divinyl-1,1,3,3-tetramethyldisiloxane complex). The reaction temperature was set at 70$^{o}$C for 6 h. After the reaction was complete, the precipitants were removed from the dispersion using an external magnet and washed with ethanol and toluene, respectively. BIBB (0.15 ml, 0.05 mmole) was slowly introduced into the reaction mixture of the PDMS-OH-coated MNP dispersion (0.1 g of the PDMS-coated MNP in 10 ml toluene) and 2 M TEA in toluene (0.25 ml) at 0$^{o}$C under nitrogen atmosphere. A white precipitate was formed upon the addition. The reaction temperature was set at room temperature for 24 h with stirring. After the reaction was complete, the precipitants of PDMS-Br-coated MNP were removed from the dispersion using an external magnet and washed with ethanol and toluene, respectively.

The mixture of the PDMS-Br-coated MNP (0.1 g) and PEGMA (3 ml, 0.01 mole) dispersed in toluene (2 ml, 60% w/v) was sonicated for 1 h and purged with nitrogen gas for 15 min. After the addition of CuBr (0.014 g, 0.1 mmole), Me6-Tren (0.025 ml, 0.1 mmole) and dialkyl bromide disiloxane (0.055 ml, 0.1 mmole) as a sacrificial initiator (the synthesis has been provided in the supporting information), ATRP reaction was carried out at room temperature for 24 h with nitrogen gas purging and magnetically stirring. After the polymerization, the particles were precipitated in ethanol and the aggregate was repeatedly washed with ethanol to remove unreacted PEGMA, CuBr and the ligand. The as-synthesized PPEGMA-coated MNP was finally dried under reduced pressure.

### 2.3. Characterization

$^{1}$H NMR spectra were performed on a 400 MHz Bruker NMR spectrometer using $CDCl_3$ as a solvent. FTIR was performed on a Perkin-Elmer Model 1600 Series FTIR Spectrophotometer in the wavenumber range of 4000-400 $cm^{-1}$. Liquid samples were directly cast onto potassium chloride plates. Solid samples were made by the pressed disc method after mixing dried solid samples with KBr. TEM was performed on Philips Tecnai 12, operated at 120 kV equipped with Gatan model 782 CCD camera. The sample solution in water or toluene was directly cast onto carbon-coated copper grids and let to slowly evaporate at room temperature. Magnetic properties of the particles were measured at room temperature using a Standard 7403 Series, Lakeshore vibrating sample magnetometer (VSM). Magnetic moment of each sample was investigated over a range of ± 10000 G of applied magnetic fields using 30 min sweep time. TGA was performed on SDTA 851 Mettler-Toledo at the temperature ranging between 25 and 600$^{o}$C at a heating rate of 20$^{o}$C/min under oxygen atmosphere. Hydrodynamic size of the particles was measured by PCS using NanoZS4700 nanoseries Malvern instrument. DI water used as a dispersing media was filtered through 0.22 μm nylon syringe filters before used. The aqueous dispersions of the particles were sonicated for 10 min before the measurement without filtration.

### 2.4 Investigation of entrapping and loading efficiencies of indomethacin in PPEGMA-coated MNP

To incorporate indomethacin, the model drug, to the particles, the drug solution (2 ml, 25 mg/ml in THF) was added dropwise with stirring to an aqueous dispersion of

PPEGMA-coated MNP (5 ml). The mixture was stirred for 30 min to remove THF and to allow fully partitioning the drug into the hydrophobic shell of the particles. Drug-loaded magnetite was then separated using an external magnet. The concentration of the excess drug in the supernatant was determined using UV-Visible spectrophotometer. The amount of the entrapped drug in the particles was determined from the difference of the weights of the loaded drug and the excess of the drug remaining dispersible in the solution. The details of the calculation are provided in the supporting information. Entrapment efficiency and drug loading efficiency (DLE) were determined as followed:

$$\text{Entrapment efficiency (\%EE)} = \frac{\text{Weight of the entrapped drug in the particles}}{\text{Weight of loaded drug}} \times 100$$

$$\text{Drug loading efficiency (\%DLE)} = \frac{\text{Weight of the entrapped drug in the particles}}{\text{Weight of the particles}} \times 100$$

## 3. Results and discussion

The primary aim of this work was to coat MNP with a novel amphiphilic surfactant to obtain bilayer surface of hydrophobic PDMS inner shell and hydrophilic PPEGMA corona. It was envisioned that the hydrophobic PDMS inner layer can be used as a reservoir for entrapment of hydrophobic entities and the hydrophilic PPEGMA brush provided steric repulsion and water dispersibility to the particles. Polysiloxane was first synthesized *via* an acid-catalyzed ring opening copolymerization of $D_4$ and $D_4H$ to obtain the Si-H-containing PDMS. This reaction was designed such that the PDMS can be covalently grafted onto the MNP surface through hydrosillylation. The PDMS-coated MNP can be then used as a macroinitiator for ATRP of PPEGMA to form water dispersible particles with double-layer surface.

### *3.1. Synthesis of difunctionalized PDMS via an acid-catalyzed ring-opening polymerization*

#### *3.1.1. Synthesis of dihydroxypropyl tetramethyl disiloxane (disiloxane diol)*

Disiloxane diol was synthesized through a hydrosillylation between 1,1,3,3-tetramethylsiloxane and allyl alcohol to obtain the hydroxyl-terminated endcapper. $^{1}$H NMR

indicated the formation of the linkages corresponding to the coupling reaction of Si-H bond to allyl alcohol: methylene protons (–C<u>H</u>$_2$–) of propyl alcohol at 0.5, 1.5 and 3.6 ppm. In addition, the disappearance of Si-H signal (4.7 ppm) signified the formation of the disiloxane diol. The resultant product appeared as transparent oil (70.5% yield). The FTIR and $^1$H NMR spectra of the product have been provided in the supporting information. $^1$H NMR (400 MHz, $CDCl_3$) $\delta_H$ : 0.05 [m, 12H, Si-C<u>H</u>$_3$], 0.50 [m, 4H, Si-C<u>H</u>$_2$], 1.60 [m, 4H, $CH_2$-C<u>H</u>$_2$-$CH_2$], 2.00 [s, 1H, $CH_2$-O<u>H</u>], 3.60 [m, 4H, $CH_2$-C<u>H</u>$_2$-OH]. FT-IR (thin film) $\upsilon_{max}$ : 3369 cm$^{-1}$ (O-H stretching), 2958 cm$^{-1}$ (C-H stretching), 1411 cm$^{-1}$ ($CH_2$ stretching), 1260 cm$^{-1}$ (Si-$CH_3$ stretching), 1078 cm$^{-1}$ (Si-O stretching) and 800 cm$^{-1}$ (Si-C stretching).

### 3.*1.2. Synthesis of hydroxyl-terminated polydimethylsiloxane (PDMS-OH)*

PDMS-OH was synthesized *via* a ring-opening polymerization of $D_4$/*$D_4H$* mixture. 1:1 Molar ratio of $D_4$ to $D_4H$ was used in this reaction in order to introduce Si-H linkages in the polysiloxane chain for further functionalization. The signal at 4.7 ppm corresponding to the hydrogen on Si (Si-<u>H</u>) indicated the presence of Si-H thoroughly dispersed in the polysiloxane chain. The $^1$H NMR spectra of the product have been provided in the supporting information. In good agreement with $^1$H NMR, FTIR spectrum manifested the presence of Si-H bond (2160 cm$^{-1}$), Si-O bond (1038 cm$^{-1}$) and Si-$CH_3$ bond (1261 cm$^{-1}$) of the PDMS-OH (Figure 2A). The 2,500 g/mol-targeted $\overline{M_n}$ of the PDMS-OH were controlled by adjusting the molar ratio of the cyclic monomers to the disiloxane diol endcapper. The methyl protons on Si (Si-C<u>H</u>$_3$, 0.06 ppm) relative to the methylene protons at the chain terminals (Si-$CH_2CH_2C$<u>H</u>$_2$OH, 3.60 ppm) were used to calculate its $\overline{M_n}$ using an endgroup analysis method *via* $^1$H NMR. The $\overline{M_n}$ of the as-synthesized PDMS-OH was approximately 2,254 g/mol (m=19, n=14).

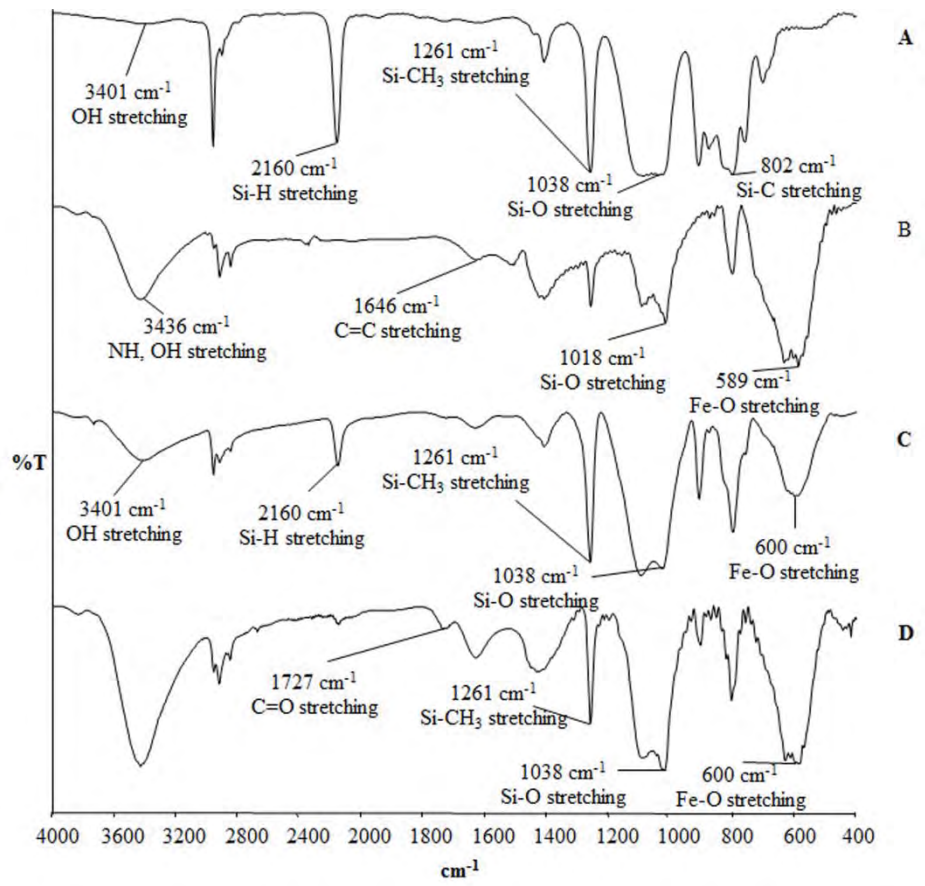


**Figure 2** FTIR spectra of A) PDMS-OH, B) allyl-grafted MNP, C) PDMS-OH-coated MNP and D) PDMS-Br-coated MNP

*3.2. Synthesis of allyl-grafted MNP*

To prepare allyl-grafted MNP, allyl-containing silane was first synthesized. It was prepared through a ring-opening reaction of epoxide ring of allyl glycidyl ether with an amino group of aminopropyl triethoxysilane to obtain allyl-containing silane compound. The resultant product appeared as yellowish oil (87% yield). The $^{1}$H NMR spectrum of the product is shown in the supporting information. In combination with the disappearance of the signals of the epoxide ring, the presence of the signals at 5.3-5.8 ppm (allyl protons), 1.2 and 3.8 ppm (ethoxy protons) indicated the formation of allyl-containing silane product. In addition, the C=C signal of allyl functional groups (1647 cm$^{-1}$) in the resultant product was apparent in FTIR spectrum. FTIR: 3412 cm$^{-1}$ (NH, O-H stretching), 2927 cm$^{-1}$ (C-H stretching), 1647 cm$^{-1}$ (C=C stretching), 1490 cm$^{-1}$ ($CH_2$ stretching), 1103 cm$^{-1}$ (C-O-C, Si-O stretching) and 800 cm$^{-1}$ (Si-C stretching). $^{1}$H NMR (400 MHz, $CDCl_3$) $\delta_H$ : 0.50 [m, 2H, $CH_2$-C<u>H</u>$_2$-Si], 1.15 [t, 9H, O-$CH_2$-C<u>H</u>$_3$], 1.50 [m, 2H, $CH_2$-C<u>H</u>$_2$-$CH_2$], 2.50 [m, 4H, C<u>H</u>$_2$-NH-C<u>H</u>$_2$], 3.40 [m, 2H, -O-C<u>H</u>$_2$-(CH-OH)-], 3.75 [m, 1H, $CH_2$-(C<u>H</u>-OH)-$CH_2$, 2H, O-C<u>H</u>$_2$-$CH_3$],

4.00 [d, 2H, -C<u>H</u>$_2$-O-CH$_2$-], 5.20 [m, 1H, CH$_2$=C<u>H</u>-CH$_2$-] and 6.80 [m, 2H, C<u>H</u>$_2$=CH-CH$_2$-]. FTIR (thin film) $\upsilon_{max}$ : 3412 cm$^{-1}$ (N-H, O-H stretching), 2927 cm$^{-1}$ (C-H stretching), 1647 cm$^{-1}$ (C=C stretching), 1490 cm$^{-1}$ (CH$_2$ stretching), 1103 cm$^{-1}$ (C-O-C, Si-O stretching) and 800 cm$^{-1}$ (Si-C stretching).

The allyl-containing silane compound was then covalently bonded onto the oleic acid-coated MNP through the combination of ligand exchange reaction and condensation of triethoxysilane to obtain allyl-grafted MNP resultant product. FTIR exhibited characteristic absorption signals of the allyl-grafted MNP: 3436 cm$^{-1}$ (N-H, O-H stretching) and 1018 cm$^{-1}$ (Si-O stretching) and 800 cm$^{-1}$ (Si-C- stretching) (Figure 2B). In combination with a strong and broad signal of Fe-O bonds (634 cm$^{-1}$), this evidenced that allyl-containing silane compound was immobilized onto the MNP surface.

*3.3 Immobilization of the PDMS onto surface of the allyl-grafted MNP and ATRP of PPEGMA from the particle surface*

To immobilize PDMS onto the surface of MNP, hydrosillylation between Si-H of the as-synthesized PDMS-OH and C=C of the allyl-grafted MNP was accomplished to obtain PDMS-coated MNP. FTIR spectrum of the PDMS-OH-coated MNP exhibited characteristic absorption signals of both PDMS-OH and MNP core: 3401 cm$^{-1}$ (O-H stretching), 1261cm$^{-1}$ (Si-CH$_3$ stretching), 1038 cm$^{-1}$ (Si-O stretching) and 600 cm$^{-1}$ (Fe-O) (Figure 2C). After the hydrosillylation, the decrease of the signal intensity of Si-H (2160 cm$^{-1}$) relative to that of Si-CH$_3$ (1261 cm$^{-1}$) indicated the depletion of Si-H linkages in the PDMS. The presence of the Si-H signal in $^1$H NMR signified the remaining of unreacted Si-H bonds after the reaction. Even though there was some Si-H trace in the PDMS, the as-synthesized PDMS-OH-coated MNP exhibited an improvement in its dispersibility in toluene when compared to the MNP without PDMS coating. TGA and VSM techniques also showed supportive results to FTIR that PDMS was bound to the MNP complexes and they have been discussed in details in the later sections.

BIBB, an active ATRP initiator, was then immobilized on the surface of PDMS-OH-coated MNP to obtain PDMS-Br-coated MNP. After the reaction, alkyl bromide groups, functioning as active ATRP initiators for PPEGMA, should present on the MNP surface. FTIR exhibited characteristic absorption signals of the PDMS-Br-coated MNP: 1727 cm$^{-1}$ (O-(C=O) carbonyl stretching), 1261 cm$^{-1}$ (Si-CH$_3$ stretching), 1038 cm$^{-1}$ (Si-O stretching) and 600 cm$^{-1}$ (Fe-O) (Figure 2D). The disappearance of Br-C=O (1767-1807 cm$^{-1}$) of BIBB

and the presence of –OC=O (1727 $cm^{-1}$) of the resultant product indicated the occurrence of the coupling reaction.

ATRP reactions of PPEGMA from the PDMS-Br-coated MNP surface were set for 24 h at room temperature. The samples were withdrawn from the reaction mixture after 1, 6 and 24 h of the reaction, ultracentrifuged to precipitate the particles, thoroughly washed with ethanol, dried *in vacuo* and characterized *via* FTIR. Figure 3 shows FTIR spectra of PEGMA oligomer and PPEGMA-coated MNP after 0, 6 and 24 h of ATRP. A progressive growth of -O(C=O)- stretching signals (1727 $cm^{-1}$) and C-O-C stretching signals (1105 $cm^{-1}$) of PPEGMA repeating units indicated that $\overline{M_n}$ of PPEGMA on MNP surfaces increased as increasing ATRP reaction time. In addition, Fe-O bond signals at 600 $cm^{-1}$ were also observed throughout the reaction.

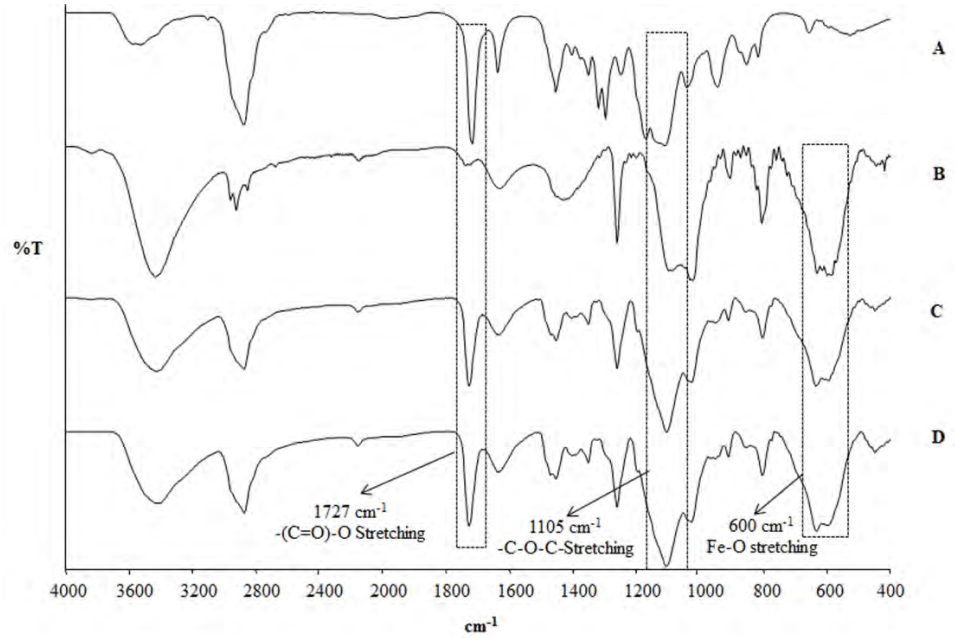


**Figure 3** FTIR spectra of (A) PEGMA oligomer, PPEGMA-coated MNP after (B) 0 h, (C) 6 h and (D) 24 h of ATRP

In the ATRP reaction, the as-synthesized dialkyl bromide disiloxane was also added into the reaction mixture as a sacrificial initiator. After ultracentrifugation of the dispersion to precipitate the particle, the supernatant containing free PPEGMA brush initiated from the sacrificial initiator was analyzed *via* $^1$H NMR to monitor the reaction progress using DMF as an internal standard. Due to the structural similarity between alkyl bromide grafted on the

particle surface and the sacrificial initiator, it was assumed that the reaction reactivities of these two initiator systems were similar.

The monomer conversion *vs* time plot of the ATRP of PPEGMA shows that the reaction rate was constant during first 7 h of the reaction and it was slowed down when the reaction was prolonged (Figure 4). In good agreement with this, the first-order plot reveals a linear relationship during the course of first 7 h of the reaction, indicating the constant consumption rate of the monomer at initial state of the reaction. After 7 h of the reaction, the rate of the reaction started to deviate from linearity at high percent monomer conversion. This was probably due the premature termination of active radicals during the polymerization due to the depletion of PEGMA concentration.

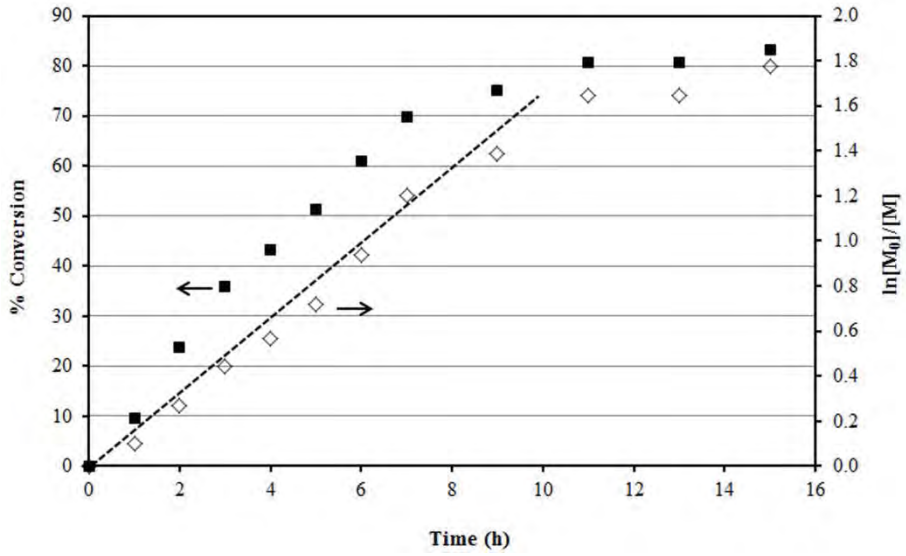


**Figure 4** Conversion *vs* time plot and first-order kinetic plot of ATRP of PPEGMA

According to the TEM measurements, the particles show narrow size distribution with the size ranging between 4 and 9 nm and the average of 7 nm in diameter (Figure 5). Figure 5B and 5C illustrate the particle distribution of the PPEGMA-coated MNP prepared from aqueous dispersions in comparison with that of the PDMS-OH-coated MNP prepared from toluene dispersion (Figure 5A). Hydrophobic PDMS in the PDMS-OH-coated MNP promoted their good dispersibility in toluene, while hydrophilic PPEGMA in the PPEGMA-coated MNP rendered them well dispersible in water. It was also noticed that dispersibility of the PPEGMA-coated MNP in water was greatly improved when ATRP reaction time was prolonged from 6 h to 24 h as indicated by the more transparent yellowish dispersion in Figure 6C (12 h) than that in Figure 6B (6 h). This implied a better coating of hydrophilic

PPEGMA on MNP surface. The slight difference in colors of the dispersions in Figure 6A and 6C was probably due to the interaction of MNP complexes in different solvents (toluene and water), which might influence the appearance of the dispersion colors. One might wonder that the color change of these dispersions may arise from the phase transformation of magnetite during the ATRP step. Selected area electron diffraction (SAED) technique was thus performed to obtain the crystal structure information of the complexes from each step of the reactions (bare MNP, PDMS-coated MNP and PPEGMA-coated MNP). Their SAED patterns revealed that the particles were crystalline and their *d*-values were in good agreement with those observed in $Fe_3O_4$ [Moisescu et al., 2008; Prai-in et al., 2012], indicating that there was no major phase transformation of magnetite core in each step. The SAED patterns of each complex are shown in the supporting information.

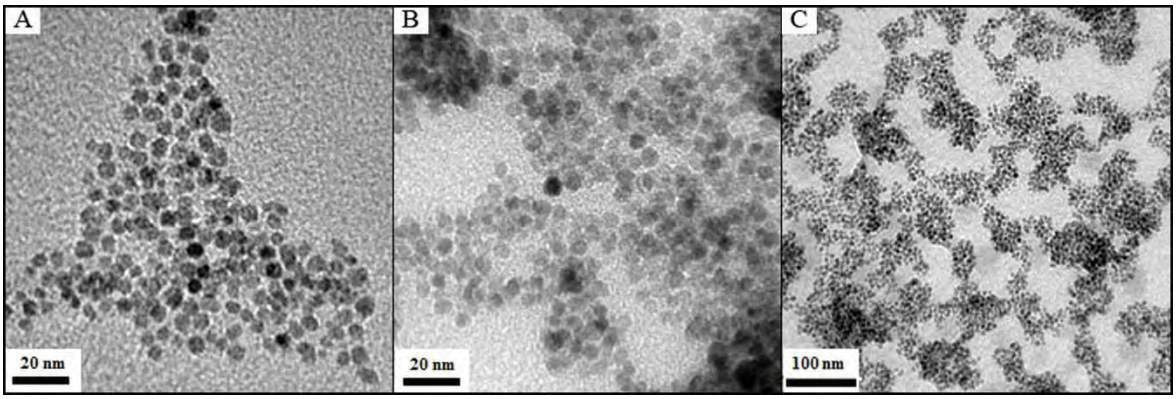


**Figure 5** TEM images of A) PDMS-OH-coated MNP prepared from toluene dispersion, B) and C) PPEGMA-coated MNP after 24 h of ATRP prepared from aqueous dispersion at different magnifications

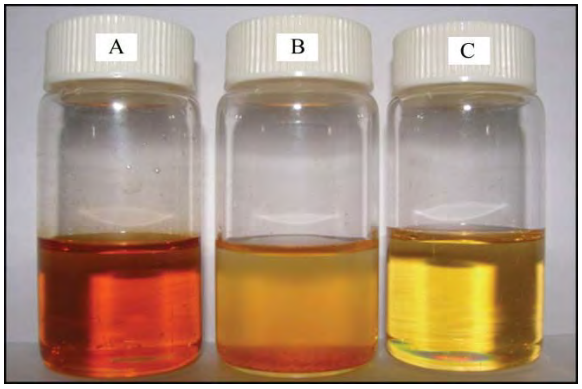


**Figure 6** Appearance of (A) PDMS-OH-coated MNP in toluene and PPEGMA-coated MNP dispersed in $H_2O$ after (B) 6 h and (C) 24 h of ATRP

PCS was conducted to investigate the hydrodynamic diameters *($D_H$)* of PDMS-OH-coated MNP dispersed in toluene and PPEGMA-coated MNP dispersed in water (Table 1). The hydrodynamic size of bare MNP in toluene was not measured because it was not well redispersible in the solvent, resulting in aggregation of the particles. In the particles stabilized with the polymers, the large $D_H$ ranging between 162 and 446 nm was attributed to the size of their complexes with some nanoscale particle aggregation. This nanoaggregate was also apparent in the TEM experiments (Figure 5C). It was also observed that $D_H$ of the PPEGMA-coated MNP after 24 h of ATRP was significantly smaller than those of the other two complexes. This was devoted to the better coating of hydrophilic PPEGMA on the particle surface, resulting in the enhancement in water dispersibility and the decrease in $D_H$ of the aggregate.

The rather large size of $D_H$ (162 nm) even after ATRP (PPEGMA-coated MNP) was probably due to the limited accessibility of PEGMA to react with the pre-formed aggregated PDMS-coated MNP. Therefore, the stability of the particles in the solvents was concerned when dispersed for long period of time. Stability studies of PDMS-coated MNP (before ATRP) in toluene and PPEGMA-coated MNP (after ATRP) in water were performed. At a given time, the dispersions were centrifuged to remove large aggregate and the concentrations of MNP remaining dispersible in the media were measured *via* atomic absorption spectroscopy (AAS). It was found that, in both samples, percentages of the dispersible particles in the solvents gradually decreased and there were about 30-50% MNP remaining dispersible in the media after 5 weeks (the plot is shown in the supporting information). One possible explanation is that the polymers might not be completely coated

on the surface of the particles, which essentially influenced their stability in the dispersions. Improvement in dispersibility of PDMS-coated MNP in toluene should also enhance dispersibility and stability of PPEGMA-coated MNP in water. This can be achieved by optimization of the reaction conditions in the PDMS-coating step of MNP such as the reaction temperature, solvent and catalyst, and this is warranted for a future study.

**Table 1** Hydrodynamic diameter ($D_H$), composition and magnetic properties of the MNP complexes

| Type of complex | $D_H$ (nm) [a] | % Char yield [b] | % in the complex [b] | | | emu/g of complex [c] | emu/g of $Fe_3O_4$ [b, c] |
|---|---|---|---|---|---|---|---|
| | | | $Fe_3O_4$ | PDMS | PPEGMA | | |
| Bare MNP | - | 88 | 100 | - | - | 44 | 44 |
| PDMS-OH-coated MNP | 446 ± 1 | 80 | 91 | 9 | - | 35 | 38 |
| PPEGMA-coated MNP | | | | | | | |
| after 6 h of ATRP | 295 ± 1 | 58 | 66 | 7 | 27 | 25 | 38 |
| after 24 h of ATRP | 162 ± 1 | 23 | 26 | 3 | 71 | 10 | 38 |

[a] Measured at room temperature *via* PCS technique

[b] Estimated from % char yield at 600 ºC *via* TGA technique

[c] Estimated from $M_s$ values at 10,000 G *via* VSM technique

Figure 7 shows the TGA thermograms of bare MNP, PDMS-OH-coated MNP and PPEGMA-coated MNP after 6 and 12 h of ATRP. The samples from each step of the reactions exhibited distinctive TGA curves giving rise to the information of the amount of PDMS and PPEGMA in the complexes. The slight drop in the weight of bare MNP was attributable to the residual benzyl alcohol used as the solvent in the MNP preparation step. According to the TGA results, there were about 9 wt% PDMS in the PDMS-OH-coated MNP and 3-7 wt% PDMS in the PPEGMA-coated MNP (Table 1). The drop in the percentage of PDMS was attributed to the increase of PPEGMA component in the complexes. The PPEGMA-coated MNP showed the weight loss stage ranging between 200 and 380$^o$C (Figure 7C and 7D), which was attributed to the decomposition of PPEGMA in the complexes. When the time periods of ATRP reaction were extended from 6 to 24 h, the percentage of PPEGMA increased from 27% to 71% and the percentage of magnetite core decreased from 66% to

26%, indicating the progressive increase of PPEGMA in the complexes. This was a supportive result to FTIR (Figure 3) and PCS experiments (Table 1) that PPEGMA chain length on their surface was extended when ATRP reaction time was prolonged.

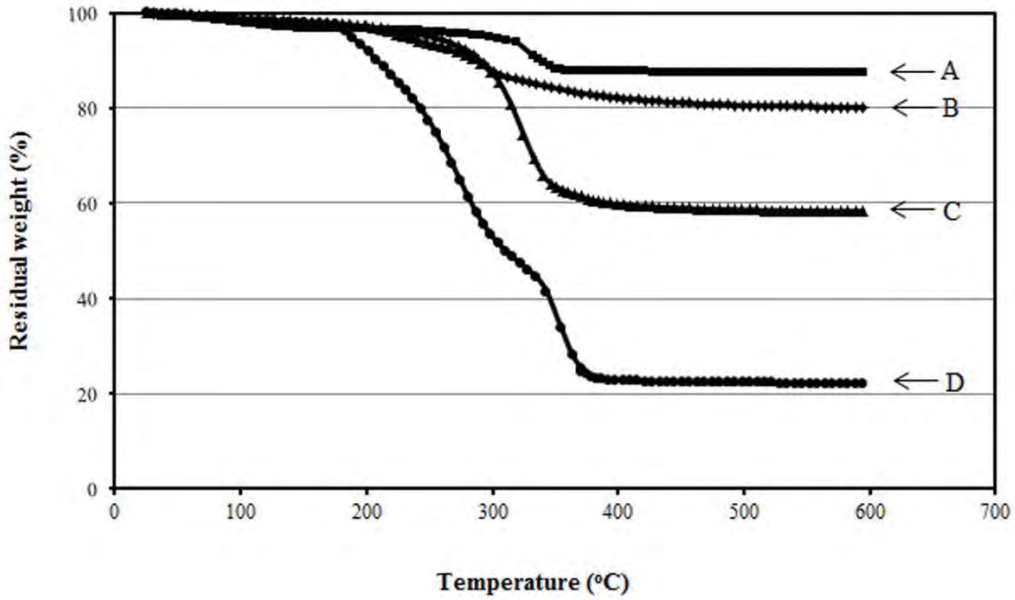


**Figure 7** TGA thermograms of (A) bare MNP, (B) PDMS-OH-coated MNP and PPEGMA-coated MNP after (C) 6 h and (D) 24 h of ATRP

Hysteresis curves of bare MNP, PDMS-OH-coated MNP, PPEGMA-coated MNP after 6 h and 24 h of ATRP were illustrated in Figure 8. They showed superparamagnetic behavior at room temperature as indicated by the absence of remanence and coercivity upon removing an external applied magnetic field. The saturation magnetization values ($M_s$) ranged between 10 and 44 emu/g complex (Table 1). As expected, the $M_s$ values decreased as the percentage of magnetite core in the complexes, determined *via* TGA technique, decreased. When taking the percentage of magnetite in the complex into account, the $M_s$ in emu/g magnetite basis of PDMS-OH-coated MNP slightly dropped from 44 to 38 emu/g magnetite. This was attributed to the use of high reaction temperature in the PDMS-coating step of MNP (hydrosillylation of PDMS-OH and allyl-grafted MNP), which might affect the magnetic properties of MNP core. Interestingly, magnetic properties of the PDMS-coated and PPEGMA-coated MNPs were not significantly different from each other, indicating that the

ATRP grafting step of PPEGMA from MNP surface did not deteriorate magnetic properties of the complexes.

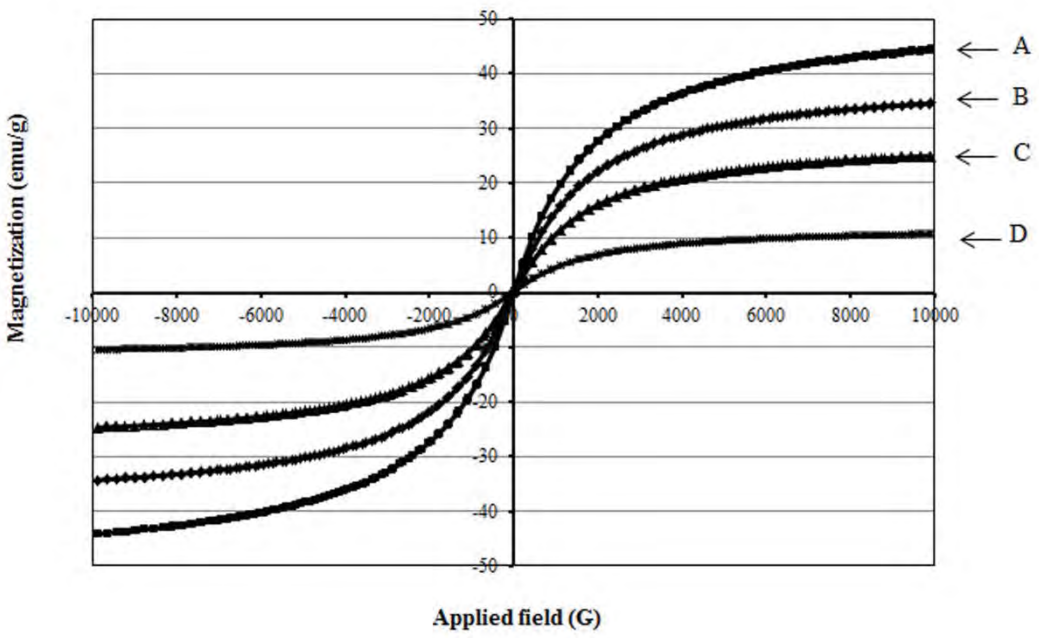


**Figure 8** Magnetization curves of (A) bare MNP, (B) PDMS-OH-coated MNP and PPEGMA-coated MNP after (C) 6 h and (D) 24 h of ATRP

The studies on drug entrapping and loading efficiencies were performed to confirm the formation of bilayer surface of MNP with a hydrophobic inner shell. Indomethacin was selected as a hydrophobic model drug in this study because its concentration can be measured *via* UV-vis spectrophotometry. It was envisioned that indomethacin should somewhat partition into the hydrophobic PDMS layer on the particle surface. It was found that percent drug entrapment efficiency (%EE) of the complex was 62% and drug loading efficiency (%DLE) was 27% (an example of the calculation is illustrated in the supporting information). This signified the formation of bilayer structure with hydrophobic PDMS inner shell on MNP surface.

## 4. Conclusions

Surface modification of MNP with PDMS-PPEGMA amphiphile *via* a "grafting from" strategy to obtain polymeric bilayer surfactant has been reported. The hydrophilic PPEGMA provided steric repulsion and water dispersibility to the particles, while